9-12-2016

Synthesis and Modification of Pristine Graphene Composites

Jennifer Bento
jennifer.bento@uconn.edu

Synthesis and Modification of Pristine Graphene Composites

Jennifer L. Bento, Ph.D.

University of Connecticut, 2016

Abstract

Graphene, a 2D allotrope of carbon, is of great interest due to its exceptional electrical, thermal, and mechanical properties. After Novoselov and Geim first isolated graphene in 2004 and later received the Nobel Prize in 2010, there has been a major effort to develop methods of graphene production for various electronic applications. However, these methods can be expensive and require strict experimental conditions. Our lab has developed a technique that overcomes these limitations by exfoliating graphite to few layer pristine graphene by trapping graphene sheets at the interface between two immiscible liquids. Vigorous mixing of the appropriate ratio of the two phases creates 2D surfactant stabilized water-in-oil emulsions. The oil phase can be a monomer and polymerized into a polymer/graphene foam.

The technique produces lightweight, mechanically robust, conductive, open-cell foam composites in a way that is simple, cheap, and scalable. This dissertation describes the electrical and thermal properties of these foams. The ability to tune the sphere size of the composites is important for filtration applications, and scanning electron microscopy (SEM) and acoustic spectrometry are the primary methods used to study the morphology and average sphere size. Since these materials are hydrophobic, a post-polymerization modification technique for porous

substrates was developed with an eye towards creating a hydrophilic poly (ethylene oxide) (PEO) surface.

PEO is a nonionic hydrophilic polymer having the same repeat unit as poly(ethylene glycol) (PEG). It is of interest in both biology and materials science, as PEO surfaces demonstrate a unique lack of protein adhesion and PEO block copolymers are widely used in applications such as drug delivery. However, the synthesis of PEO can be experimentally challenging, requiring air sensitive organometallic reagents to form reactive potassium alkoxides followed by the removal of compounds such as naphthalene from the final product. In this dissertation, we report a synthetic route that avoids these difficulties by forming the propagating alkoxides by azeotropic distillation, removing water from the alcohol / alkoxide equilibrium.

Synthesis and Modification of Pristine Graphene Composites

Jennifer L. Bento

B.S. Simmons College, 2011

A Dissertation

Submitted in Partial Fulfillment of the

Requirements for the Degree of

Doctor of Philosophy

at the

University of Connecticut

2016

APPROVAL PAGE

Doctor of Philosophy Dissertation

Synthesis and Modification of Pristine Graphene Composites

Presented by

Jennifer L. Bento, B.S.

Major Advisor: _____

Prof. Douglas H. Adamson

Associate Advisor: _____

Prof. Anson W. K. Ma

Associate Advisor: _____

Prof. Jeffrey R. McCutcheon

Associate Advisor: _____

Prof. Leslie M. Shor

Associate Advisor: _____

Prof. Richard S. Parnas

University of Connecticut
2016

Dedication

This work is dedicated to Shaun who has been my rock throughout my educational journey and to my parents for their unconditional love and encouragement.

Acknowledgements

I would first like to thank my advisor Dr. Adamson. Thank you for having me as a REU student in your lab 6 years ago and to advise me 1 year later as a graduate student. Thank you for challenging and motivating me. The group dynamic in the Adamson lab is very positive, collaborative, friendly, and exciting. I believe this is from having an outstanding advisor and mentor who leads by example. Next, I would like to thank my committee members: Dr. Ma, Dr. McCutcheon, Dr. Parnas, and Dr. Shor, for their helpful discussions throughout my graduate career. I would also like to thank the technical staff at IMS who have taught me many characterization techniques that were vital to my research. Specifically, Dr. Laura Pinatti for her help with thermal analysis instrumentation and for helpful discussions on my future career. Thank you to Mark Dudley and Gary Lavigne for their training on GPC and FT-IR. I would like to thank Dr. Roger Ristau and Dr. Lichun Zhang for all of their SEM help and countless questions they have answered. Thank you to JoAnne Ronzello for allowing me to use the thermal conductivity meter in her lab and for making my time spent in her lab enjoyable. I would also like to thank YoungHee for encouraging me to apply to the UConn Polymer Program for graduate school after my REU.

Next, I would like to thank all Adamson lab members past and present. They have all helped create a supportive and fun work environment. I would like to thank Dr. AJ Oyer, Dr. Andre Martinez, Dr. Kevin Huang, and Dr. Zhenhua Cui for welcoming me into the group when I started and always willing to discuss any research topic/question in lab. I would especially like to thank Dr. Chetan Hire. He was my mentor during my REU program and is a major reason why I chose to pursue Polymer Science in graduate school. He is not only a mentor today but a great

friend who continues to give me advice on school, life and anything to do with computers. I would like to thank Dr. Steve Woltornist, Dr. Reihaneh Mohammadi, Deepthi Varghese, and Garrett Kraft for the fun times we have had inside and outside the lab. I look forward to working with Steve again at Solvay. In addition, Drona Madugula, Shawn Ward, Liz Brown, Chau Vy, Martin Hui, Harish Kumar, and Fei Chen have made working in the lab both entertaining and inspiring. Thank you to my six classmates who I started the Polymer Program with, especially Yang Guo, who has been a great study partner, friend and sister to me throughout the past 5 years.

Lastly and most importantly, I would like to thank my family. Shaun, thank you for always supporting me, for being understanding, and for listening to my "chemistry talk." I could not have done these past 5 years without you by my side. To my parents: I would not be where I am today if it wasn't for the both of you. As educators you have always taught me that I can accomplish anything I put my mind to. Thank you for always believing in me and teaching me to work hard no matter what. To my Voa, Voo, Grandma, and VooVoo: Thank you for instilling values in me that I have used many times throughout my educational journey. They were truly invaluable. To Betty and Ryan: Thank you for always thinking of me and sending your well wishes in anything I was tackling. To Lee, Carlos, Josh, Becca, and Connor: thank you for always supporting me and being my cheerleaders back home.

Table of Contents

List of Figures

Chapter 1:
Introduction to the methods of graphene production

Section 1: Introduction

1.1.1 Graphene

Graphene, a two-dimensional allotrope of carbon, has many desirable properties, such as high thermal conductivity[1,2], electrical conductivity[3,4,5], mechanical properties[6,7] and large surface area[8,9]. Figure 1-1 shows graphene, the individual layers found in graphite, on the top right, and graphite in the top left image. These are relatives of carbon nanotubes and fullerenes shown on the bottom of the image, respectively. Individual graphene sheets were first isolated in 2004 by Novoselov and Geim[3] through a technique called micromechanical exfoliation.[3,10] The technique starts with a piece of highly-oriented pyrolytic graphite (HOPG) and scotch tape.[3] By using the scotch tape to pull apart the HOPG, eventually single layer graphene was produced.[10] The single layer of pristine graphene was transferred to another substrate, such as a Si wafer, and then analyzed further with techniques including AFM.

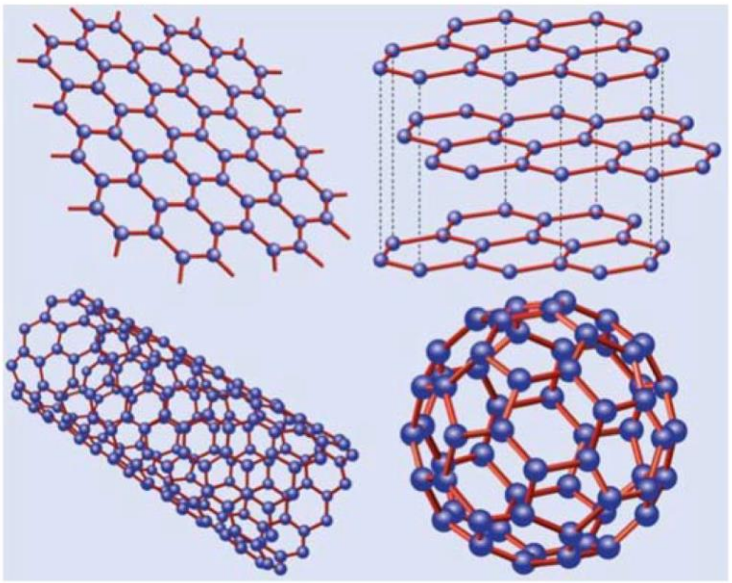

Figure 1-1. Graphene (top left), Graphite (top right), Carbon Nanotube (bottom left), Fullerenes (C_{60}) (bottom right).[5]

Due to graphene's extraordinary properties, there has been a large amount of research devoted to this 2D material and utilizing it in various applications. Specifically, graphene has a thermal conductivity of ~5000 W/mK,[1] a surface area of 2630 m^2/g,[9] a tensile modulus of 1TPa,[6] and an electron mobility of 250,000 $cm^2/(V.s)$.[11] With all of these incredible properties, graphene has a fairly low density of 2.2 g/cm^3 as compared to metals such as silver (10.49 g/cm^3) and copper (8.96 g/cm^3). There is a wide range of applications that are currently being studied with graphene such as transparent conductive electrodes[12–14], sensors[15,16], and energy storage devices.[17–19] Furthermore, graphene is utilized in composites[20–22] as well as in environmental applications, such as water treatment.[23,24] However, due to issues with scale up of the micromechanical exfoliation technique to produce pristine graphene for these types of applications, other methods have been developed.

1.1.2 Chemical Vapor Deposition and Epitaxial Growth

Chemical vapor deposition (CVD) is used to form large-area, high-quality graphene using metal substrates such as copper[25,26] or nickle.[27] A mixture of gases, such as methane, hydrogen or argon, is flowed over the substrate while heated at ~1000 °C.[28] Once the system is cooled, the most thermodynamically stable form of carbon, graphene, is formed on the surface.[29] The growth mechanism for Cu-based graphene is shown in Figure 1-2.[29]

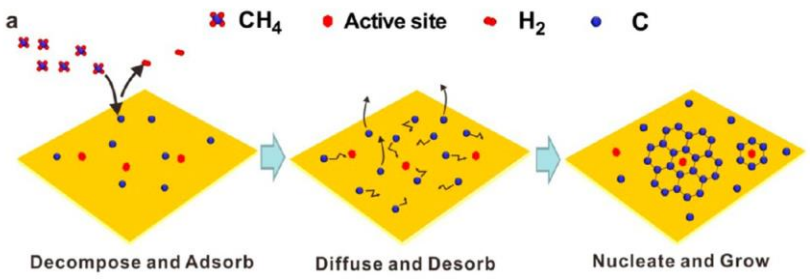

Figure 1-2. CVD graphene growth mechanism.[29]

Epitaxial growth uses a substrate like in CVD, however it is either silicon carbide, SiC, as shown in Figure 1-3[30] or ruthenium.[31] The system is heated in a vacuum or inert atmosphere and in the case of SiC, the silicon atoms leave the surface while graphene spontaneously forms on the surface.[30] Both techniques, CVD and epitaxial growth, are expensive and sensitive to experimental conditions. Also, a drawback of CVD is the chemical etching step required in order to transfer the graphene film from the metal substrate.[28]

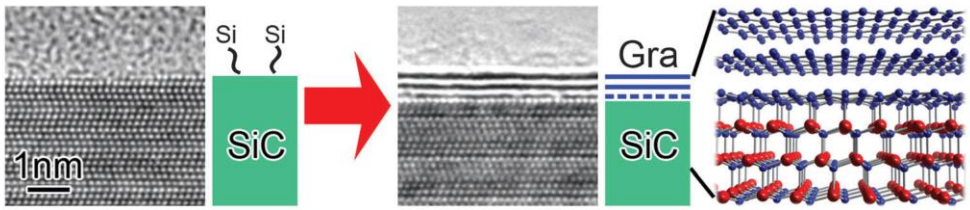

Figure 1-3. Epitaxial graphene growth on SiC.[30]

1.1.3 Oxidation and Reduction of Graphite

Graphite oxide is prepared by the oxidation of bulk graphite. The first method to produce graphite oxide was developed by Brodie[32] in the mid-1800s followed by Staudenmaier[33] and Hummer[34]. Oxygen functionalities such as hydroxyl, epoxide, carbonyl, and carboxyl groups are

introduced into the system.[35] These oxygen functionalities aid in the exfoliation or separation of the sheets into graphene oxide.[36] Graphene oxide is hydrophilic and therefore one advantage of GO over graphene is that it can be dispersed in water. However, GO is an insulator. In order to create an electrically conducting material, researchers have then taken GO and modified it further by reducing it to reduced graphene oxide or rGO.[37,38,39] An example of this is shown in Figure 1-4 where hydrazine is used to chemically reduce GO to rGO.[36] Although similar to pristine graphene, rGO still contains residual functional groups and lattice defects that degrade the final properties of the material.[40,41] In addition to chemical treatments, rGO can also be produced through thermal reduction.[42] In this way, GO is synthesized and thermally exfoliated at the same time without the need to remove any chemicals at the end.

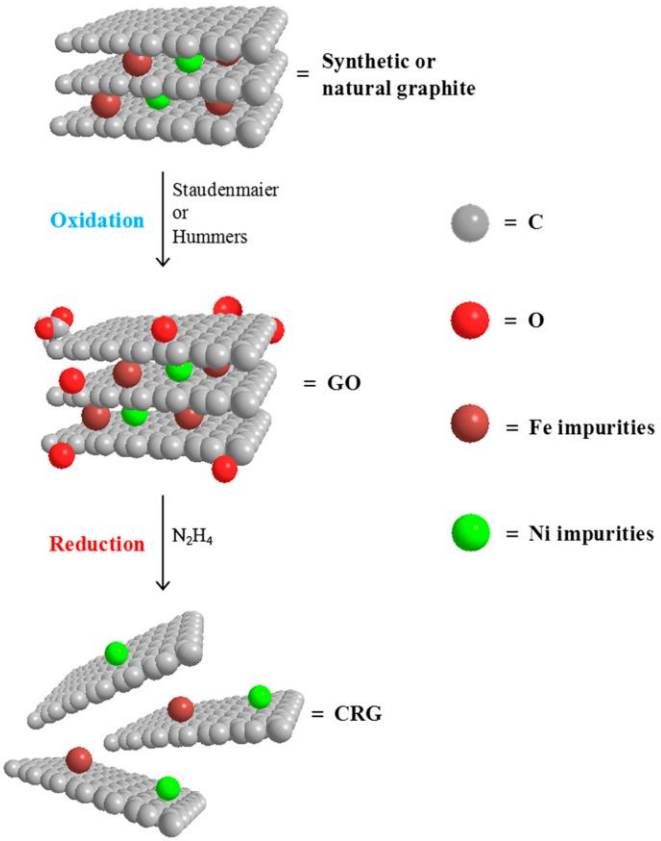

Figure 1-4. An example of a method to prepare chemically reduced graphene.[36]

1.1.4 Solvent Exfoliation and Surfactant Aided Exfoliation

Common solvents that are used in the exfoliation of graphite are *N*-Methyl-2-pyrrolidone (NMP)[43], *N*,*N*-Dimethylformamide (DMF), and *ortho*-Dichlorobenzene (DCB).[44] In order to successfully separate the sheets, the van der Waals forces between the layers must be overcome. Ultrasonication is used as a source of energy for dispersing the graphite into the solvents. Unfortunately, solvents such as NMP and DMF are hard to remove and have negative health effects.[44] In addition, the concentration of graphene in the organic solvents is low at around 0.01 mg/mL. Surfactant aided exfoliation[45], with surfactants such as sodium dodecylbenzene sulfonate (SDBS)[46], although safer than using organic solvents via surfactant-water solutions, require purification to remove the adsorbed surfactant molecules. Figure 1-5 demonstrates both liquid-phase exfoliation with and without surfactant molecules.[44]

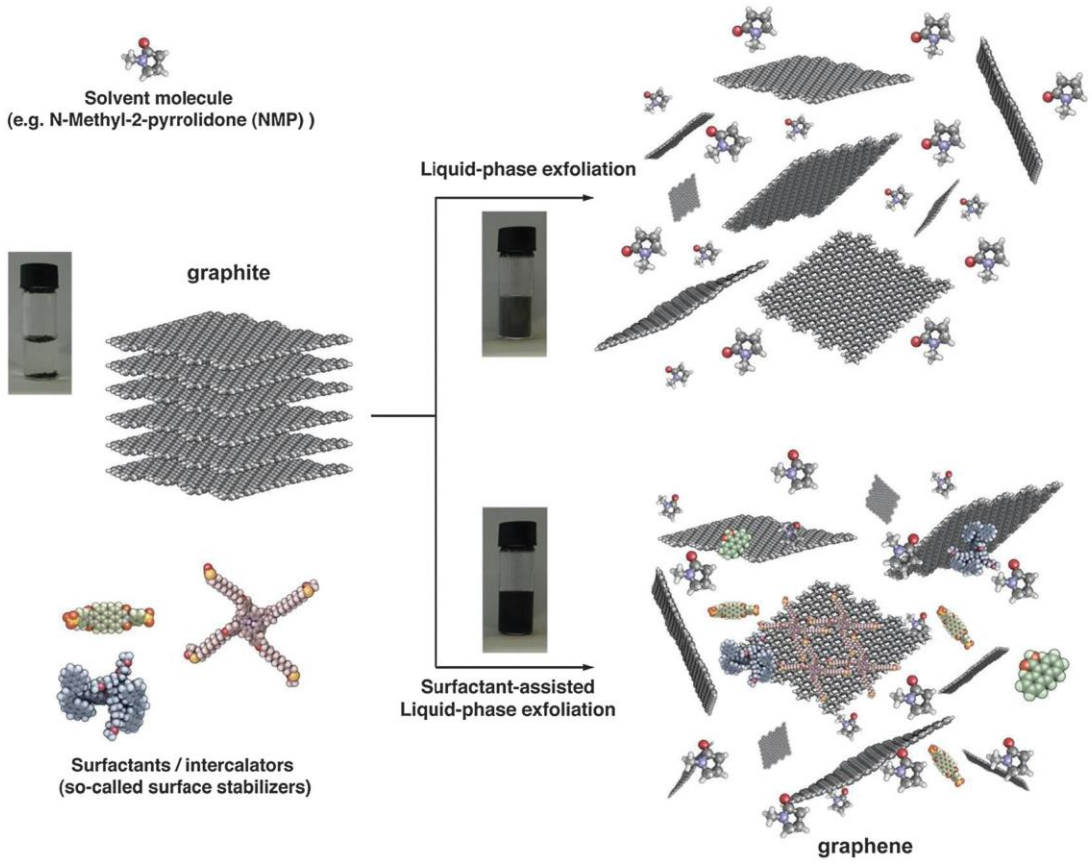

Figure 1-5. Liquid-phase exfoliation of graphite in the absence (top right) and presence (bottom right) of surfactant molecules.[44]

In order to overcome the limitations discussed in Sections 1.1.2 – 1.1.4, our group has developed a new technique to exfoliate graphite into pristine graphene that is simple, cheap, and scalable, without the need for removing surfactant molecules or using harsh chemicals or high temperatures.

1.1.5 Interfacial trapping method

Our group has discovered an interfacial trapping technique where bulk graphite is exfoliated to few layer graphene by trapping the graphite at the interface between two immiscible

liquids.[47] The system is driven by lowering the overall interfacial energy of the system. Transparent and conductive thin films are produced through this technique. These macroscopic films are up to 95% transparent and achieve conductivities of 400 S/cm.[47] There are no chemical modifications that are made to the graphite. The interfacial trapping method is a very simple and inexpensive technique.

Depending on the water-to-oil ratio, the pristine graphene can act as a two-dimensional surfactant and stabilize water-in-oil emulsions, as shown in Figure 1-6 below.[21,48] Similarly, graphene oxide can be used with this technique but instead form oil-in-water emulsions.[49]

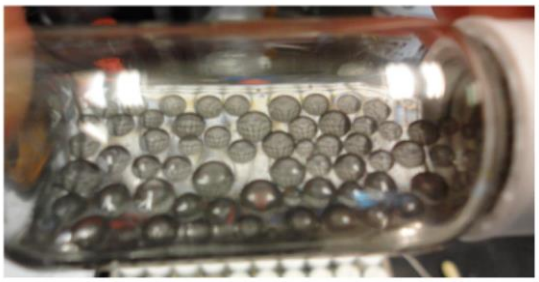

Figure 1-6. Water-in-oil spheres stabilized by pristine graphene.[47]

1.1.6 Polystyrene/graphene (PS-G) composite foams

Polymer-graphene nanocomposites can be synthesized for various applications, based on the same underlying principle of the interfacial trapping method.[20] The oil phase is replaced with a monomer and the continuous phase is polymerized, leaving behind water filled spheres stabilized by overlapping graphene sheets locked into place in a polystyrene matrix. One requirement with this technique is that the surface energy of the monomer must be below the surface energy of graphene, which is 54.8 mN/m.[50] Water has a surface energy of 72.9 mN/m.[20] Figure 1-7A and B demonstrate the scalability of the PS/G composites and homogeneity in the sphere size distribution. The graphene sheets are visible lining the inside of the spheres, in Figure

1-7C, where the smooth regions are polystyrene. In Figure 1-7D, the sphere-to-sphere contact point provides a percolating network of graphene sheets that allows these composites to be electrically conductive.

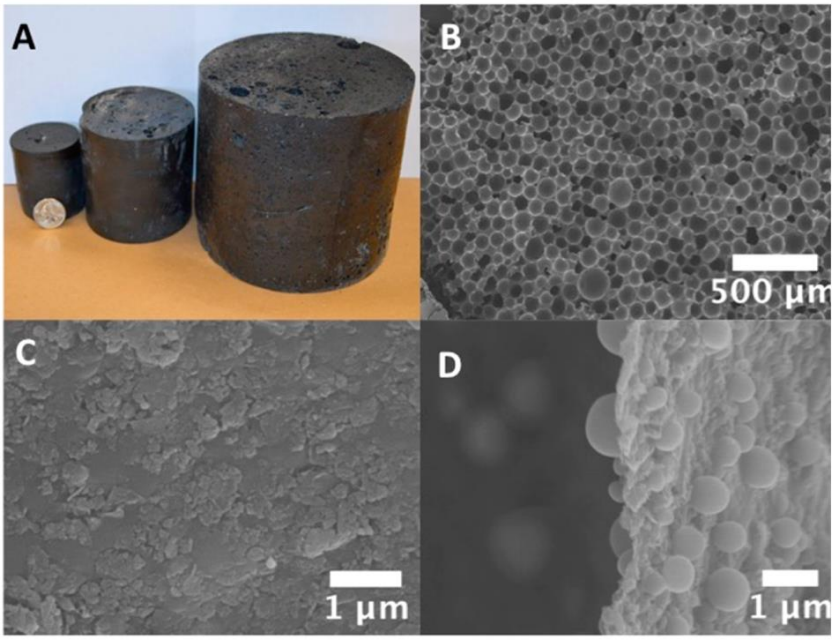

Figure 1-7. (A) Scalability of Polystyrene/Graphene foams (B) SEM image of the cross section of the graphene composite (C) SEM image of zooming into one of the spheres to see the graphene sheets (D) A SEM image of a sphere-to-sphere contact point.[20]

The open-cell, scalable foams have very low densities, between 0.25 to 0.35 g/cm^3, making them extremely lightweight. The PS/G composites also have excellent mechanical and electrical properties. Compressive strengths of 8.3 MPa (1200 psi) and bulk conductivities of 7 S/m can be achieved.[20] In addition to electrical properties, we are very interested in the thermal properties of the foams, for applications as porous electrodes or thermoelectric materials.

References

(1) Balandin, A. A.; Ghosh, S.; Bao, W.; Calizo, I.; Teweldebrhan, D.; Miao, F.; Lau, C. N. *Nano Lett.* **2008**, *8*, 902–907.

(2) Stankovich, S.; Dikin, D. A.; Dommett, G. H. B.; Kohlhaas, K. M.; Zimney, E. J.; Stach, E. A.; Piner, R. D.; Nguyen, S. T.; Ruoff, R. S. *Nat. Lett.* **2006**, *442*, 282–286.

(3) Novoselov, K. S.; Geim, A. K.; Morozov, S. V.; Jiang, D.; Zhang, Y.; Dubonos, S. V.; Grigorieva, I. V.; Firsov, A. A. *Science (80-.).* **2004**, *306*, 666–669.

(4) Geim, A. K.; Novoselov, K. S. *Nat. Mater.* **2007**, *6*, 183–191.

(5) Castro Neto, A. H.; Guinea, F.; Peres, N. M. R.; Novoselov, K. S.; Geim, A. K. *Rev. Mod. Phys.* **2009**, *81*, 109–162.

(6) Lee, C.; Wei, X.; Kysar, J. W.; Hone, J. *Science (80-.).* **2008**, *321*, 385–388.

(7) Chatterjee, S.; Wang, J. W.; Kuo, W. S.; Tai, N. H.; Salzmann, C.; Li, W. L.; Hollertz, R.; Nuesch, F. A.; Chu, B. T. T. *Chem. Phys. Lett.* **2012**, *531*, 6–10.

(8) Barg, S.; Perez, F. M.; Ni, N.; do Vale Pereira, P.; Maher, R. C.; Garcia-Tuñon, E.; Eslava, S.; Agnoli, S.; Mattevi, C.; Saiz, E. *Nat. Commun.* **2014**, *5*, 1–10.

(9) Stoller, M. D.; Park, S.; Zhu, Y.; An, J.; Ruoff, R. S. *Nano Lett.* **2008**, *8*, 3498–3502.

(10) Novoselov, K. S.; Jiang, D.; Schedin, F.; Booth, T. J.; Khotkevich, V. V.; Morozov, S. V.; Geim, A. K. *Proc. Natl. Acad. Scienes United States Am.* **2005**, *102*, 10451–10453.

(11) Orlita, M.; Faugeras, C.; Plochocka, P.; Neugebauer, P.; Martinez, G.; Maude, D. K.; Barra, A.-L.; Sprinkle, M.; Berger, C.; de Heer, W. A.; Potemski, M. *Phys. Rev. Lett.* **2008**, *101*, 1–5.

(12) Cai, W.; Zhu, Y.; Li, X.; Piner, R. D.; Ruoff, R. S. *Appl. Phys. Lett.* **2009**, *95*, 123115–1 – 123115–3.

(13) Li, X.; Zhu, Y.; Cai, W.; Borysiak, M.; Han, B.; Chen, D.; Piner, R. D.; Colombo, L.; Ruoff, R. S. *Nano Lett.* **2009**, *9*, 4359–4363.

(14) Zhu, Y.; Murali, S.; Cai, W.; Li, X.; Suk, J. W.; Potts, J. R.; Ruoff, R. S. *Adv. Mater.* **2010**, *22*, 3906–3924.

(15) He, Q.; Sudibya, H. G.; Yin, Z.; Wu, S.; Li, H.; Boey, F.; Huang, W.; Chen, P.; Zhang, H. *ACS Nano* **2010**, *4*, 3201–3208.

(16) Schedin, F.; Geim, A. K.; Morozov, S. V.; Hill, E. W.; Blake, P.; Katsnelson, M. I.; Novoselov, K. S. *Nat. Mater.* **2007**, *6*, 652–655.

(17) Huang, Y.; Liang, J.; Chen, Y. *Small* **2012**, *8*, 1–30.

(18) Mao, S.; Lu, G.; Chen, J. *Nanoscale* **2015**, *7*, 6924–6943.

(19) Shao, Y.; El-Kady, M. F.; Wang, L. J.; Zhang, Q.; Li, Y.; Wang, H.; Mousavi, M. F.; Kaner, R. B. *Chem. Soc. Rev.* **2015**, *44*, 3639–3665.

(20) Woltornist, S. J.; Carrillo, J.-M. Y.; Xu, T. O.; Dobrynin, A. V.; Adamson, D. H. *Macromolecules* **2015**, *48*, 687–693.

(21) Woltornist, S. J.; Adamson, D. H. *Ind. Eng. Chem. Res.* **2016**, *55*, 6777–6782.

(22) Huang, X.; Qi, X.; Boey, F.; Zhang, H. *Chem. Soc. Rev.* **2012**, *41*, 666–686.

(23) Kemp, K. C.; Seema, H.; Saleh, M.; Le, N. H.; Mahesh, K.; Chandra, V.; Kim, K. S. *Nanoscale* **2013**, *5*, 3149–3171.

(24) Perreault, F.; Fonseca de Faria, A.; Elimelech, M. *Chem. Soc. Rev.* **2015**, *44*, 5861–5896.

(25) Wang, Y.; Zheng, Y.; Xu, X.; Dubuisson, E.; Bao, Q.; Lu, J.; Loh, K. P. *ACS Nano* **2011**, *5*, 9927–9933.

(26) Li, X.; Cai, W.; An, J.; Kim, S.; Nah, J.; Yang, D.; Piner, R.; Velamakanni, A.; Jung, I.; Tutuc, E.; Banerjee, S. K.; Colombo, L.; Ruoff, R. S. *Science (80-.).* **2009**, *324*, 1312–

1314.

(27) Reina, A.; Jia, X.; Ho, J.; Nezich, D.; Son, H.; Bulovic, V.; Dresselhaus, M. S.; Kong, J. *Nano Lett.* **2009**, *9*, 30–35.

(28) Kim, K. S.; Zhao, Y.; Jang, H.; Lee, S. Y.; Kim, J. M.; Kim, K. S.; Ahn, J.-H.; Kim, P.; Choi, J.-Y.; Hong, B. H. *Nature* **2009**, *457*, 706–710.

(29) Yan, Z.; Lin, J.; Peng, Z.; Sun, Z.; Zhu, Y.; Li, L.; Xiang, C.; Samuel, E. L.; Kittrell, C.; Tour, J. M. *ACS Nano* **2012**, *6*, 9110–9117.

(30) Norimatsu, W.; Kusunoki, M. *Phys. Chem. Chem. Phys.* **2014**, *16*, 3501–3511.

(31) Sutter, P. W.; Flege, J.-I.; Sutter, E. A. *Nat. Mater.* **2008**, *7*, 406–411.

(32) Brodie, B. C. *Philos. Trans. R. Soc. London* **1859**, *149*, 249–259.

(33) Staudenmaier, L. *Berichte der Dtsch. Chem.* **1898**, *31*, 1481–1487.

(34) Hummers Jr., W. S.; Offeman, R. E. *J. Am. Chem. Soc.* **1958**, *80*, 1339–1339.

(35) Stankovich, S.; Dikin, D. A.; Piner, R. D.; Kohlhaas, K. A.; Kleinhammes, A.; Jia, Y.; Wu, Y.; Nguyen, S. T.; Ruoff, R. S. *Carbon N. Y.* **2007**, *45*, 1558–1565.

(36) Ambrosi, A.; Chua, C. K.; Khezri, B.; Sofer, Z.; Webster, R. D.; Pumera, M. *Proc. Natl. Acad. Sci.* **2012**, *109*, 12899–12904.

(37) Eda, G.; Fanchini, G.; Chhowalla, M. *Nat. Nanotechnol.* **2008**, *3*, 270–274.

(38) Wang, G.; Yang, J.; Park, J.; Gou, X.; Wang, B.; Liu, H.; Yao, J. *J. Phys. Chem. C* **2008**, *112*, 8192–8195.

(39) Liu, H.; Zhang, L.; Guo, Y.; Cheng, C.; Yang, L.; Jiang, L.; Yu, G.; Hu, W.; Liu, Y.; Zhu, D. *J. Mater. Chem. C* **2013**, *1*, 3104–3109.

(40) Pei, S.; Cheng, H.-M. *Carbon N. Y.* **2012**, *50*, 3210–3228.

(41) Becerril, H. A.; Mao, J.; Liu, Z.; Stoltenberg, R. M.; Bao, Z.; Chen, Y. *ACS Nano* **2008**, *2*,

463–470.

(42) Schniepp, H. C.; Li, J.-L.; McAllister, M. J.; Sai, H.; Herrera-Alonso, M.; Adamson, D. H.; Prud'homme, R. K.; Car, R.; Saville, D. A.; Aksay, I. A. *J. Phys. Chem. B* **2006**, *110*, 8535–8539.

(43) Hernandez, Y.; Nicolosi, V.; Lotya, M.; Blighe, F. M.; Sun, Z.; De, S.; McGovern, I. T.; Holland, B.; Byrne, M.; Gun'Ko, Y. K.; Boland, J. J.; Niraj, P.; Duesberg, G.; Krishnamurthy, S.; Goodhue, R.; Hutchison, J.; Scardaci, V.; Ferrari, A. C.; Coleman, J. N. *Nat. Nanotechnol.* **2008**, *3*, 563–568.

(44) Ciesielski, A.; Samorì, P. *Chem. Soc. Rev.* **2014**, *43*, 381–398.

(45) Nicolosi, V.; Chhowalla, M.; Kanatzidis, M. G.; Strano, M. S.; Coleman, J. N. *Science (80-.).* **2013**, *340*, 1226419–1 – 1226419–18.

(46) Lotya, M.; Hernandez, Y.; King, P. J.; Smith, R. J.; Nicolosi, V.; Karlsson, L. S.; Blighe, F. M.; De, S.; Wang, Z.; McGovern, I. T.; Duesberg, G. S.; Coleman, J. N. *J. Am. Chem. Soc.* **2009**, *131*, 3611–3620.

(47) Woltornist, S. J.; Oyer, A. J.; Carrillo, J.-M. Y.; Dobrynin, A. V.; Adamson, D. H. *ACS Nano* **2013**, *7*, 7062–7066.

(48) Woltornist, S. J.; Alamer, F. A.; McDannald, A.; Jain, M.; Sotzing, G. A.; Adamson, D. H. *Carbon N. Y.* **2015**, *81*, 38–42.

(49) Kumar, H. V.; Woltornist, S. J.; Adamson, D. H. *Carbon N. Y.* **2016**, *98*, 491–495.

(50) Wang, S.; Zhang, Y.; Abidi, N.; Cabrales, L. *Langmuir* **2009**, *25*, 11078–11081.

Chapter 2:
Outline of dissertation

This dissertation is divided into six chapters and is centered around the use of pristine graphene as a two-dimensional surfactant to stabilize water-in-oil emulsions for the production of lightweight, open-cell foams for applications in resistive heating and adsorption. The previous chapter, Chapter 1, described the background of various methods of graphene production in the literature. Most methods are expensive and require strict experimental conditions. Other disadvantages to the current methods are that harsh chemicals are used and removal of high boiling point solvents or surfactants is required at the end of the production of graphene. In addition, the resultant "graphene", without exception, will have residual functional groups from reduction of graphene oxide to reduced graphene oxide and defects in the 2D carbon lattice that degrade the final properties of the material. A method that was developed in our lab is introduced: the interfacial trapping method. This technique uses the insolubility of bulk graphite in both organic and aqueous media to our advantage. The spreading and self-assembly of graphene sheets at a high energy oil/water interface takes place and is driven by lowering the overall energy of the system. No chemical treatments, surfactants, high boiling solvents, or purification steps are necessary. Pristine graphene acts as a two-dimensional surfactant and stabilizes water-in-oil emulsions.

The oil phase in the water-in-oil emulsions stabilized by overlapping graphene sheets can be replaced with a monomer, such as styrene, and polymerized to form a rigid continuous phase. The water-filled, graphene-stabilized spheres within the polystyrene matrix can be evaporated from gentle heating and a lightweight, open-cell foam is produced. Due to the overlapping graphene sheets and sphere-to-sphere contact, the polystyrene-graphene composites are electrically conductive. The scalability and tunability of the foams is briefly introduced at the end of the first chapter.

Next, the thermodynamically-driven exfoliation and self-assembly of pristine graphene sheets at a liquid/liquid interface is shown to provide thermally and electrically-functional polymer composites in Chapter 3. The spreading of graphene sheets at a high energy liquid/liquid interface is driven by lowering the overall energy of the system, and provides for the formation of water-in-oil emulsions stabilized by overlapping graphene sheets. Polymerization of the oil phase, followed by removal of the dispersed water phase, produces inexpensive and porous composite foams. Contact between the graphene-stabilized water droplets provides a pathway for electrical and thermal transport through the composite. Unlike other reports of graphene foams, the graphite used to synthesize these composites is natural flake material, with no oxidation, reduction, sonication, high temperature thermal treatment, addition of surfactants, or high shear mixing required. The result is an inexpensive, low-density material that exhibits Joule heating and displays increasing electrical conductivity with decreasing thermal conductivity. Reproducible Joule heating up to ~100 °C is shown with no degradation of the material with the average resistance of the composite staying the same pre and post-heating.

In Chapter 4, an investigation into the mechanism of formation of polymer foams templated by emulsions stabilized by two-dimensional pristine graphene surfactants is presented. The thermodynamically-driven exfoliation of natural flake graphite at a high-energy monomer/water interface produces stabile water-in-oil emulsions stabilized by a thin layer of overlapping graphene sheets. The process requires no additional surfactant or pretreatment of the graphite, such as oxidization, reduction, sonication or high shear mixing. Subsequent polymerization of the continuous monomer phase produces polymer foams with cells lined by graphene. With a combination of acoustic spectrometry and electron microscopy, the effects of graphite concentration and temperature are studied, as is the correlation between droplet size in

the emulsion and the size of the cells in the final polymer foam. Additionally, results are presented demonstrating the application of this polymer foam for the adsorption of an organic dye and as a filter for dispersed oil.

The polymer/graphene foams are hydrophobic and we have been developing methods for the post-polymerization modification of the composites to add some hydrophilic character to the material. One possible modification is through the attachment of poly (ethylene oxide) chains to the surface of the porous composite. Poly(ethylene oxide) (PEO) is a nonionic hydrophilic polymer having the same repeat unit as poly(ethylene glycol) (PEG). It is of interest in both biology and materials science, as PEO surfaces demonstrate a unique lack of protein adhesion and PEO block copolymers are widely used in applications such as drug delivery. However, the synthesis of PEO can be experimentally challenging, requiring air sensitive organometallic reagents to form reactive potassium alkoxides followed by the removal of compounds such as naphthalene from the final product. In Chapter 5, we report a novel synthetic route that avoids these difficulties by forming the propagating alkoxides by azeotropic distillation, removing water from the alcohol / alkoxide equilibrium. Removing the water drives the equilibrium to the potassium alkoxide without the use of pyrophoric organometallics. GPC and NMR are used to characterize the PEO polymers made by this approach from various alcohols, including small molecular weight alcohols, hydroxyl terminated pre-formed PEO, and macromers such as polystyrene endcapped with a hydroxyl group.

Lastly, a summary of all the work throughout the dissertation and potential ideas for future work are described in Chapter 6. The potential for post-modification of the foams to make them more hydrophilic, changing the monomer to create different polymer/graphene foams, and continuing the use of the composites in filtration applications is discussed.

Chapter 3:
Thermal and electrical properties of nanocomposites based on self-assembled pristine graphene

Objective:

To study the electrical and thermal properties of polystyrene/graphene nanocomposites, which are made by the self-assembly of pristine graphene at an oil/water interface. Different positions within a composite provide a platform to see the effect of graphene density on the properties of the material. Joule heating applications are also of interest for these foams.

Section 1: Introduction

The remarkable thermal,[1,2] electrical,[3–5] and mechanical properties[6,7] of graphene, combined with its large surface area,[8,9] have inspired an explosion of interest for its use in functional nanocomposites. However, the difficulty associated with exfoliating and dispersing pristine graphene in a polymer matrix has meant that, almost without exception, such composites are made with either graphene oxide (GO), or reduced graphene oxide (rGO). Although rGO is often referred to as graphene in many articles, its use requires separate oxidation and reduction steps and results in sheets with diminished properties as compared to pristine graphene. In the investigations described in this chapter, we describe the electrical, thermal, and Joule heating properties of a pristine graphene-based functional nanocomposite synthesized by the self-assembly of natural flake graphite without any pretreatment, added surfactant, or extended high energy mixing or sonication.

The thermal and electrical properties of these polystyrene/graphene (PS/G) emulsion templated nanocomposites are a result of the contact between the graphene-coated dispersed water droplets in the emulsion. The settling and packing of these droplets prior to polymerization thus has a significant effect on the electrical and thermal properties of the composite. After polymerization of the oil phase, the water phase is removed by way of windows between the droplets that result from tears in the very thin graphene skin separating the droplets. The composition of the graphene shell surrounding each water droplet, and thus lining each cell in the composite foam after removal of the water, is inferred from spreading studies of a model system at a heptane/water interface.[10] The graphitic skin surrounding each water droplet appears to be a combination of graphene and graphite, with the graphene sheets at the interface, along with graphite flakes that did not exfoliate further once the liquid/liquid interface was covered with graphene.

In addition, our composite is capable of Joule heating, a process of directly heating a sample by passing a current through a percolated network of nanocarbons within a matrix.[14,15] This type of heating has been previously studied using carbon nanotubes (CNTs),[16–21] reduced graphene oxide (rGO),[15,22] pure graphite,[18,23] and CVD grown graphene,[24,25] with proposed applications such as defoggers, composite manufacturing and repair,[18] the detection of internal and surface damage *in situ* using thermographic imaging,[17] and as an external stimulus for stimuli responsive materials in shape memory or recovery.[14,26]

This chapter presents an inexpensive, electrically and thermally conductive pristine graphene based composite material that demonstrates Joule heating. It is synthesized by the thermodynamically-driven exfoliation and self-assembly of graphite and graphene sheets to form a continuous graphene network within a polymer matrix.[27] No added surfactants, oxidation, high

sheer mixing, high temperature treatment or sonication is required. These composites are of interest for filtration, as porous electrodes, and as thermoelectric materials with material and production costs expected to be less than that for simple polystyrene packing foam.

Section 2: Experimental

3.2.1 Synthesis of polystyrene/graphene composite foams

The procedure to synthesize a typical polystyrene/graphene composite was used as described elsewhere.[11] The following modifications have been made to the procedure. For all composites, regardless of graphite type and concentration, a 7/3 water/styrene volume ratio was used. An Erlenmeyer flask was charged with the necessary amount of graphite (Asbury Graphite Mills, Inc. grade Nano 24 lot # 2148 or grade Micro 890 lot # 16787), 140 ml water (Deionized), 60 ml styrene (Sigma-Aldrich, ≥99%), 14.4 ml divinylbenzene (DVB) (Aldrich, 80%), 180 mg azobis(isobutyronitrile) (AIBN) (Aldrich, 98%) and a stir bar, then stirred for 1 minute on a stir plate. The stir bar was then removed and the flask placed under the mixing tip of a Silverson laboratory mixer (Model L5M-A, Silverson Machines Inc.) for 1 minute. The emulsion was transferred into a 240 mL jar, capped with a lid and placed in a convection oven (Blue M, Stabil-Therm) at ~70 °C for 24 h. The rigid nanocomposites were then removed from the jars and heated at ~70 °C for an additional ~2 – 3 days to remove the remaining water. The simple process of creating a water-in-oil emulsion and subsequently polymerizing the oil phase is shown in Figure 3-1 for a 1.3 wt% graphite emulsion. The bulk polystyrene top layer was then cut from the composites, and composite slices ~ 1 cm in thickness were cut from the sample for analysis.

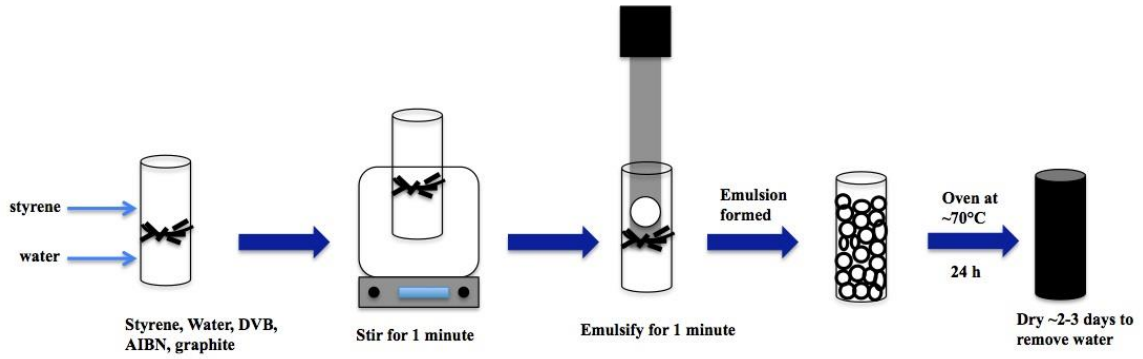

Figure 3-1. Schematic of the synthesis of a theoretical 1.3 wt% graphite PS/G composite.

There was a slight variation in the sample preparation between a standard composite (1.3% graphite by weight) and the composites with higher graphite loadings due to an increase in the viscosity of the emulsions containing more graphite. The weight percent of graphite was calculated as the ratio of graphite to the total mass of the oil phase and graphite. The calculated 3.4 wt% (2.4 g graphite) and 6.9 wt% (5 g graphite) graphene-stabilized emulsions were stirred on a stir plate for 1 minute after all of the reagents were added, however the Silverson mixer was not used and the dispersion was instead shaken for 1 minute. The calculated 14 wt% (11 g) was not blended using the Silverson nor stirred on a stir plate. After all reagents were added, the dispersion was shaken in 10s intervals for 1 minute. When changing graphite flake size, from the Nano 24 (~1 μm) to the Micro 890 (~10 μm), samples were blended for 1 minute with the Silverson mixer, then shaken for an additional 1 minute to increase the amount of emulsion present in the jar prior to polymerization.

3.2.2 Scanning Electron Microscopy (SEM)

Microscopy samples were prepared by breaking off small pieces from the composite disc with a razor blade. The pieces were placed on aluminum stubs covered with carbon tape to

adhere the sample to the stub. The stubs were coated with Au/Pd in a sputter coater (Polaron Unit E5100) and characterized with a JEOL JSM-6335F FESEM using a 10 kV accelerating voltage. The acquired images were analyzed with Image J software to determine the average sphere size. To account for the spheres not being cut in the center when making a sample for SEM, the average radius from Image J was multiplied by four and divided by π to calculate the radius. This method was used for all average sphere size calculations.

Two graphite flake sizes, Nano 24 (~1 μm) and Micro 890 (~10 μm), are used throughout this chapter and the morphology of the sheets, characterized by SEM, is important for the results and the discussion of the thermal and electrical properties of the PS/G nanocomposites. The average lateral sheet size of Asbury grade Nano 24 is on the order of a few microns. In Figure 3-2A, B, and C, the synthetic Nano 24 can be seen. Nano 24 is provided by Asbury Carbons.

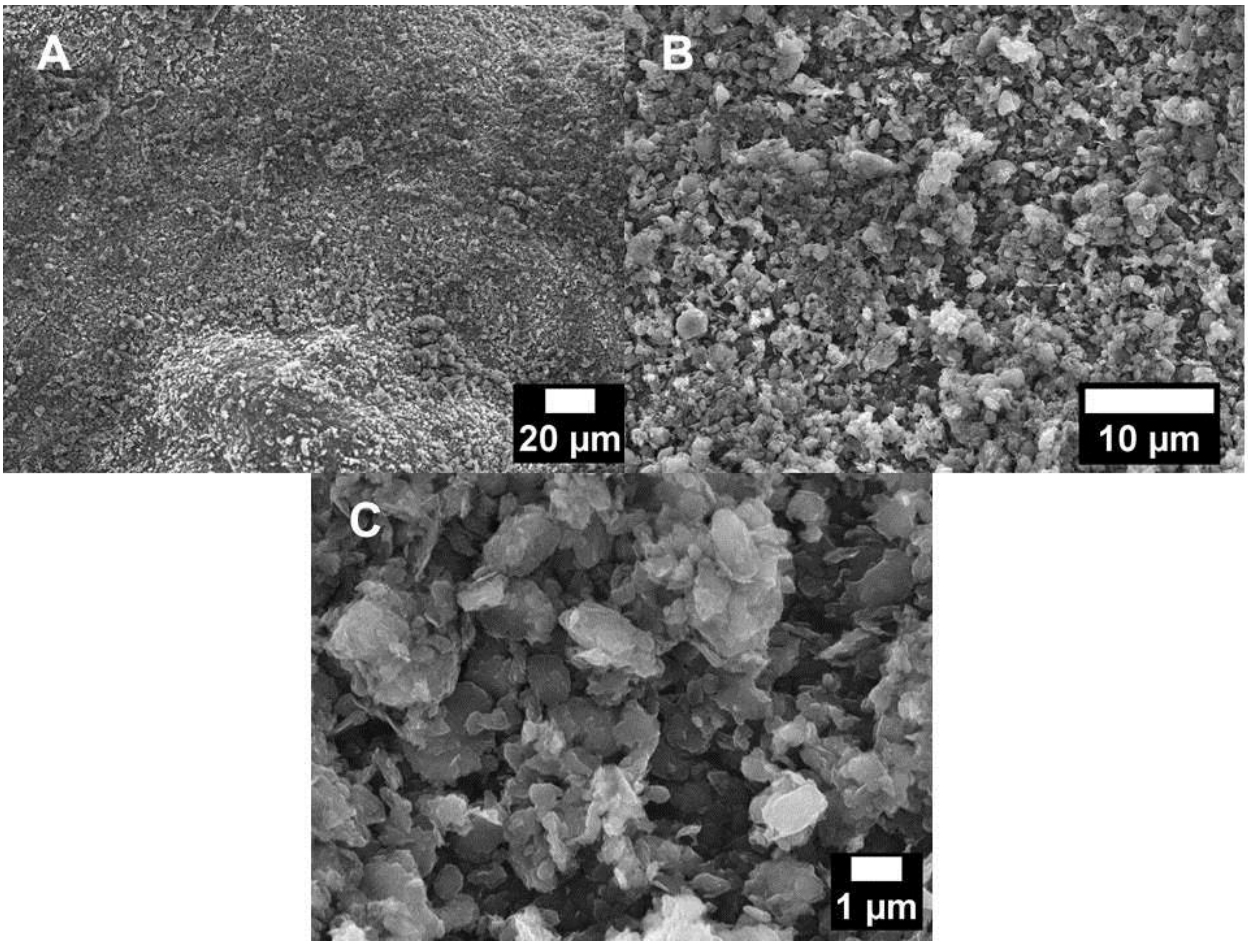

Figure 3-2. Scanning electron microscopy images of Asbury Carbons graphite grade Nano 24.

The average lateral sheet size of Asbury grade Micro 890 is around 10 µm. The natural flake graphite can be seen in Figure 3-3A, B, and C. Micro 890 is provided by Asbury Carbons.

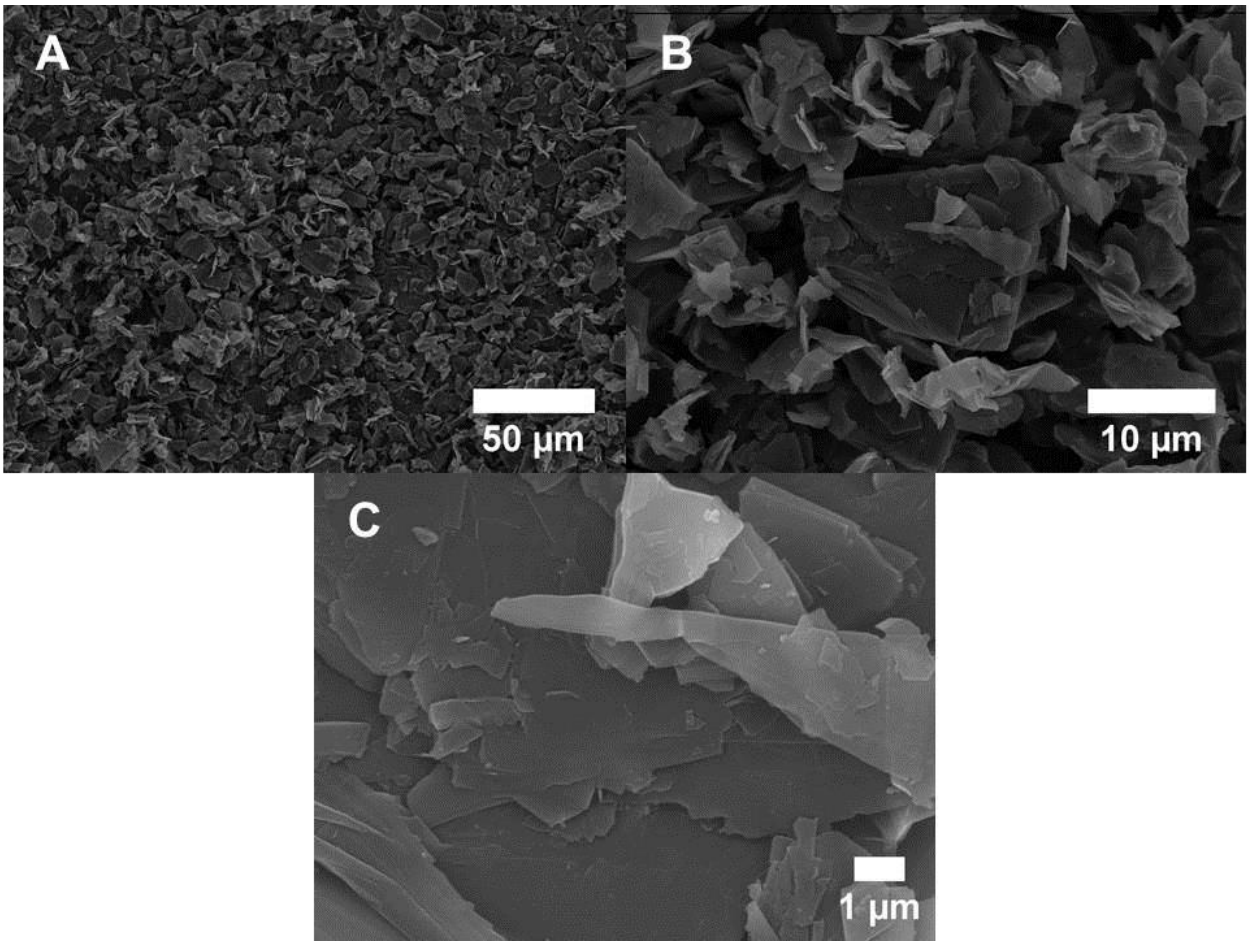

Figure 3-3. Scanning electron microscopy images of Asbury Carbons graphite grade Micro 890.

3.2.3 Thermal gravimetric analysis (TGA)

Small pieces of the composite were cut with a razor blade for thermal analysis. Approximately 20 mg of composite was placed in a platinum pan and heated to 800 °C using a heating rate of 10 °C/min in a TA Instruments TGA Q-500. Nitrogen gas was used in the chamber. The percent residue was analyzed at 795 °C for each sample to ensure no polymer remained. Figure 3-4 shows a typical TGA profile for a PS/G composite, with a small weight loss at ~100 °C for any water remaining, a major peak at ~400 °C from the decomposition of the polymer, and anything remaining in the system taken as graphite at 795 °C.

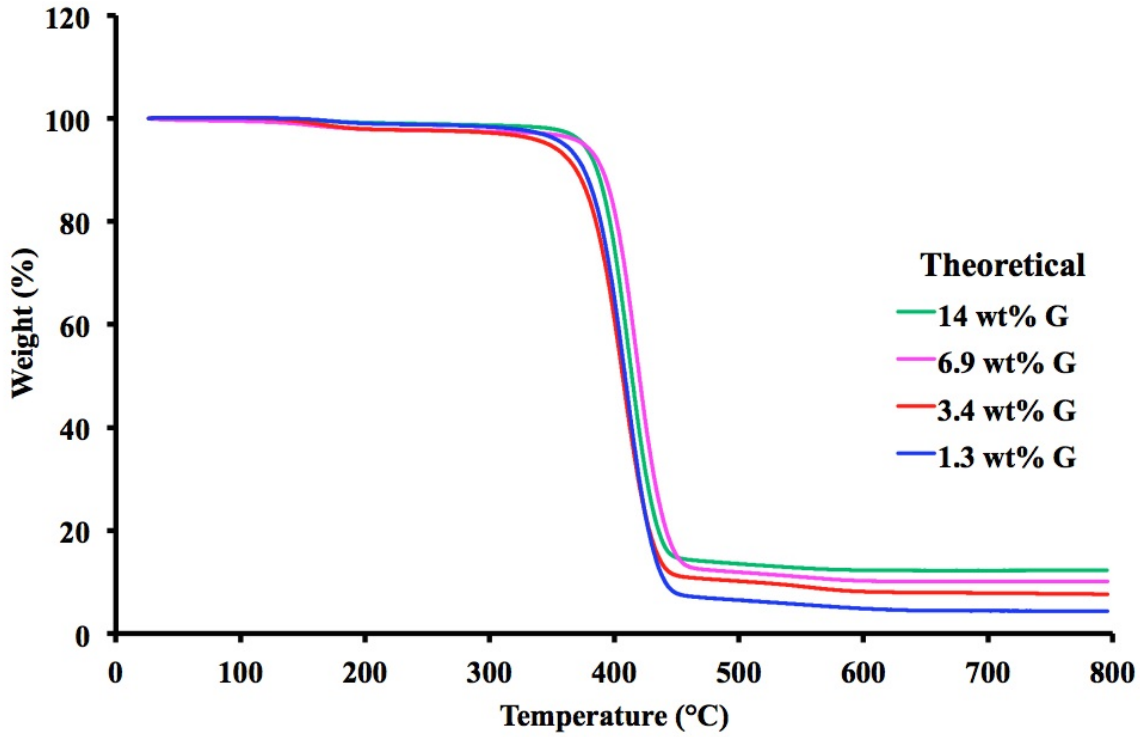

Figure 3-4. Typical TGA trace of weight % versus temperature for four different theoretical weight percentages of graphite in PS/G nanocomposites. This method is used throughout the results and discussion regardless of weight % or flake size of graphite in PS/G foams to determine actual weight % graphite.

3.2.4 Thermal conductivity

1 cm thick discs were cut from a composite sample, starting from directly below the bulk polystyrene layer and moving downward. A thin layer of thermal joint compound, type 120 silicone (Wakefield Solutions) was placed on both sides of the disc to make contact with the two electrodes. The thermal conductivity of each disc was measured at 20 °C using a TA Instruments thermal conductivity meter (DTC-300).

3.2.5 Electrical measurements

The procedure for cutting composite slices as mentioned above was repeated. From these discs, two rectangular prisms were cut (3 cm x 1.5 cm x 1 cm). The ends of the prisms were painted with Pelco® colloidal silver paste (Ted Pella, Inc.) and allowed to dry overnight. Copper tape (Electron Microscopy Sciences) was then attached to the silver covered ends and the current was measured using a Keithly Model 2420 sourcemeter. A voltage sweep from 0.001 to 0.1 V was performed with each sample using the sourcemeter and the average resistance was obtained. The dimensions of the sample and the average resistance were used to calculate the conductivity.

3.2.6 X-ray diffraction (XRD)

The samples that were used for electrical conductivity measurements were crushed using a mortar and pestle. These samples were then used for XRD, using a Bruker D2 Phaser and DIFFRAC.Measurement Center software, Version 4.0. Data was collected from a 2θ value of 7 – 35°, time of 0.5 s, and an increment of 0.01. The area under each peak was analyzed using DIFFRAC.EVA software, Version 4.1.1 and the G/PS ratio was compared.

3.2.7 Resistive Heating

Rectangular prisms were used to study the resistive heating of the composites. After attaching copper tape to the silver-coated ends of the composite, a Keithly Model 2420 sourcemeter was used to pass a constant current through the material. A systematic study was performed to determine the maximum amount of current that could pass through the composite without degrading the material and to achieve reproducible heating. The voltage versus time was monitored. The temperature over time was also measured using a thermal imaging camera (FLIR

ONE) while heating. The setup is shown in Figure 3-5, where the PS/G composite is on the left with the Keithly sourcementer and a computer on the right to run the software. The Keithly sourcemeter with the PS/G rectangular prism is highlighted in the bottom image.

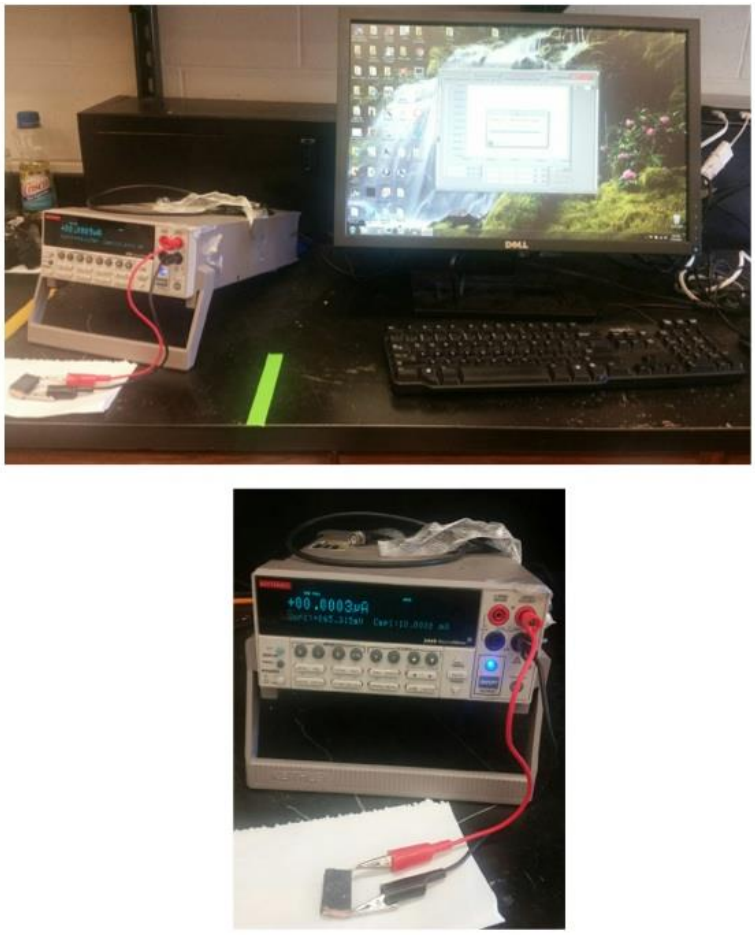

Figure 3-5. Image of test setup for resistance measurements in addition to resistive heating experiments. A PS/G rectangular prism with silver coated ends and copper tape is attached to a Keithly sourcementer and a computer to run the appropriate software.

Section 3: Results & Discussion

Polymerization of the oil phase of the emulsion is not instantaneous, and some settling of the graphene-coated water droplets occurs prior to polymerization. As the spheres settle, they pack more closely at the bottom of the reaction vessel, decreasing the volume of the interstitial oil (monomer) phase and creating a density gradient in the material. Figure 3-6A shows an image of a typical polystyrene/graphene (PS/G) nanocomposite. A bulk layer of PS forms on the top of the emulsion due to the settling and packing of the denser dispersed phase (water), forcing some of the continuous phase (styrene) out from between the droplets. This excess oil phase rises to the top of the emulsion and polymerizes. The bottom of the composite thus has more water and less monomer per unit volume than the top, and because the water is removed following polymerization, the density of the bottom material is lower than that of the top. Conversely, as there is less polymer at the bottom, the relative density of graphene at the bottom is greater. To investigate the effect of changing graphene density, 1 cm thick discs are taken from the composite, as shown in Figure 3-6A. These slices are used for thermal conductivity and electrical conductivity measurements to investigate the effect of graphene density on those properties.

SEM images shown in Figure 3-6B through Figure 3-6E show the spherical morphology of the composites and illustrate the decreasing amount of interstitial polymer as one moves towards the bottom of the composite. Figure 3-6B shows an image of the composite from the 0 – 1 cm region, which is the closest position to the top PS bulk layer. The black arrows indicate the interstitial PS between the graphene-lined spheres. Due to settling of the emulsion prior to polymerization, the spheres are more tightly packed at the bottom of the composite than at the top. This results in less interstitial polymer between spheres, smaller spheres, lower material density, and higher relative graphene density.

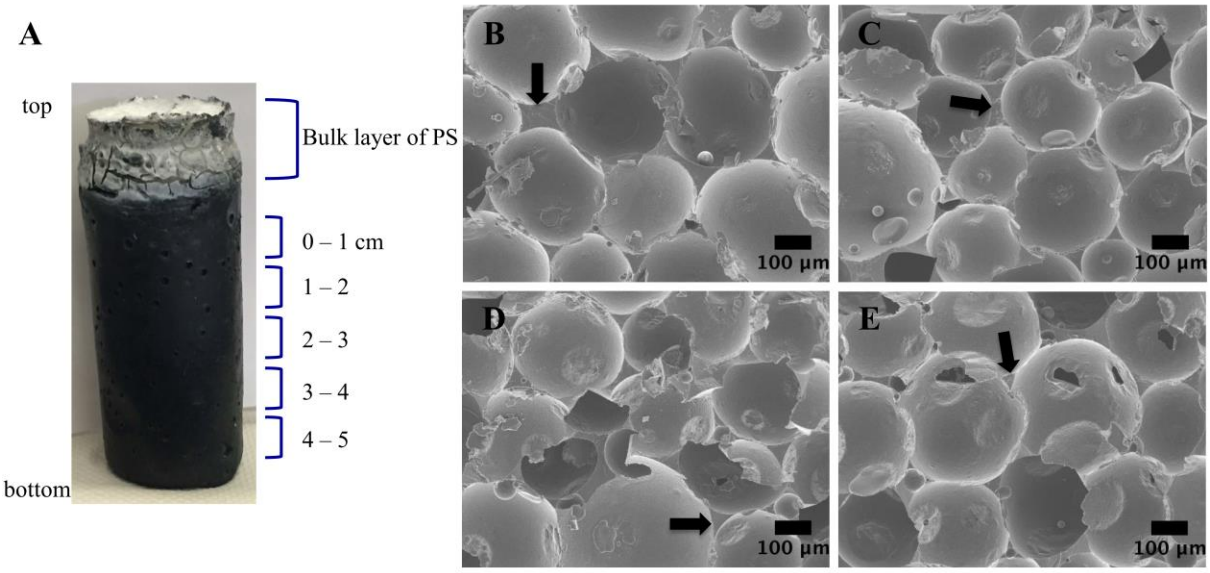

Figure 3-6. (A) Typical PS/G nanocomposite with a bulk layer of PS on top, illustrating from where the ~1 cm slices are taken for thermal and electrical measurements (B-E) Scanning electron microscopy (SEM) images of PS/G composite slices from a 70/30 (water/oil) emulsion with a theoretical 1.3 wt% of a 1 µm graphite (B) 0 – 1 cm, (C) 1 – 2 cm, (D) 2 – 3 cm, and (E) 3 – 4 cm slices.

The decrease in sphere size is confirmed by analyzing the SEM images from different positions within a 1.3 wt% graphite PS/G composite and is shown graphically in Figure 3-7. The average sphere size for the 0 – 1 cm layer is 334 µm. The 1 – 2 and 2 – 3 cm regions of the composite have similar sphere sizes of 304 and 312 µm, respectively, and in the 3 – 4 cm position the sphere size decreases to 270 µm. The change in relative graphene density with respect to position in the sample is determined by TGA, and in all cases is found to increase from top to bottom.

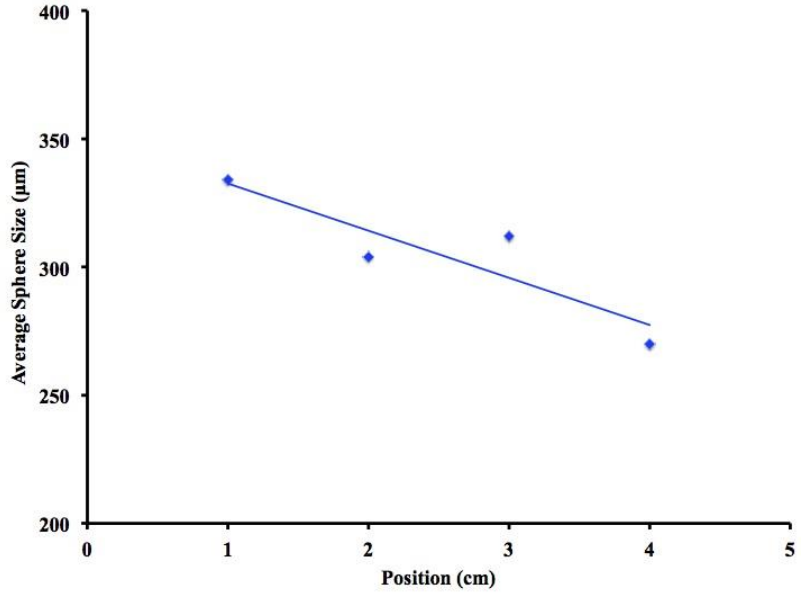

Figure 3-7. Average sphere size determined by Image J analysis from SEM images vs position in a theoretical 1.3 wt% PS/G. Line is used to guide the eye.

The effect of relative graphene content on the electrical conductivity of the composites is studied using a series of PS/G composites synthesized with increasing amounts of added graphite. The percent residue that remains after heating to 800 °C is used as the experimental wt% of graphene. This means that a composite with a 1.3 wt% theoretical loading can have a different experimental wt% of graphene that depends on how far from the top the sample was taken. In this way, the role of the graphene can be analyzed independently of the matrix.

The electrical conductivity of PS/G composites with four different theoretical weight percentages of graphite (1.3, 3.4, 6.9, and 14 %) is determined as described in Appendix A, Figure A-5, and the results are shown in Figure 3-8. Electrical conductivity normalized by sample mass is plotted as a function of experimentally determined graphene wt%. The weight percent of

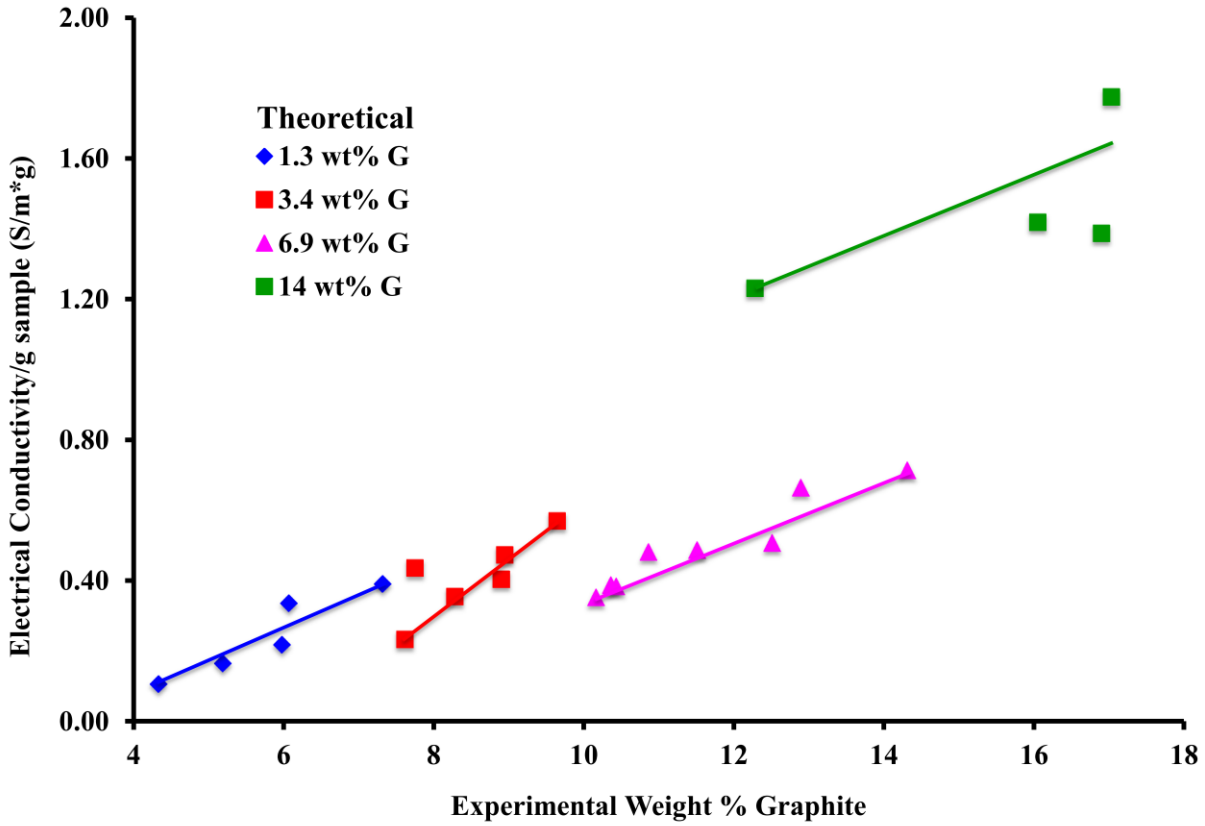

Figure 3-8. Electrical conductivity normalized by mass of sample plotted versus experimental weight percent of graphite determined by TGA for four PS/G composites of different theoretical weight percentages: 1.3 wt% (blue), 3.4 wt% (red), 6.9 wt% (pink), 14 wt% (green). Lines are to guide the eye.

graphite increases in tandem with normalized electrical conductivity moving from the top to bottom within a composite. It is found that the greater the mass of graphene relative to PS, the greater the electrical conductivity of the composite. One outlier in this study is the theoretical 14 wt% graphite sample. The addition of 14 wt% graphite creates an emulsion significantly more viscous than those at lower wt% and with little to no PS layer on the top. The experimental wt% of graphene thus more closely matches the theoretical value, as nearly all of the initial styrene is incorporated in the final composite. However, in all cases, the greater the wt% of graphite in the composite, the higher the electrical conductivity within each sample.

Thermal conductivity, however, is observed to be significantly different. The same samples that are used for electrical conductivity are used for thermal conductivity measurements, and can thus be directly compared. Shown in Figure 3-9 is the thermal conductivity of the same samples, normalized by the mass of each composite disc, as a function of experimental graphene wt%. For comparison, the thermal conductivity of a control PS disc, without any graphite, has a value of 0.144 W/mK (before normalization), which agrees well with the literature value of 0.15 W/mK.[28] When the thermal conductivity is normalized by the mass of the disc, as is done for the PS/G composite discs, its value is 0.0091 W/mK, approximately three times less than the PS/G composites.

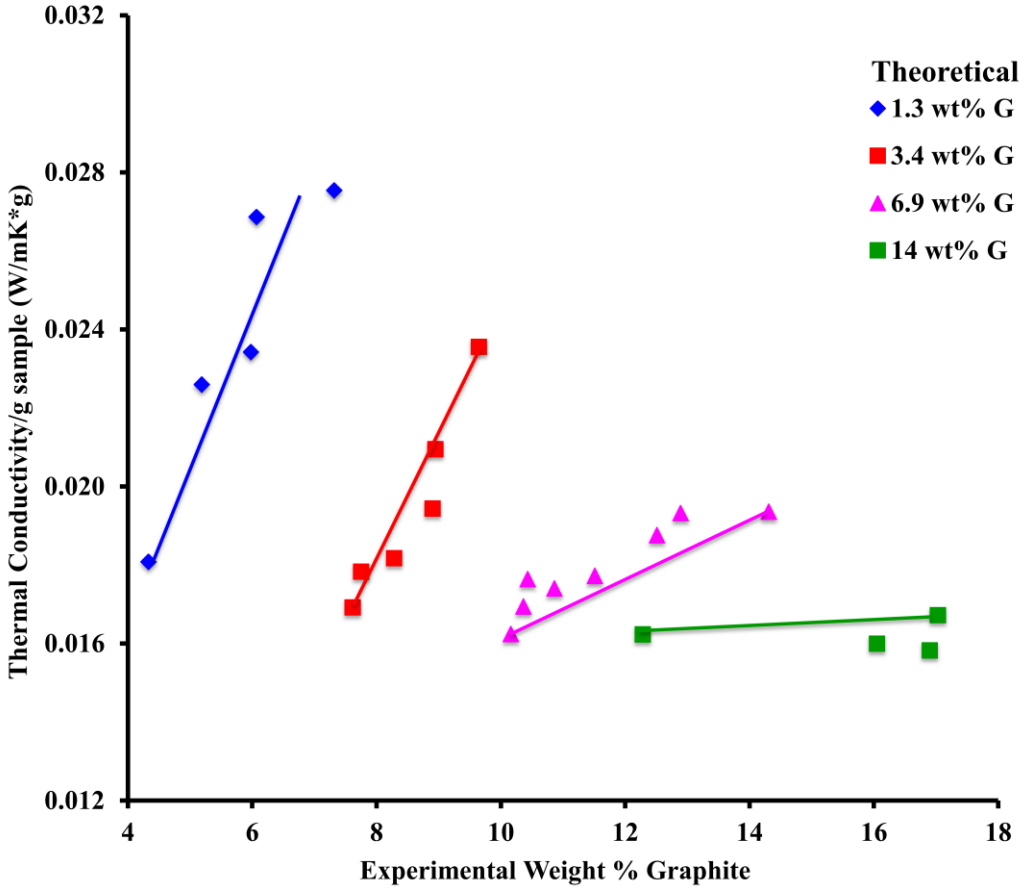

Figure 3-9. Thermal conductivity normalized by mass of sample plotted against experimental weight percent of graphite as determined by TGA for four PS/G composites of different

theoretical weight percentages: 1.3 wt% (blue), 3.4 wt% (red), 6.9 wt% (pink), 14 wt% (green). Lines are used to guide the eye.

In sharp contrast to electrical conductivity, as more graphite is added into the system (higher theoretical wt%), the normalized thermal conductivity decreases. As mentioned earlier, the graphitic "skin" surrounding the water droplets in the emulsion is a combination of overlapping exfoliated graphene sheets 1 to 4 layers thick, and unexfoliated graphite flakes. While an increase in the amount of added graphite leads to a decrease in the size of the water droplets as more surface area can be stabilized, there is a limit to how small the droplets can be due to the stiffness of the graphene sheets.[27] Once the high-energy oil/water interface has been stabilized, there is no driving force for exfoliation of the excess graphite. This excess graphite appears to increase the electrical conductivity of the composites to some degree, but has the opposite effect on thermal conductivity. Rather than acting as an additional route for conduction, it appears instead to act as a phonon scattering center, decreasing the thermal conductivity of the composite. Examining the thermal conductivity of the composites normalized by the mass of graphite, as seen in Appendix A, Figure A-4, shows that the addition of more graphite actually decreases the effectiveness of the graphite towards thermal conductivity. It is thus possible to increase the electrical conductivity of the composite while simultaneously decreasing the thermal conductivity, a unique feature of our composites and one that suggests exciting possibilities for their use in thermoelectric devices.

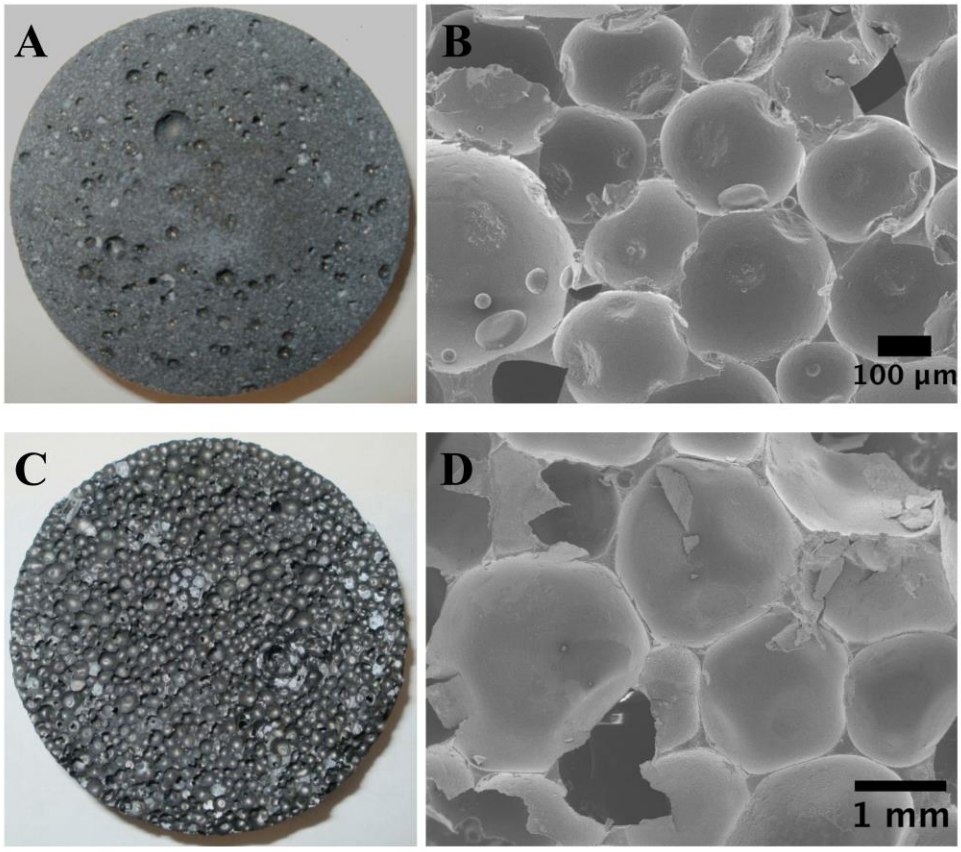

Figure 3-10. Images of a theoretical 1.3 wt% graphite PS/G nanocomposite using a 1 µm graphite flake size 1-2 cm from the top (A) macroscopically (diameter = 47 mm) (the large holes in the composite are due to coalescence) and (B) via SEM. Same weight percent of graphite in PS/G using a 10 µm graphite flake size (C) macroscopically (diameter = 43 mm) and (D) via SEM.

Adjusting the ratio of components, however, is only one approach to tailor the conductive properties of these composites. Changing the graphite flake size also affects sphere size and subsequently the electrical and thermal properties of the material. Shown in Figure 3-10 are images comparing composites made from 1 µm and 10 µm flake size graphite. A comparison of the average sphere size of each composite, as obtained from SEM images of samples taken from slices from the 1 – 2 cm region reveal that the average sphere size for the composite made with 1 µm graphite is 304 µm and with 10 µm graphite it is 1,770 µm. It is also shown that the size of

flakes not only affects the size of the spheres; it also has a significant effect on the conductive properties of the composites.

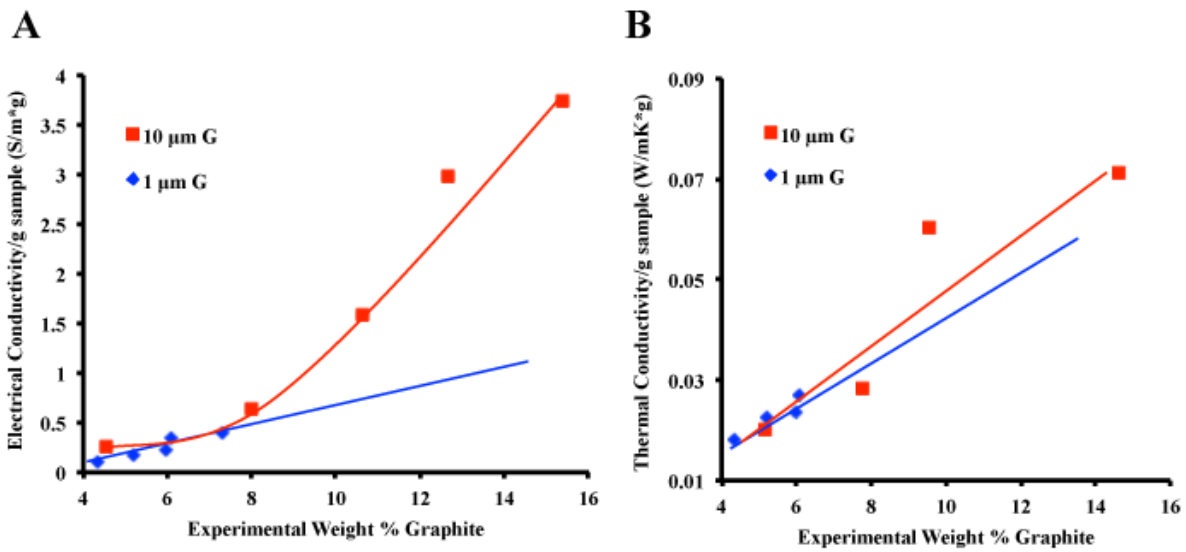

Figure 3-11. (A) Electrical conductivity normalized by mass of sample versus experimental weight percent of graphite determined by TGA for different flake sizes of graphite: 1 µm (blue), 10 µm (red) (B) Thermal conductivity normalized by mass of sample plotted versus experimental weight percent of graphite determined by TGA for different flake sizes of graphite: 1 µm (blue), 10 µm (red). Lines are to guide the eye.

The effect of the starting graphite flake size is studied in the same way as previously described for the study of graphite loading. Similar to the previous set of experiments, in which flake size was kept constant and the graphite loading was increased, electrical conductivity is normalized by the mass of the samples as shown in Figure 3-11A. The wt% of graphite, determined from TGA, increases going from the top of the composite to the bottom, as seen before. However, the volume of the emulsion phase is less in the case of the 10 µm graphite stabilized emulsions. Therefore, a smaller volume of composite results from polymerization of the oil phase, leading to the experimental wt% of the composite being greater. From Figure 3-11A, the rate of increase in electrical conductivity with increasing experimental wt% graphite

appears to be greater for the larger flake graphite composites, while Figure 3-11B shows the rate of increase in thermal conductivity with increasing experimental graphite wt% to be similar for the two flake sizes. The overall density of the materials also differs, as the density of composites made with 10 μm graphite decreases from 0.21 to 0.04 g/cm^3 from top to bottom while the 1 μm flake size material decreases from 0.22 to 0.15 g/cm^3. This overall decrease in density corresponds to a normalized increase in graphene wt%.

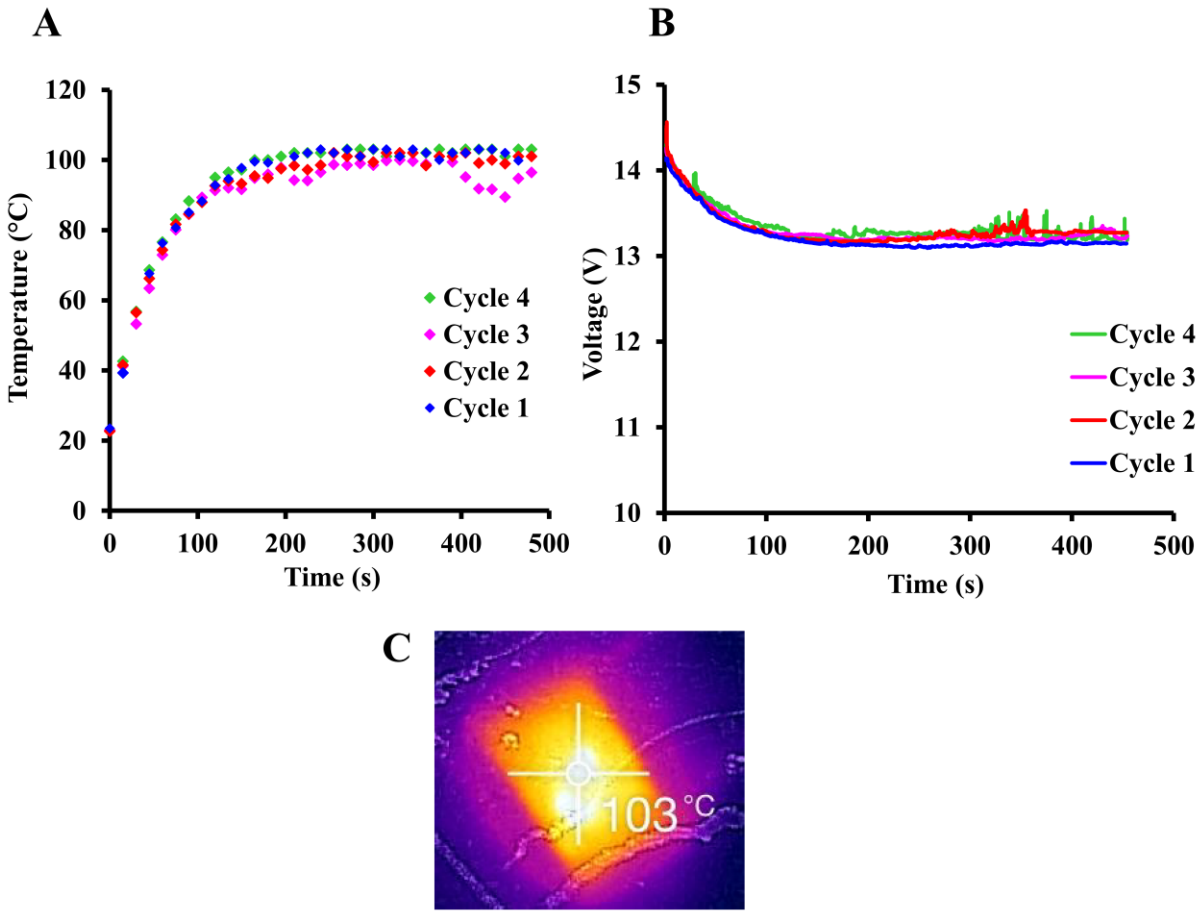

Figure 3-12. (A) Time verses temperature plot illustrating Joule Heating of a theoretical 6.9 wt% graphite PS/G composite reaching 100 °C (B) Voltage verse time measurements of four consecutive heating cycles (C) Thermal image of the PS/G composite undergoing Joule heating.

The presence of a percolating network of graphene also allows for Joule heating of the composites. As seen in Figure 3-12A, passing a 0.09 amp current through the material results in a steady temperature of ~100 °C. Higher currents and temperatures are limited by the polymer matrix, and increased currents can lead to the production of smoke as the polymer degrades. At 0.09 amps, however, heating and cooling cycles show little to no hysteresis, suggesting no degradation of the sample. In fact, as shown in Figure 3-12B, the potential required to produce a 0.09 amp current remains the same after four heating and cooling cycles, with the potential required to drive the current decreasing with increasing temperature. This suggests better contact between the conducting graphene sheets at higher temperature, possibly due to the increased mobility of PS allowing closer contact between sheets. Additionally, the heating of the composite appears to be fairly uniform, as shown in a thermal image seen in Figure 3-12C. There appears to be no high temperature regions next to the contacts, and no cool regions to suggest electrically isolated material.

3.3.1 Conclusion

Taking advantage of graphene's ability to act as a 2D surfactant in the stabilization of emulsions, inexpensive porous graphene nanocomposites have been developed that are thermally and electrically conducting. Polymerizing the continuous phase of graphene-stabilized water-in-oil emulsions leads to structured composite materials containing a percolating network of graphene sheets. This self-assembled network provides both electrical and thermal conduction pathways, as well as providing a route for increasing electrical conductivity while simultaneously decreasing thermal conductivity, a long sought after property for thermoelectric materials. In addition, the composites are shown to exhibit Joule heating, with multiple heating

and cooling cycles showing no hysteresis. These composites use pristine graphite, with no oxidation, reduction, sonication, high sheer mixing, added surfactants, high temperature treatment, or high boiling solvents required. Spreading at a high-energy liquid/liquid interface provides an approach to the large scale, inexpensive exfoliation of graphite and commercially viable composite foam materials. These foams are of interest for applications in filtration, porous electrodes, sensors, and thermoelectric materials.

3.3.2 References

(1) Balandin, A. A.; Ghosh, S.; Bao, W.; Calizo, I.; Teweldebrhan, D.; Miao, F.; Lau, C. N. *Nano Lett.* **2008**, *8*, 902–907.

(2) Stankovich, S.; Dikin, D. A.; Dommett, G. H. B.; Kohlhaas, K. M.; Zimney, E. J.; Stach, E. A.; Piner, R. D.; Nguyen, S. T.; Ruoff, R. S. *Nat. Lett.* **2006**, *442*, 282–286.

(3) Novoselov, K. S.; Geim, A. K.; Morozov, S. V.; Jiang, D.; Zhang, Y.; Dubonos, S. V.; Grigorieva, I. V.; Firsov, A. A. *Science (80-.).* **2004**, *306*, 666–669.

(4) Geim, A. K.; Novoselov, K. S. *Nat. Mater.* **2007**, *6*, 183–191.

(5) Castro Neto, A. H.; Guinea, F.; Peres, N. M. R.; Novoselov, K. S.; Geim, A. K. *Rev. Mod. Phys.* **2009**, *81*, 109–162.

(6) Lee, C.; Wei, X.; Kysar, J. W.; Hone, J. *Science (80-.).* **2008**, *321*, 385–388.

(7) Chatterjee, S.; Wang, J. W.; Kuo, W. S.; Tai, N. H.; Salzmann, C.; Li, W. L.; Hollertz, R.; Nuesch, F. A.; Chu, B. T. T. *Chem. Phys. Lett.* **2012**, *531*, 6–10.

(8) Barg, S.; Perez, F. M.; Ni, N.; do Vale Pereira, P.; Maher, R. C.; Garcia-Tuñon, E.; Eslava, S.; Agnoli, S.; Mattevi, C.; Saiz, E. *Nat Commun* **2014**, *5*.

(9) Stoller, M. D.; Park, S.; Zhu, Y.; An, J.; Ruoff, R. S. *Nano Lett.* **2008**, *8*, 3498–3502.

(10) Woltornist, S. J.; Oyer, A. J.; Carrillo, J.-M. Y.; Dobrynin, A. V.; Adamson, D. H. *ACS Nano* **2013**, *7*, 7062–7066.

(11) Woltornist, S. J.; Adamson, D. H. *Ind. Eng. Chem. Res.* **2016**, *55*, 6777–6782.

(12) Woltornist, S. J.; Alamer, F. A.; McDannald, A.; Jain, M.; Sotzing, G. A.; Adamson, D. H. *Carbon N. Y.* **2015**, *81*, 38–42.

(13) Kim, J.; Cote, L. J.; Kim, F.; Yuan, W.; Shull, K. R.; Huang, J. *J. Am. Chem. Soc.* **2010**, *132*, 8180–8186.

(14) Koerner, H.; Price, G.; Pearce, N. A.; Alexander, M.; Vaia, R. A. *Nat. Mater.* **2004**, *3*, 115–120.

(15) Menzel, R.; Barg, S.; Miranda, M.; Anthony, D. B.; Bawaked, S. M.; Mokhtar, M.; Al-Thabaiti, S. A.; Basahel, S. N.; Saiz, E.; Shaffer, M. S. P. *Adv. Funct. Mater.* **2015**, *25*, 28–35.

(16) Lee, J.; Stein, I. Y.; Kessler, S. S.; Wardle, B. L. *ACS Appl. Mater. Interfaces* **2015**, *7*, 8900–8905.

(17) Guzmán de Villoria, R.; Yamamoto, N.; Miravete, A.; Wardle, B. L. *Nanotechnology* **2011**, *22*, 1–7.

(18) Mas, B.; Fernández-Blázquez, J. P.; Duval, J.; Bunyan, H.; Vilatela, J. J. *Carbon N. Y.* **2013**, *63*, 523–529.

(19) Jang, H.-S.; Jeon, S. K.; Nahm, S. H. *Carbon N. Y.* **2011**, *49*, 111–116.

(20) Janas, D.; Koziol, K. K. *Carbon N. Y.* **2013**, *59*, 457–463.

(21) Kim, D.; Lee, H.-C.; Woo, J. Y.; Han, C.-S. *J. Phys. Chem. C* **2010**, *114*, 5817–5821.

(22) Zheng, Z.; Jin, J.; Xu, G.-K.; Zou, J.; Wais, U.; Beckett, A.; Heil, T.; Higgins, S.; Guan, L.; Wang, Y.; Shchukin, D. *ACS Nano* **2016**, *10*, 4695–4703.

(23) Li, C.; Xu, Y.-T.; Zhao, B.; Jiang, L.; Chen, S.-G.; Xu, J.-B.; Fu, X.-Z.; Sun, R.; Wong, C.-P. *J. Mater. Sci.* **2016**, *51*, 1043–1051.

(24) Kang, J.; Kim, H.; Kim, K. S.; Lee, S.-K.; Bae, S.; Ahn, J.-H.; Kim, Y.-J.; Choi, J.-B.; Hong, B. H. *Nano Lett.* **2011**, *11*, 5154–5158.

(25) Bae, J. J.; Lim, S. C.; Han, G. H.; Jo, Y. W.; Doung, D. L.; Kim, E. S.; Chae, S. J.; Huy, T. Q.; Van Luan, N.; Lee, Y. H. *Adv. Funct. Mater.* **2012**, *22*, 4819–4826.

(26) Leng, J.; Lan, X.; Liu, Y.; Du, S. *Smart Mater. Struct.* **2009**, *18*, 1–7.

(27) Woltornist, S. J.; Carrillo, J.-M. Y.; Xu, T. O.; Dobrynin, A. V.; Adamson, D. H. *Macromolecules* **2015**, *48*, 687–693.

(28) Yu, S.; Hing, P.; Hu, X. *Compos. Part A* **2002**, *33*, 289–292.

Chapter 4:
Tuning the sphere size of water-in-oil emulsions with pristine graphene as a 2D surfactant

Objective:

To study the droplet size in graphene-stabilized water-in-oil emulsions by acoustic spectrometry and to see how the size of the cells in the final nanocomposite compare via SEM analysis. The effect of the temperature on the emulsion stability is of interest. To look at adsorption of dye and oil with the polymer/graphene foams due to the ability to tune the pore size of the foam with different concentrations of graphite.

Section 1: Introduction

The use of amphiphilic surfactant stabilized emulsions as polymerization templates is well known.[1] After polymerization of the continuous phase, the dispersed phase is removed, yielding porous polymer foams with potential applications in filtration and catalyst supports. However, the functionality of these materials is limited to the functionality of the matrix polymer, with the surfactant contributing only to the porous morphology of the foam. If, instead of using an amphiphilic surfactant, two-dimensional graphene sheets are used to stabilize the templating emulsion, the cells of the resulting polymer foam are lined with graphene, offering the possibility of inexpensive and robust filters for the removal of oils and dyes with no further functionalization of the polymer foam required.

Emulsions are metastable dispersions of immiscible liquids[2–4] with a wide range of industrial applications in the food, cosmetics, pharmaceutical, and paint industries.[2,5] They are not thermodynamically stable, but can persist for some time due to kinetic stability provided by an emulsifier.[6] A common approach to choosing the proper emulsifier is based on the hydrophilic-lipophilic balance (HLB),[7,8] and if the right emulsifier is not used, the emulsion may be unstable. In contrast, graphene sheets are neither hydrophilic nor lipophilic, and their function as a surfactant is in part due to their being trapped at the liquid/liquid interface due to the energy cost associated with entering either phase.[9] As the graphite exfoliates, or spreads, at the high-energy liquid/liquid interface, the graphene sheets lower the free energy of the system, thus acting as a surfactant by surrounding each water droplet with a very thin layer of overlapping graphene sheets.

When the oil phase of the graphene stabilized water-in-oil emulsion is a monomer such as styrene, the continuous phase of the emulsion can be polymerized and lightweight, robust, electrically conductive, open-cell foams are created.[10,11] Where the droplets are in contact prior to polymerization, only a thin layer of graphene separates the dispersed phase. During drying, these regions are observed to tear, creating "windows" between the spheres through which water can pass and be removed from the foam. Also of importance is that the emulsions formed with graphene are water-in-oil rather than the oil-in-water emulsions formed with graphene oxide (GO) or reduced graphene oxide (rGO). Polymerizing the oil phase of oil-in-water emulsions leads to a powder rather than a porous polymer foam. In addition, the use of GO or rGO requires the oxidation and reduction of graphite, adding expense and complexity to the material synthesis. The synthesis of the pristine graphene based foam requires only graphite, monomer, water, initiator, and simple emulsification.

Of general interest in porous materials is the ability to control the pore size. In the case of our nanocomposite foam, this is directly related to controlling the size of the foam cells. We find one approach to this is to change the concentration of graphite in the emulsion. As stated earlier, filtration based on adsorbing contaminates on the graphene surfaces of the polymer foam is an exciting potential application for our material. Adsorption of synthetic dyes from wastewater is of interest due to the wide range of applications in the textile, paper, and food industries.[12] Approximately 7 x 10^5 tons of dye per year are produced, and adsorption is the most efficient method for dye removal.[13,14] Commercial activated carbon is a common adsorbent, however due to the high expense, researchers are looking for inexpensive materials for adsorption with similar efficiency as activated carbon.[15] Carbon nanotubes (CNTs) and CNT based composites have been studied for the removal of dyes from aqueous solutions, but CNTs are also expensive and have been known to have toxic effects.[16] Graphene-based derivatives such as graphene oxide (GO)[17] and reduced graphene oxide (rGO)[18,19] have been studied for dye removal, but these materials require expensive chemical or high temperature (~800 °C) treatments in order to oxidize and subsequently reduce the graphite to rGO. Our system does not require any prior treatment of the graphite, and thus promises a much more economically viable and environmentally friendly approach.

In this chapter, we investigate graphene-stabilized emulsions in terms of the effect of changing graphite concentration and temperature on the droplet size and stability of the emulsion. We also study the relationship between the emulsion droplet size observed by acoustic spectrometry and the size of the cells in the final polymer foam. Finally, we present preliminary results describing the use of these foams as filters for the removal of organic dyes and dispersed oil.

Section 2: Experimental

4.2.1 Formation of emulsions for acoustic spectrometry

The procedure to form a typical water-in-styrene emulsion was used as described elsewhere.[11] The following modifications have been made to the procedure. For all emulsions, regardless of the graphite concentration, a 7/3 water/styrene ratio was used. The appropriate amount of graphite (Asbury Graphite Mills, Inc. grade Nano 24 lot # 2148), 70 ml water (Deionized), 30 ml styrene (Sigma-Aldrich, ≥99%), 7.2 ml divinylbenzene (DVB) (Aldrich, 80%), and a magnetic stir bar were placed into a 125 ml jar. The capped jar was placed on a stir plate for 1 minute. The stir bar was removed and the jar shaken for 1 minute. The contents were then poured into a DT-1202 Acoustic and Electroacoustic Spectrometer (Dispersion Technologies Inc.) sample cell. For the calculated 1.3 wt% graphite water/styrene emulsions, a bulk layer of styrene occurred very quickly at the top layer of the emulsion after shaking the jar and was poured off first before pouring the emulsion into the sample chamber.

4.2.2 Synthesis of PS/G composites

Emulsions were made the same way as described above but the continuous phase was polymerized. In addition to the graphite, styrene (60 ml), Deionized water (140 ml), DVB (14.4 ml), and a magnetic stir bar, 180 mg of the initiator azobis(isobutyronitrile) (AIBN) (Aldrich, 98%), was added to a 240 ml jar, to synthesize a larger sample size for analysis. The capped jar was placed on a stir plate for 1 minute. The stir bar was removed and the jar shaken for 1 minute. All jars, regardless of the concentration of graphite in the emulsion, were placed into a

convection oven (Blue M, Stabil-Therm) at ~70 °C for 24 h to polymerize the styrene. After the reaction was complete, the rigid, water-filled composites were removed from the jars and returned to the ~70 °C oven for ~2-3 days to remove the water from inside the cells of the composite. If the composites had a bulk polystyrene layer on top (1.3 wt% graphite PS/G), it was cut from the composites. The remainder of the composite was used for analysis (SEM and batch test).

4.2.3 Methylene blue batch test

The ability of the polymer foam to adsorb methylene blue dye, chemical structure shown in Figure 4-1, (methylene blue trihydrate, Fisher) was tested by batch tests with calculated 1.3 and 6.9 wt% graphite PS/G composites along with a mass of graphite roughly equal to the mass of graphite contained in the composite samples as a control. A 100 mL solution of 10 $mg \cdot L^{-1}$ dye, and ~1.5 g of PS/G composite, crushed and sieved to 38 – 250 μm, was placed into a 250 mL plastic beaker with a magnetic stir bar. A stir rate of 500 rpm was used. Samples (4 mL) were removed from the dye solutions over a 16-hour time period and analyzed by UV-Vis spectroscopy (PerkinElmer Lambda 1050 UV/VIS/NIR Spectrometer) at a wavelength of 630 nm.

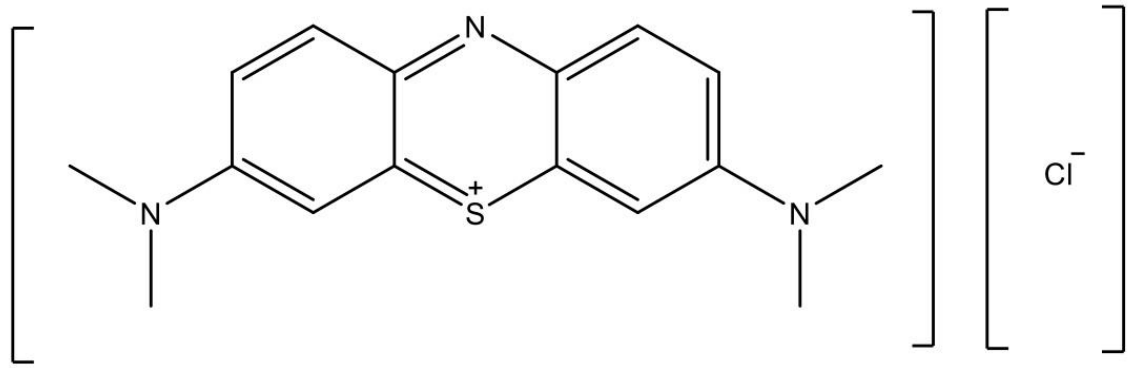

Figure 4-1. Chemical structure of the cationic dye, methylene blue.

4.2.4 Synthesis of PS/G composites in pipes

For filtration applications, the same procedure to create the PS/G foams as described above is used to synthesize the PS/G foams in metal pipes. For the calculated 1.3 wt% graphite emulsions, the Silverson laboratory mixer (Model L5M-A, Silverson Machines Inc.) was used for 1 minute after stirring on a stir plate for 1 minute. For higher concentrations of graphite (3.4 wt%), the jar was shaken after stirring on a stir plate for 1 minute. All were done in 125 ml jars. After the dispersions were either blended or shaken and a homogenous emulsion had formed, the jars were allowed to sit for 30 minutes. Some bulk layer of pure monomer, styrene, was removed using a pipet. This was to ensure that there was not a bulk layer present in the final pipes that would block the open-cell structure after polymerization. Stainless steel pipes with 4 inches in length and a ½ inch diameter (McMaster-Carr) were used, as shown in Figure 4-2 on the right. If aluminum pipes were used instead of stainless steel, the image on the left in Figure 4-2 was what occurred. The PS/G composite can be removed right out of the pipe.

Figure 4-2. PS/G composite after removal from an aluminum pipe with a U.S. penny for scale (left) PS/G composite adhered to wall in pipe (right).

The emulsion without any bulk monomer layer was poured into the pipes. Teflon tape was used to wrap around the outer threads of the pipe to easily remove the caps after polymerization. The bottom cap was sealed tightly in order to prevent the emulsion from leaking and the top cap was placed loosely on the top of the pipe, in order to prevent pressure from building up inside the pipes. The pipe was placed into a convection oven (Blue M, Stabil-Therm) at ~70 °C for 24 h. Figure 4-3 shows the process of making a typical 1.3 wt% graphite PS/G foam in a pipe.

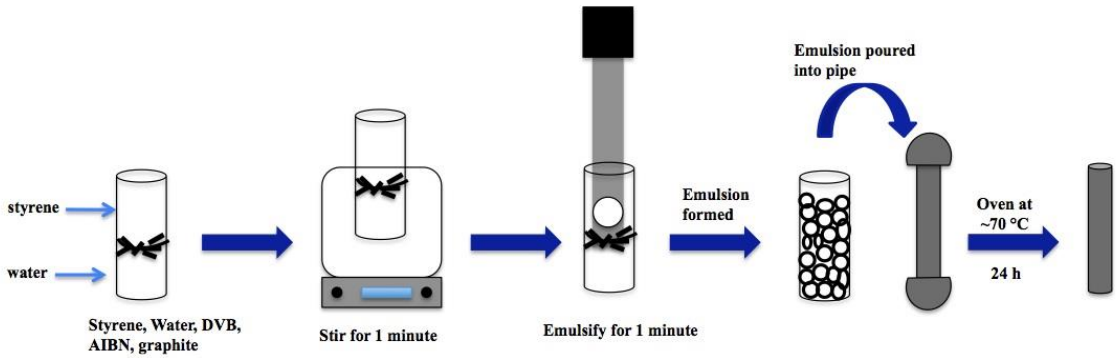

Figure 4-3. Schematic of emulsification and transfer of graphene-stabilized emulsion into pipes before polymerization of the styrene phase for a 1.3 wt% graphite emulsion.

The same method to prepare the water-in-styrene emulsions was used as above but plastic pipes were used instead of metal pipes. A calculated 1.3 wt% graphite loading was used. Plastic pipes were of interest for other applications and poly (vinyl chloride) (PVC) pipes (4 in length, ½ in diameter, McMaster-Carr) were first tried. There were different types of PVC such as dark grey and clear. Different loadings of initiator were tried, up to 4X the original initiator concentration with the dark grey PVC pipes. Light grey CPVC (4 in length, ½ in diameter, McMaster-Carr) was also tried. However, the PS/G composites were not successfully polymerized inside the plastic pipes and metal pipes were used throughout the remainder of our studies. We believe this is due to a plasticizer or additive that was leaching out of the pipe and quenching the reaction.

4.2.5 Acoustic spectrometry

Water-in-styrene emulsion samples were analyzed using a DT-1202 Acoustic and Electroacoustic Spectrometer (Dispersion Technologies Inc.), shown in an image in Figure 4-4. Attenuation spectra were analyzed with Dispersion Technology software for polydisperse emulsions.[20]

Figure 4-4. Image of acoustic spectrometer from Dispersion Technologies with an arrow indicating the sample chamber where the emulsion is poured.[21]

4.2.6 Scanning electron microscopy (SEM)

The composite samples from three samples with different graphite loadings were prepared by breaking off small pieces from the center of the composite with a razor blade. The pieces were then placed on aluminum stubs covered with carbon tape to adhere the sample to the stub. The stubs were coated with Au/Pd in a sputter coater (Polaron Unit E5100). The samples were characterized with a JEOL JSM-6335F FESEM using a 10 kV accelerating voltage. The acquired images were analyzed with Image J analysis software for the average sphere size and distribution. To account for the spheres in the composite not being completely cut in the center when making a sample for SEM, an equation was used to calculate the actual average sphere size. The average radius from Image J was multiplied by four and divided by π to calculate the radius.

4.2.7 Ultraviolet-visible (UV-Vis) spectroscopy

Samples from the batch test with PS/G composite and methylene blue dye are tested using a UV-Vis spectrometer (PerkinElmer Lambda 1050 UV/VIS/NIR Spectrometer) at a wavelength of 630 nm. The concentration of emulsified oil (petroleum oil, Sigma-Aldrich) exiting the PS/G foam in a metal pipe was monitored at 260 nm using UV-Vis spectroscopy.

4.2.8 Raman Spectroscopy

The PS/G composite samples were powdered using a mortar and pestle. The powdered sample was placed on a glass slide and flattened. A Raman run was then performed at 25% laser power due to the composites getting burnt. The laser wavelength was 514 nm. A 40% focus was used and multiple points along the sample were taken.

Section 3: Results & Discussion

The effects of graphite concentration and temperature are studied, with a combination of acoustic spectrometry and electron microscopy, to determine the correlation between the droplet size in the emulsion and the size of the cells in the final polymer foam. First looking at electron microscopy, Figure 4-5A shows a 1.3 wt% graphite PS/G composite, with an average sphere size of 312 μm. Figure 4-5B shows the 3.4 wt% graphite PS/G with an average sphere size of 171 μm. However, as the loading of graphite increases to 6.9 wt% graphite, as seen in Figure 4-5C, the sphere size distribution becomes less homogeneous and the amount of interstitial polystyrene in between the spheres decreases. The average sphere size for the 6.9 wt% graphite composite is 125 μm. The smaller sphere size corresponds to more interfacial area, and as more graphene is available in the system, the more liquid/liquid interface can be stabilized.

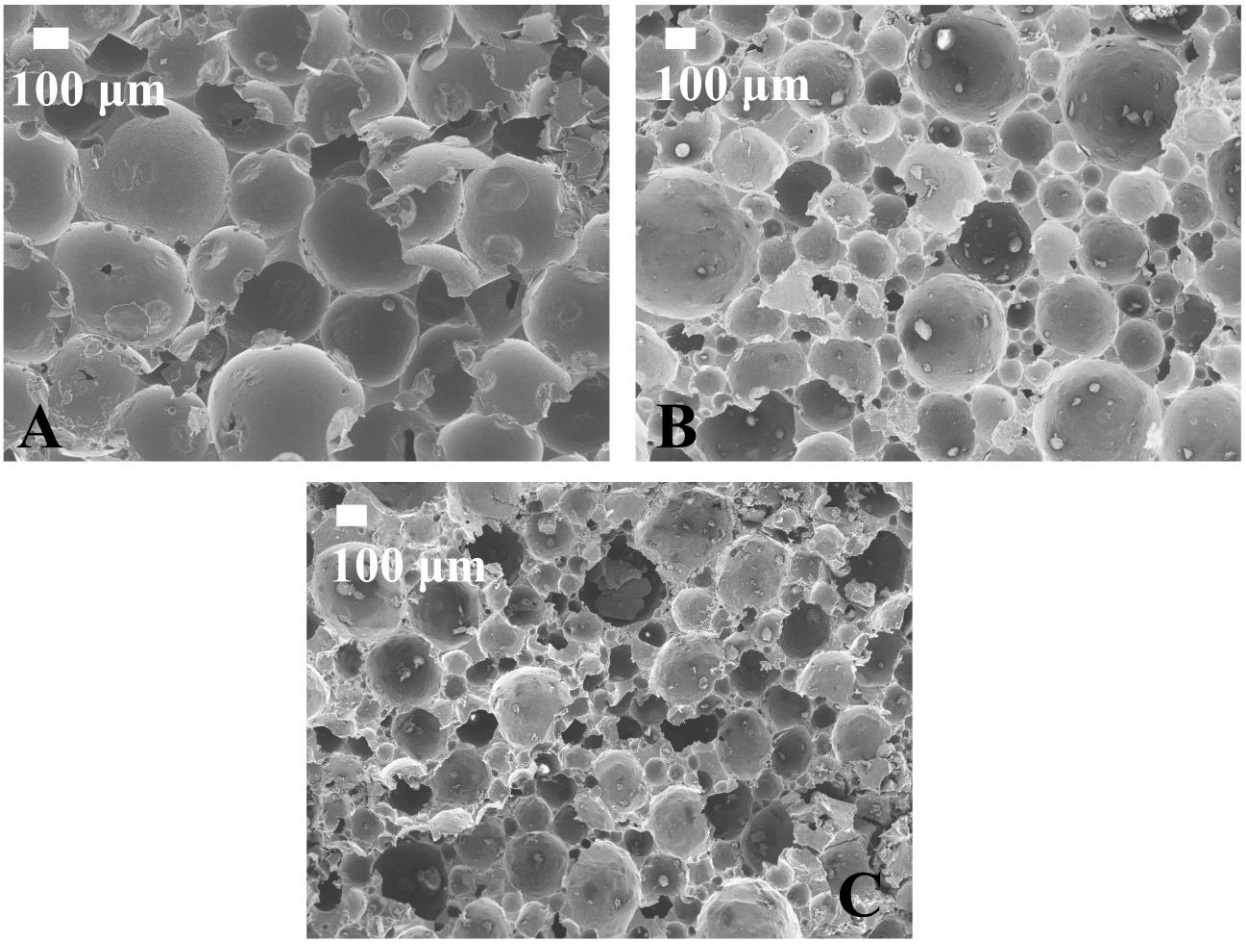

Figure 4-5. Scanning Electron Microscopy (SEM) images of three different theoretical graphite weight percentages in PS/G composites with (A) 1.3 wt% graphite, (B) 3.4 wt% graphite, and (C) 6.9 wt% graphite.

An unanswered question, however, is how the size of the droplets in the emulsion compares to the size of the cells after polymerization of the styrene. Light scattering based sizing techniques do not work with black samples such as these. Instead, we study the emulsions via acoustic spectrometry, using a DT-1202 Acoustic and Electroacoustic Spectrometer and analyzing the attenuation spectra with Dispersion Technology software for polydisperse emulsions.[20] Emulsions are made with varying graphite loadings and poured into the spectrometer sample cell. Emulsions made the same way are polymerized in order to directly compare with SEM images from solid samples.

Figure 4-6 shows the comparison between the droplet size determined by acoustic spectrometry and the cell size observed by SEM. The left side of Figure 4-6A shows the sphere size distribution of a 1.3 wt% graphite stabilized water-in-styrene emulsion determined by acoustic spectrometry. On the right, a histogram of the sphere size distribution of the 1.3 wt% graphite PS/G composite is shown. The average sphere size calculated from SEM analysis is 312 μm. This correlates well with the average sphere size of 337 μm determined by acoustic spectrometry. Both sphere size distributions, from acoustic and SEM, appear to be roughly symmetrical. It is important to note that the acoustic plots shown in Figure 4-6 are obtained after each emulsion reaches a steady size, typically requiring more than 9 h at RT. The sphere size after this time better matches the average sphere size of the final composite due to settling and possible coalescence that may take place in the oven before the polymerization of styrene occurs. Settling and packing of spheres, with monomer being pressed out from between the spheres, especially with the 1.3 wt% graphite emulsions, can lead to a layer of PS on the top of the polymer foam in some cases.

As the amount of graphite is increased to 3.4 wt%, the average sphere size by acoustic spectrometry, shown on the left in Figure 4-6B, decreases to 155 μm, with the histogram showing the average sphere size to be 171 μm as determined by SEM analysis. These two values correlate well, as do the sphere size distributions. Increasing the concentration of graphite to 6.9 wt% gives an average sphere size of 148 μm determined by acoustic measurements, shown in Figure 4-6C on the left. Again, the acoustic and SEM values match well, with an average sphere size of 125 μm from SEM, as does the sphere size distribution.

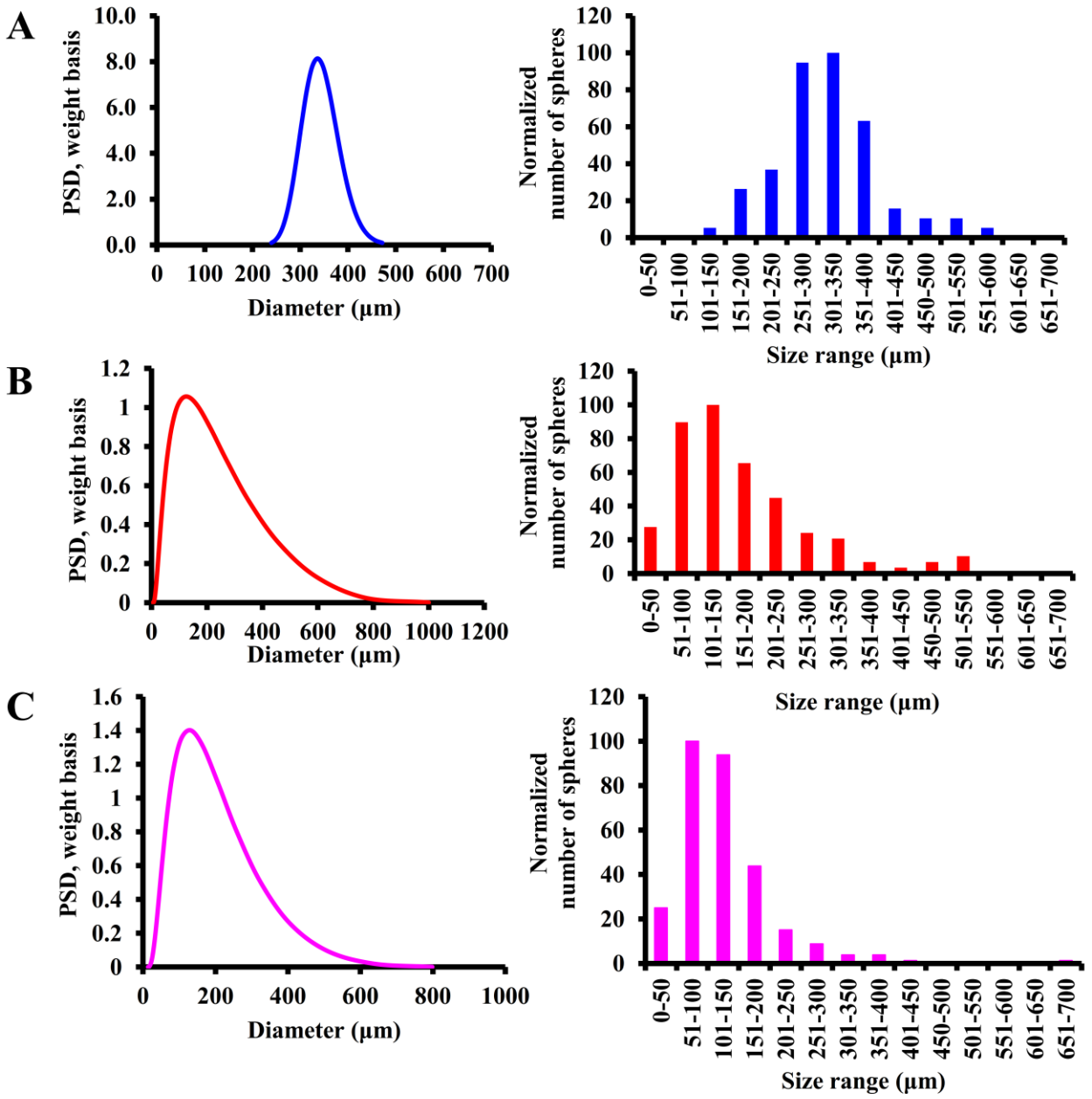

Figure 4-6. Sphere size distributions determined by acoustic spectrometry of water-in-styrene emulsions with different theoretical loadings of graphite paired with histograms of sphere size distributions from the final PS/G composites with (A) 1.3 wt% graphite, (B) 3.4 wt% graphite, (C) 6.9 wt% graphite.

Acoustic spectrometry also allows for the study of the emulsions over time. This is done both at room temperature and at 70 °C to observe the effect of temperature on the rate of coalescence. As an emulsion sample is heated to initiate polymerization, rate of settling, packing

of spheres, and coalescence may increase at the elevated temperature before the continuous phase polymerizes. To test this, two 3.4 wt% graphite emulsion samples are prepared as described previously, but with no initiator present. One sample is heated while the other is left at RT. As shown in Figure 4-7, the emulsion fractions at room temperature change very little in sphere size, from ~33 to 35 μm, during this time. However, heating the emulsions at 70 °C, caused the sphere size to increase from ~34 to 82 μm. The kinetics of coalescence are thus strongly influenced by temperature.

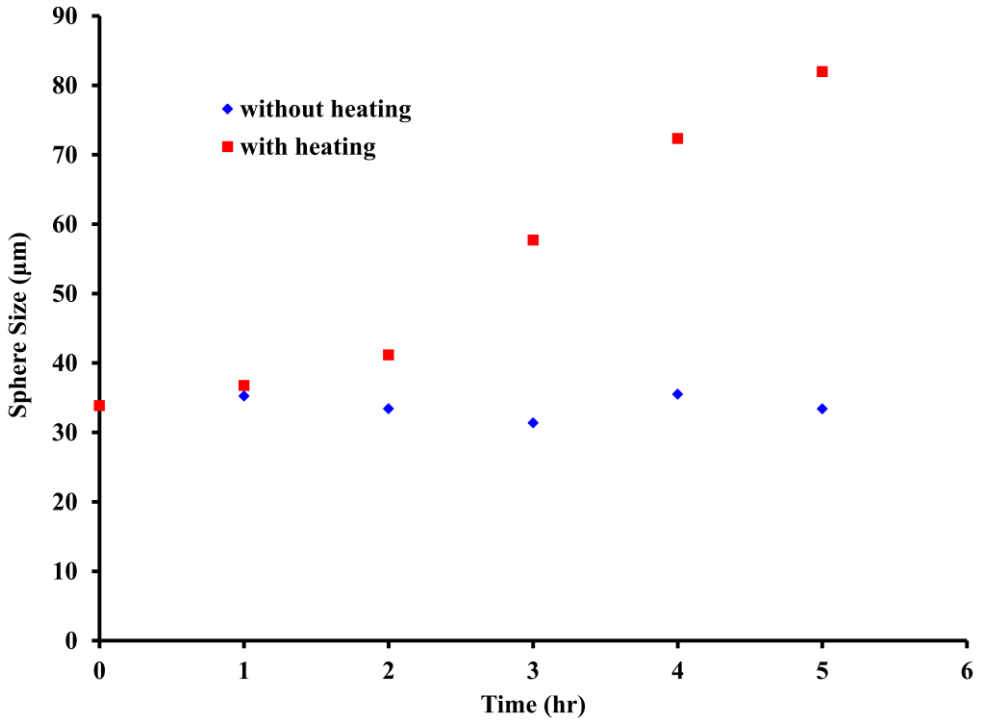

Figure 4-7. The effect of temperature on the rate of coalescence for a theoretical 3.4 wt% graphite water-in-styrene emulsion with an emulsion heated at 70 °C (red) and a control at room temperature (blue).

As our graphene based polymer foam composites are formed by polymerizing styrene in contact with the graphene at the liquid/liquid interface, it is possible that the graphene is coated

with a layer of polystyrene, limiting its adsorption potential. Comparing the three samples with different concentrations of graphite in a batch test study with methylene blue, as shown in Figure 4-8, shows the 6.9 wt% composite to be as effective in adsorbing the dye as is the neat graphite. This indicates that even if there is some PS covering the graphene sheets, the additional surface area afforded by exfoliation is enough to compensate. The lower adsorption by the 1.3 wt% material is important as well, as it demonstrates that graphene plays a role in the adsorption and it is not simply a matter of the dye adsorbing to the surface of a particle. If that were the case, there would be no difference expected between the two composite samples, as they were ground to the same particle size.

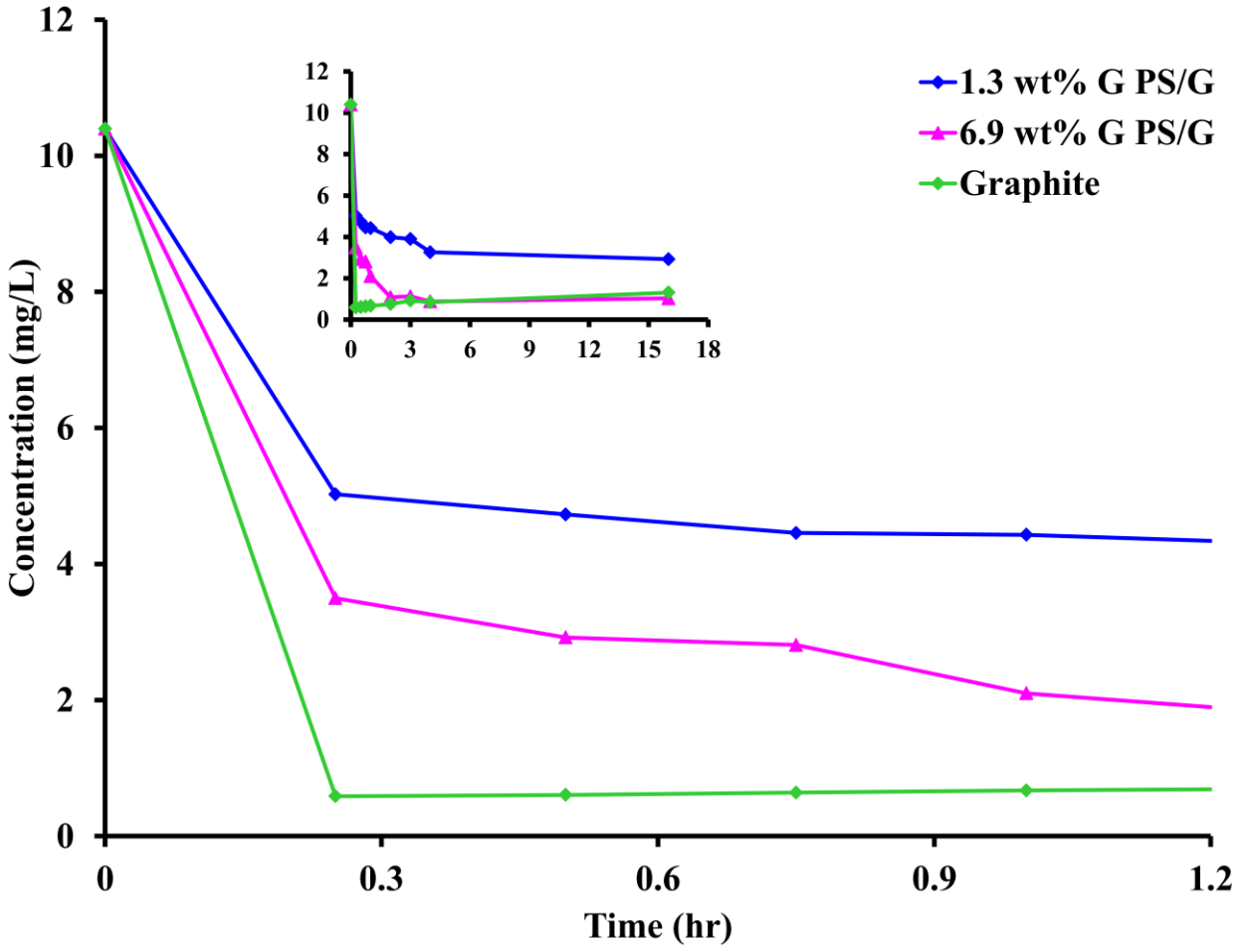

Figure 4-8. Adsorption of methylene blue dye verses time for a 1.3 wt% graphite foam (blue), 6.9 wt% graphite foam (pink), and a neat graphite control (green).

Preliminary results of using the polymer foams for filtration are shown in Figure 4-9. Filters are constructed by curing the emulsion in threaded stainless steel pipes, as previously described in the experimental section. Steel threaded caps fitted with tubing adaptors are then placed on both ends and the pipe containing the polymer foam connected to a syringe pump and a pressure gauge. An emulsion of oil in water is then flowed through the system at a rate of 50 $mL \cdot h^{-1}$. The backpressure for the 1.3 wt% filter rose from 2 psi to 6 psi during the trial, and rose from 12 psi to 19 psi for the 3.5 wt% sample. The concentration of oil exiting the filter is monitored by UV-Vis spectroscopy. The effect of graphite concentration in the filters is clear, with the 3.5 wt% polymer foam filter taking nearly 40 minutes before an increase in oil concentration is observed, as compared to the 1.3 wt% polymer foam filter showing an increase in oil concentration after only a few minutes. These results are important for several reasons. First, they demonstrate the potential of the material for the removal of dispersed oil from water. More than that, however, they demonstrate that the graphene in the composite plays a vital role in the filtration mechanism; otherwise the change in graphite concentration would have little to no effect.

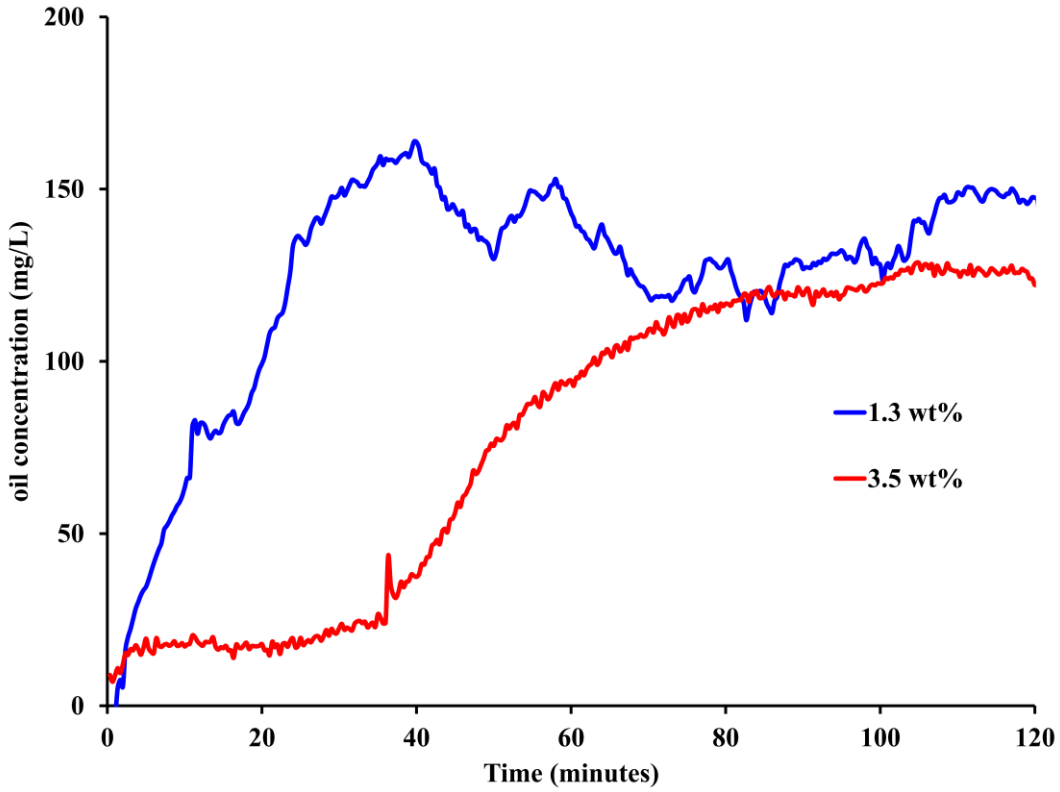

Figure 4-9. Plot of filtration of emulsified oil in water as a function of time. The blue line is filtration by a 1.3 wt% graphene polymer foam, and the red line is a 3.5 wt% foam. Saturation is seen to occur around 40 minutes for the 1.3 wt% sample, and after approximately 90 minutes for the 3.5 wt% sample.

4.3.1 Conclusion

In conclusion, pristine graphene based polymer nanocomposites are produced by an inexpensive and scalable interface trapping technique that results in the thermodynamically driven exfoliation of pristine graphite to stabilize water-in-oil emulsions. Polymerizing the continuous phase of the graphene stabilized emulsion produces polymer foam materials with graphene-lined cells of tunable size. The correlation of emulsion droplet size as measured with acoustic spectrometry is shown to correlate closely with the size of the foam cells as determined

by SEM. The coalescence of the emulsions is studied as a function of temperature, and the application of the foam as a filter is demonstrated. The ease of production and the low cost of the starting materials suggest these foams can be produced with a cost similar to styrene foam, suggesting they may play an import role in future filtration applications.

4.3.2 References

(1) Cameron, N. R. *Polymer (Guildf).* **2005**, *46*, 1439–1449.

(2) Bibette, J.; Calderon, F. L.; Poulin, P. *Rep. Prog. Phys.* **1999**, *62*, 969–1033.

(3) Thomas, A. W. *J. Ind. Eng. Chem.* **1920**, *12*, 177–181.

(4) Madaan, V.; Chanana, A.; Kataria, M. K.; Bilandi, A. *Int. Res. J. Pharm.* **2014**, *5*, 533–542.

(5) Tadros, T. F. In *Emulsion Formation and Stability*; Wiley-VCH Verlag GmbH & Co. KGaA: Weinheim, Germany, 2013; pp 1–75.

(6) Dickinson, E. *Food Hydrocoll.* **2003**, *17*, 25–39.

(7) Bos, M. A.; Vliet, T. van. *Adv. Colloid Interface Sci.* **2001**, *91*, 437–471.

(8) Myers, D. *Surfactant Science and Technology*, 3rd ed.; 2006.

(9) Woltornist, S. J.; Oyer, A. J.; Carrillo, J.-M. Y.; Dobrynin, A. V; Adamson, D. H. *ACS Nano* **2013**, *7*, 7062–7066.

(10) Woltornist, S. J.; Carrillo, J.-M. Y.; Xu, T. O.; Dobrynin, A. V.; Adamson, D. H. *Macromolecules* **2015**, *48*, 687–693.

(11) Woltornist, S. J.; Adamson, D. H. *Ind. Eng. Chem. Res.* **2016**, *55*, 6777–6782.

(12) Forgacs, E.; Cserháti, T.; Oros, G. *Environ. Int.* **2004**, *30*, 953–971.

(13) Kannan, N.; Sundaram, M. M. *Dye. Pigment.* **2001**, *51*, 25–40.

(14) Rafatullah, M.; Sulaiman, O.; Hashim, R.; Ahmad, A. *J. Hazard. Mater.* **2010**, *177*, 70–80.

(15) Crini, G. *Bioresour. Technol.* **2006**, *97*, 1061–1085.

(16) Gupta, V. K.; Kumar, R.; Nayak, A.; Saleh, T. A.; Barakat, M. A. *Adv. Colloid Interface Sci.* **2013**, *193-194*, 24–34.

(17) Yang, S.-T.; Chen, S.; Chang, Y.; Cao, A.; Liu, Y.; Wang, H. *J. Colloid Interface Sci.* **2011**, *359*, 24–29.

(18) Liu, T.; Li, Y.; Du, Q.; Sun, J.; Jiao, Y.; Yang, G.; Wang, Z.; Xia, Y.; Zhang, W.; Wang, K.; Zhu, H.; Wu, D. *Colloids Surfaces B Biointerfaces* **2012**, *90*, 197–203.

(19) Ramesha, G. K.; Vijaya Kumara, A.; Muralidhara, H. B.; Sampath, S. *J. Colloid Interface Sci.* **2011**, *361*, 270–277.

(20) Dukhin, A. S.; Goetz, P. J. *Characterization of Liquids, Nano-and Microparticulates, and Porous Bodies Using Ultrasound*; Elsevier: Oxford UK, 2010.

(21) Dispersion Technologies, Inc. http://www.dispersion.com/model-dt-1202_ (accessed Aug 10, 2016).

Chapter 5:
Improved synthesis of
Poly (ethylene oxide)

Objective:

To study the novel synthesis of poly(ethylene oxide) homopolymers and block copolymers that was developed in our lab, driven by the equilibrium between an alcohol/KOH and

alkoxide/water, as a potential post-polymerization modification method for the porous, hydrophobic polymer/graphene nanocomposites.

Section 1: Introduction

5.1.1 Amphiphilic block copolymers and their applications

Amphiphilic block copolymers are made up of hydrophobic and hydrophilic segments which assemble in aqueous media into polymeric micelles with a size range of 10 – 100 nm.[1,2] The formation of micelles from amphiphilic diblock copolymers is shown in Figure 5-1. This process is thermodynamically favored above the critical micelle concentration or CMC.[3,4,2] Below the CMC, only single chains are present.[5] Polymeric micelles are of interest for applications such as drug delivery systems.[6,7]

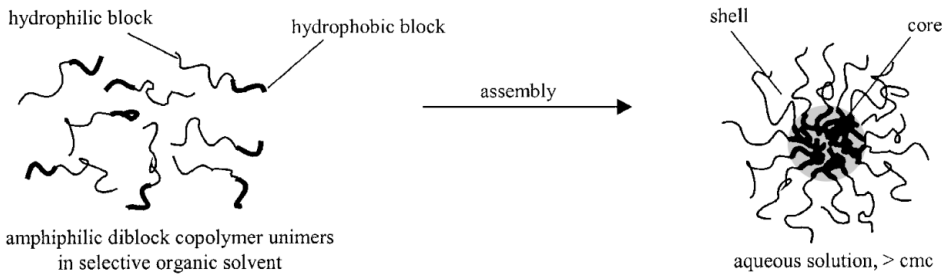

Figure 5-1. Micellization process for an amphiphilic diblock copolymer.[8]

There are some common hydrophobic blocks in amphiphilic block copolymers used in drug delivery applications. The hydrophobic segments consist of poly(ester)[9], such as poly (lactic

acid) (PLA)[4] or poly(propylene oxide) (PPO)[10]. The most widely used hydrophilic segment is poly (ethylene oxide) (PEO) or poly(ethylene glycol) (PEG).[8] PEO or PEG, is a water soluble,[11] nonionic semi-crystalline polymer[12] that is biocompatible,[13] nontoxic,[14] and chemically stable.[13] Due to PEO's ability to inhibit the adhesion of proteins, polymers containing PEO have a range of applications that include polymeric surfactants,[15] emulsifiers,[16] drug carriers,[17-21] and anti-fouling coatings for medical implants[22,23] and ship hulls.[24] The synthesis of these materials, however, requires the use of moisture sensitive, pyrophoric organometallics in order to convert hydroxyl functional groups to the metal alkoxides required for the polymerization of ethylene oxide (EO). In this chapter we introduce a new mechanism for the formation of the necessary alkoxides from alcohols and hydroxyl functionalized polymers: the use of azeotropic distillation to remove water from the equilibrium between alcohol/KOH and alkoxide/water, as illustrated in Figure 5-2. This approach uses KOH as the source for potassium cations, avoiding the use of moisture sensitive reagents that often need to be synthesized immediately prior to use. We have been developing methods to make our hydrophobic polymer/graphene foams more hydrophilic. One technique that could be used is this azeotropic method for growth of PEO for post polymerization modification of porous materials, such as our polymer/graphene nanocomposites that were studied in Chapters 1-4, to make them more hydrophilic for other applications, including filtration.

5.1.2 Anionic Ring Opening Polymerization (ROP)

Industrially, PEO homopolymers are synthesized at high temperatures and pressures (100-200 °C and 520 kPa) by adding ethylene oxide (EO) to an alcoholic aqueous solution containing a caustic.[25] For lab scale synthesis, the anionic ring-opening polymerization (ROP) of

EO is typically employed, with the initiator being a potassium alkoxide.[13,26] Potassium, rather than lithium, is normally used due to the strong association between the lithium cation and the propagating oxygen anion[27,28,29] that results in tight ion pairs and little to no chain propagation.[27,28] This inability of lithium cations to propagate the growth of PEO means that adding EO to a anion with a lithium counter ion results in only one monomer unit being added to the chain. This is a useful approach to form hydroxyl terminated polymers, and is often used as a route to the hydroxyl terminated polymers from which PEO is subsequently grown.

5.1.3 Previous methods of synthesizing Poly (ethylene oxide)

The synthesis of PEO polymers typically begins by reacting a hydroxyl group with an alkyl or aromatic potassium organometallic to form a potassium alkoxide. The compounds most frequently used are cumylpotassium,[30,31] diphenylmethyl potassium (DPMK),[32-34] benzyl potassium,[11,35,36] α-phenyl ethyl potassium,[37] and potassium naphthalenide.[16,38] Examples include work by Allgaier *et al.*, where cumylpotassium was added to hydroxyl terminated polymers to initiate the polymerization of EO to form poly[1,4-isoprene-*b*-(ethylene oxide)] (PI-PEO) and poly[ethylene-*co*-propylene-*b*-(ethylene oxide)] (PEP-PEO) block copolymers.[30] As is common for such potassium reagents, the cumylpotassium had to be synthesized and used within a short period of time.[30] Castle *et al.* synthesized block copolymers containing norbornene derived polymer blocks with a PEO block using DPMK,[33] and as is often the case, PEO homopolymer was found as an impurity in the synthesized poly(styrene)comb-*b*-poly(ethylene oxide)combs.[32] Benzyl potassium has also been used for the polymerization of EO in the synthesis of PEO homopolymers, polystyrene-*b*-poly(ethylene oxide) (PS-*b*-PEO), and for PI-*b*-P2VP-*b*-PEO copolymers.[11] α-Phenyl ethyl potassium has been used to synthesize PS-*b*-PEO and PS-*b*-PEO-*b*-

PS copolymers[37] with high conversion of EO (95%), but purification of the final product was necessary to remove PS and PEO homopolymers. Lastly, potassium naphthalide has been used in the synthesis of polyolefin-PEO block copolymers[16] by forming the potassium alkoxide of hydrogenated polydienes containing hydroxyl end groups. Although this is far from a complete review of PEO block copolymer synthesis, these investigations are representative of the typical current approaches.

Other, much less common approaches have also been employed. Potassium methoxide was used to synthesize PS-*b*-PEO block copolymers,[39] requiring a reaction time of 11 days, heating gradually from 30 °C to 70 °C for 7 days, followed by holding the reaction at 70 °C for another 4 days followed by the removal of PS and PEO homopolymers. Potassium metal has also been used directly to create potassium alkoxide initiators. In one example, potassium metal was added piecewise to a reaction mixture containing dimethylaminoethanol to form the potassium alkoxide.[40] The addition of ethylene oxide was then followed by butylene oxide to produce a copolymer after 20 days. Another example of using potassium metal is the use of a potassium mirror to synthesize PS-*b*-PEO copolymers from hydroxyl terminated PS.[41]

Methods for growing PEO that do not involve potassium have been reported, but they are the exception. One route to PEO containing block copolymers allows for the use of lithium as a counterion by adding a phosphazene base.[28,42] The phosphazene base complexes with the lithium counterion and allows for the propagation of EO. Polybutadiene-PEO (PBd-PEO) and PI-PEO block copolymers have been synthesized using this approach.[28] Another route used a lithium alkoxide with small amounts of a potassium alkoxide in a benzene/DMSO mixture. PEO homopolymer was found in the final block copolymer product, but other alkoxides, such as potassium 2,6-di-t-butylphenoxide, produced less PEO homopolymer.[43] Finally, to avoid the

presence of potassium in the final material, an N-heterocyclic carbene was used to initiate EO polymerization, followed by the sequential polymerization of ε-caprolactone.[13]

5.1.4 Our Method: Azeotropic Distillation

Figure 5-2. Equilibrium responsible for forming potassium alkoxide initiator. The removal of water drives the equilibrium to the right.

A common theme in nearly all of these methods is the conversion of an alcohol to a metal alkoxide by way of a reactive organometallic. In our approach, rather than adding a reactive and air sensitive pyrophoric compound to form the necessary potassium alkoxide, we add potassium hydroxide without any need for moisture-free conditions or prior synthesis of the organometallic. Additionally, at the end of the reaction, there are no compounds, such as naphthalene, that must be removed. The equilibrium between alcoholic potassium hydroxide and a potassium alkoxide, as shown in Figure 5-2, generally favors the reactants. By Le Chatelier's principle, removal of the water from the right hand side drives the equilibrium towards the potassium alkoxide, eliminating the need for the addition of organometallic reagents or potassium metal. A typical reaction starts by dissolving the hydroxyl-containing molecule in toluene and adding a stoichiometric amount of KOH dissolved in methanol. The toluene is then partially distilled off, observing the boiling temperature of the toluene. Initially, the boiling temperature is far lower than the standard boiling temperature for toluene, as first the methanol, then the water in the form of an azeotrope with toluene, are removed. Once all the water in the system is removed, the boiling temperature reaches its literature value. After complete removal of the water, dry THF is

added to provide a polar solvent for chain propagation, followed by the addition of the EO monomer. As examples of this approach we discuss: growing PEO off small molecular weight alcohols, extending the chain length of a PEO homopolymer, and synthesizing a block copolymer of polystyrene and PEO (PS-*b*-PEO) from a hydroxyl terminated PS.

Section 2: Experimental

5.2.1 Synthesis of Macroinitiators

The synthesis of polystyrene endcapped with a hydroxyl group (PS-OH) was performed in a glove box. The solvent, cyclohexane, was previously dried over *sec*-butyllithium and 1,1-diphenylethylene on a vacuum line. Cyclohexane was then distilled into a vacuum flask and brought into the glove box. The initiator, *sec*-butyllithium, was then added to the dried cyclohexane. Styrene was added and the reaction allowed to stir overnight at room temperature.

The color of the solution turned deep orange. Excess ethylene oxide was then added and the color of the solution faded. The vacuum flask was removed from the glove box and degassed methanol was added to terminate the reaction. The cloudy solution was allowed to stand overnight. The polymer solution was filtered, followed by precipitation in excess methanol. The resulting solid was dried under vacuum for several days. GPC and ^{1}H NMR were used to characterize the molecular weight and polydispersity of the polymer. PEO homopolymer (2 kg/mol) and 1-octanol were used as received.

5.2.2 Method 1: Vacuum Distillation

The polymerization of PEO was performed by the following general procedure that varied slightly depending on the starting alcohol. For the hydroxyl endcapped PS, the polymer (3 g, 1.15 mmol) was placed in a 500 ml round-bottom vacuum flask equipped with a magnetic stir bar and a high vacuum Teflon valve. To this was added approximately 50 ml of DMSO and 300 ml toluene. Next, an equimolar amount of KOH was added. The reaction flask was attached to a vacuum line and the toluene slowly removed by vacuum distillation. After the toluene was removed, degassed THF dried over sodium/benzophenone was added by vacuum distillation, followed by the addition of ethylene oxide (1.7 ml, 34 mmol) by way of vacuum distillation.

The flask was then removed from the line under vacuum by closing the Teflon stopcock and placed in an oil bath. The reaction mixture was heated to 60 $^{\circ}$C for 5-7 days, then quenched with degassed methanol. The polymer solution was filtered and then precipitated by pouring into cold diethyl ether. The solid was collected and placed in a vacuum oven at ambient temperature to dry. GPC and ^{1}H NMR were used to characterize the molecular weight and polydispersity of the

PEO polymers. The PEO extension reaction was performed with benzene as an initial solvent instead of toluene. Toluene was used as the initial solvent for all other polymerizations.

5.2.3 Method 2: Atmospheric Pressure Distillation

A second method to synthesize PEO with a Dean-Stark apparatus was used to perform the azeotropic distillation. For a typical synthesis, a 1L vacuum flask, equipped with a stir bar, approximately 300 ml toluene, 50 ml of DMSO, and an equimolar amount of 0.1 N KOH in methanol and 1-octanol (0.111 ml, 0.7064 mmol) were added. The Dean-Stark apparatus was equipped with a ground-glass joint thermometer and a water-cooled condenser. The vacuum flask was placed in an oil bath on a hot/stir plate and then connected to the Dean-Stark apparatus, leaving the Teflon valve open. The reaction mixture was distilled, with the end point determined by monitoring the temperature of the vapor. Once the water was removed, the Teflon valve was closed as the heat was removed. The reaction flask was allowed to cool to room temperature, fixed to a vacuum line and approximately 200 ml of dry THF was distilled into the flask. Further reaction steps then proceeded as in Method 1.

5.2.4 Gel permeation chromatography (GPC)

Gel permeation chromatography (GPC) was used to determine the molecular weight and polydispersity of the PEO polymers. A Waters GPC-1, 1515 HPLC Pump and Waters 717Plus Autoinjector was used. The instrument contains Jordi Gel fluorinated DVB columns (1-100,000, 2-10,000, 1-500Å) and a Varian 380-LC Evaporative Light Scattering Detector (ELSD). THF

was used as the mobile phase. Empower 1, Waters software, was used to run the samples and analyze the data.

5.2.5 Nuclear magnetic resonance (NMR) spectroscopy

Proton NMR was obtained on a Bruker DMX 500MHz High Resolution Nuclear Magnetic Resonance (NMR) Spectrometer with Bruker Topspin 1.3 software. MestReNova software was utilized to analyze the spectra.

Section 3: Results & Discussion

5.3.1 PEO homopolymer

5.3.1.1 1-octanol

The equilibrium between alcoholic potassium hydroxide and potassium alkoxide, as shown in Figure 5-2, lies far to the left. By Le Chatelier's principle, removal of the water from the right hand side drives the equilibrium towards the alkoxide. Toluene is our solvent of choice, as it forms an azeotrope with both water and methanol, solubilizes a variety of polymers, has a reasonably low boiling temperature, and has fewer health and environmental concerns than benzene. The binary positive azeotrope between methanol and toluene distills at 63.8 °C, with the vapor containing a 0.883 mole fraction of methanol, or 72.4 wt% methanol. The azeotrope with methanol is convenient, as we typically add the KOH by way of a 0.1 N standard solution of KOH in methanol. The positive binary azeotrope between water and toluene distills at 84.1 °C, with the vapor containing a 0.444 mole fraction of water, or 13.5 wt% water.[44] The differences between the boiling temperature of the azeotropes and of pure toluene (110.6 °C) are large enough to clearly distinguish them during the distillation.

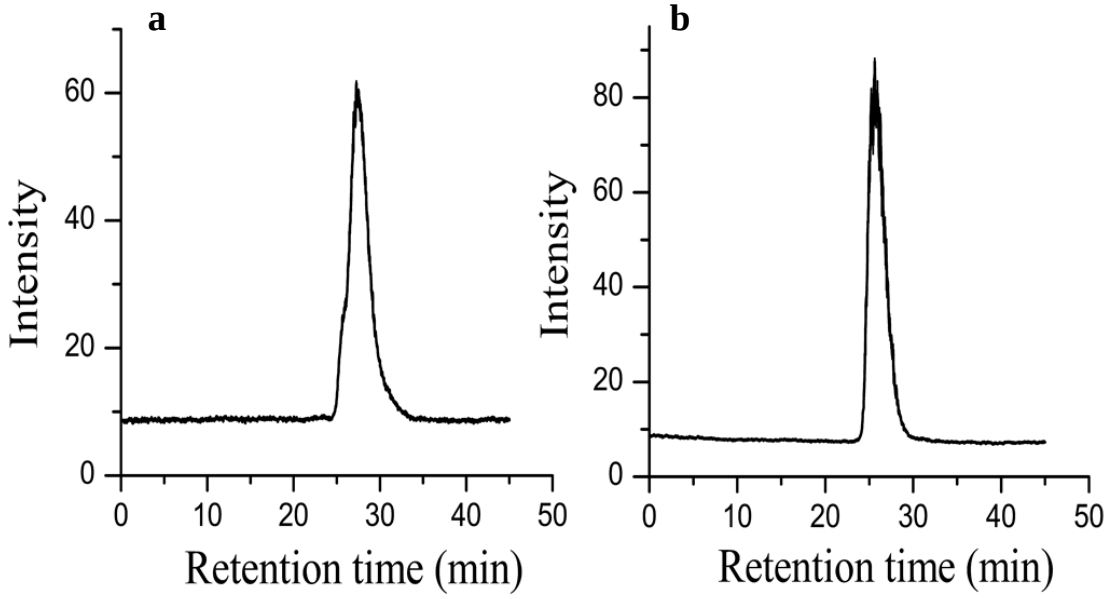

Figure 5-3. (a) GPC trace of PEO homopolymer from 1-octanol initiator with DMSO (b) GPC trace of PEO homopolymer from 1-octanol without DMSO.

To demonstrate the growth of PEO from a small molecular weight alcohol, we use 1-octanol, an alcohol with sufficiently low vapor pressure to remain in solution while the water is removed by azeotropic distillation with the toluene co-solvent. A PEO polymer with a target MW of 10 kg/mol is synthesized in a solution of toluene and THF, both with and without DMSO. The use of DMSO as a co-solvent is studied based on literature reports that it aids in the polymerization of EO.[43] During the reaction, the mixture with DMSO turned yellow once the alkoxide had formed, indicating an anion was present. The reaction mixture in the absence of DMSO remained clear.

The PEO homopolymer thus synthesized from 1-octanol is analyzed with ^{1}H NMR and GPC. The polydispersity index (PDI) determined by GPC for the polymer made with DMSO present is 1.21, while without DMSO the PDI is 1.19. The GPC chromatograms of the PEO homopolymers from 1-octanol with and without DMSO are shown in Figure 5-3(a) and 5-3(b).

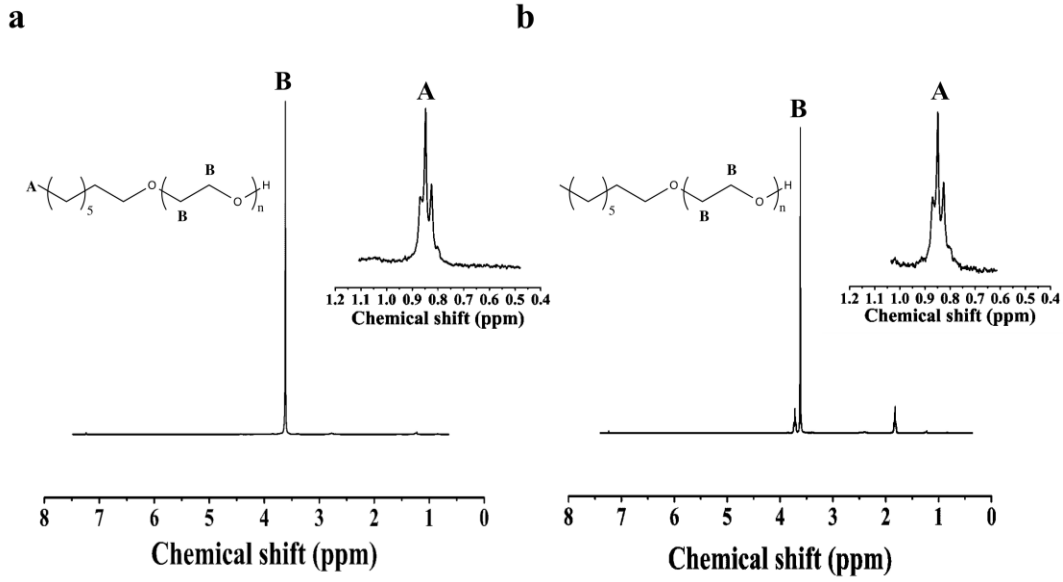

Figure 5-4. (a) ^{1}H NMR of PEO homopolymer from 1-octanol initiator with DMSO (b) ^{1}H NMR of PEO homopolymer from 1-octanol without DMSO.

^{1}H NMR MW results are shown in Figure 5-4. Assigning the singlet at 3.62 ppm to the methylene protons in the backbone of the PEO chain, and the triplet at 0.85 ppm to the terminal methyl group of the 1-octanol, integration of the peak areas gives M_n values of 6.5 kg/mol for the polymer grown with DMSO and 10.0 kg/mol for the polymer synthesized without DMSO. The lower MW of the PEO with DMSO corresponds with a lower yield, likely due to EO being less soluble in the reaction mixture containing DMSO. The nearly identical PDI with and without DMSO argues against a termination event. Slower rates of reaction due to lower concentrations of EO dissolved in the reaction mixture are supported by several observations. The first is that the isolated yield of the reaction with DMSO is 77%, and the measured molecular weight is roughly 70 % of the target. The second observation is that using a 1:1 ratio of DMSO:THF results in PEO with a MW roughly 10% of the of the target. Changing the ratio to 1:4 DMSO:THF results in PEO with a MW 70% of the target, with all other reaction conditions held constant. Without any DMSO at all, the yield is 99.5%.

^{1}H NMR also provides evidence that the PEO chains are indeed initiated from the alcohol, as the presence of PEO chains not initiated from the alcohol would result in ^{1}H NMR results, which are based on the peak areas associated with the alcohol, being far different than the target MW. The presence of free alcohol is unlikely due to the precipitation of the polymer during workup. Looked at a different way, this means that there was no significant amount of PEO “homopolymer”, or polymer initiated without the intended initiator. As our approach works by removing the water present in the system, no water is available to initiate polymerization and produce homopolymer.

5.3.1.2 Propargyl alcohol

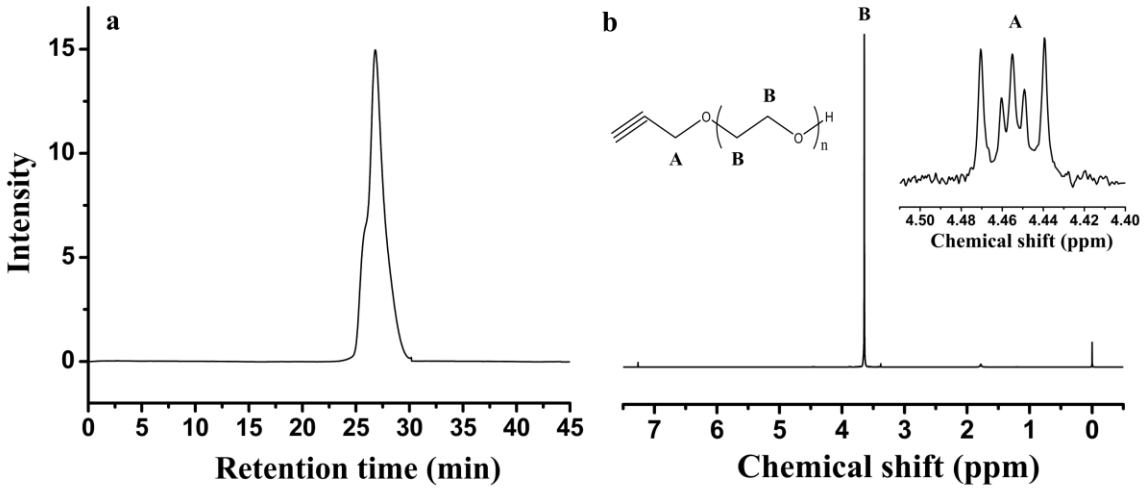

Figure 5-5. (a) GPC of PEO homopolymer from propargyl alcohol initiator (b) ^{1}H NMR of PEO homopolymer from propargyl alcohol.

In addition to 1-octanol, propargyl alcohol is used to grow PEO with a target molecular weight of 5 kg/mol. Due to its thermal sensitivity, method 1, or vacuum distillation, is used to form the alkoxide and no DMSO is present in the system. Once the alkoxide forms, a colorless liquid remains. After distilling in dry THF, the solution turns cloudy white prior to heating at 60 °C for 7 days. The synthesized PEO from propargyl alcohol is analyzed with ^{1}H NMR and GPC, giving a M_n value of 6.8 kg/mol and a polydispersity index (PDI) of 1.37. Figure 5-5 shows the GPC chromatogram and ^{1}H NMR spectrum for the polymer. The chemical shift value at 4.45 ppm corresponds to the methylene group in the initiator. The methylene group in the backbone of the polymer chain is shown as a singlet at 3.60 ppm. Comparing the integration of the peak areas, the calculated M_n from ^{1}H NMR is 6.8 kg/mol, slightly higher than the target MW, possibly due to not all of the propargyl initiator being converted to the alkoxide. The yield of the reaction is 96%.

5.3.2 PS-*b*-PEO copolymer

Next, block copolymers of PS-*b*-PEO are synthesized. Hydroxyl terminated polystyrene macroinitiator (PS-OH) is used as the alcohol, and is analyzed by GPC and ^{1}H NMR before using the azeotropic method to grow the PEO block. The PDI by GPC is 1.19, and the M_n is 2.6 kg/mol by NMR. From this macroinitiator, PEO with a target MW of 1.3 kg/mol is synthesized using method 1. Figure 5-6(a) and 5-6(b) show the overlay of the original polymer (in red) and the block copolymer (in black). The ^{1}H NMR spectrum of the PS-OH macromer is shown in Figure 5-6(c)**,** with the relevant peaks labeled.

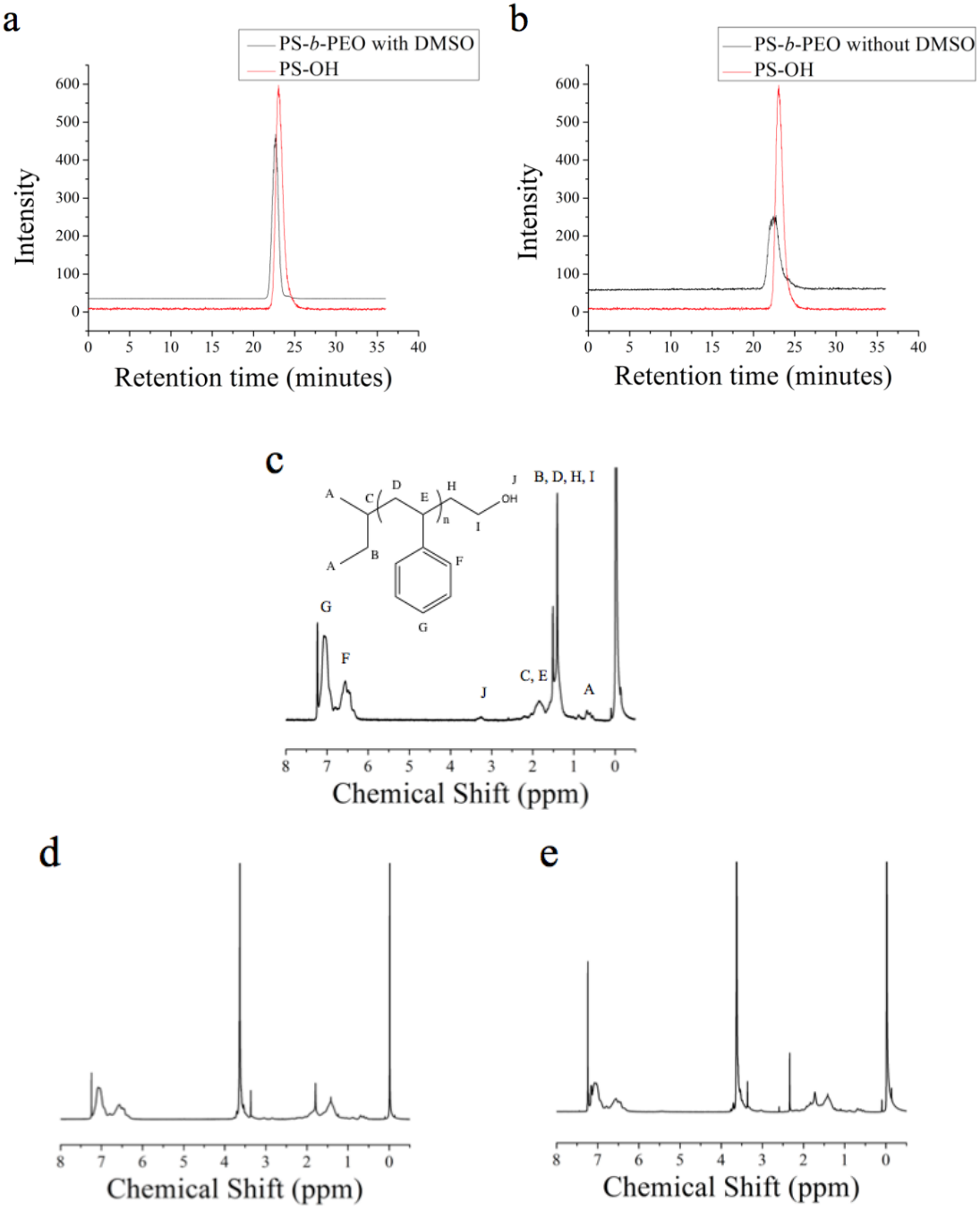

Figure 5-6. (a) Overlapping GPC traces of PS-OH and PS-*b*-PEO with DMSO (b) Overlapping GPC traces of PS-OH and PS-*b*-PEO without DMSO (c) ^{1}H NMR of PS-OH (d) ^{1}H NMR of PS-*b*-PEO with DMSO (e) ^{1}H NMR of PS-*b*-PEO without DMSO.

As with the 1-octanol initiated polymerization, the effect of DMSO on the azeotropic initiated PS-OH macromer is investigated. In both cases, with and without DMSO, the yield of the polymerization is better than 98%, and polymers are characterized by GPC and ^{1}H NMR. The GPC chromatogram of the PS-*b*-PEO with DMSO is shown in Figure 5-6(a), with an overlaid trace of the PS-OH macromer, and a PDI of 1.21. In comparison, Figure 5-6(b) shows the GPC trace of PS-*b*-PEO without DMSO, with a PDI of 1.50. The presence of the DMSO appears in this case to give a narrower molecular weight distribution, as seen previously by Quirk *et al*.[43] Figure 5-6(d) and 5-6(e) show the ^{1}H NMR spectra of PS-*b*-PEO with and without DMSO, respectively, each containing the characteristic PEO peak at around 3.6 ppm. The M_n of the PEO block made with DMSO from ^{1}H NMR is 1.1 kg/mol, close to the target of 1.3 kg/mol, while the molecular weight of the PEO block without DMSO is 1.9 kg/mol. It thus appears the effect of the DMSO may be to make the PS-OH macromer a better initiator, possibly by stabilizing the charged chain end outside of the polymer coil, where it is likely buried in more nonpolar solvents.

5.3.3 PEO extension

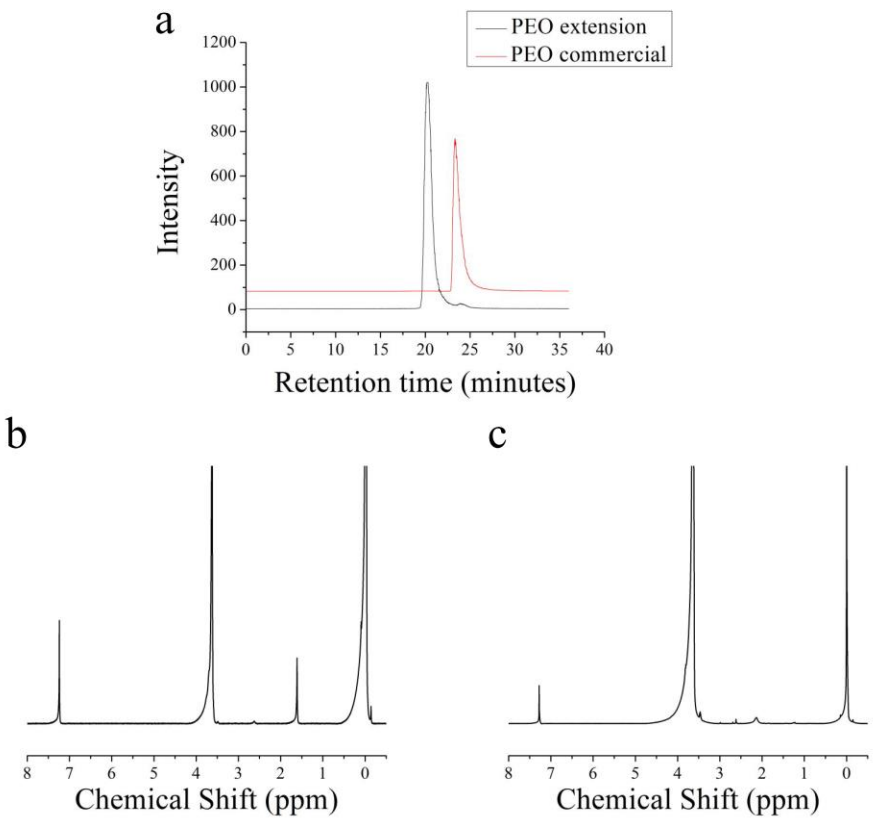

Figure 5-7. (a) Overlapping GPC traces of PEO commercial and PEO extension (b) ^{1}H NMR of commercial PEO (c) ^{1}H NMR of extended PEO chain

This method is also used to extend the molecular weight of preformed hydroxyl-terminated PEO polymers. A commercial PEO with a molecular weight of 2.0 kg/mol is used with a target of 20 kg/mol for the extended polymer. After azeotropic distillation, the reaction mixture turns yellow, suggesting the presence of an anion. Figure 5-7(a) shows overlaid GPC traces of the commercial PEO and the extended PEO chain. The commercial PEO has a PDI of 1.30, and after extension, the PDI decreases to 1.16. Figure 5-7(b) shows the ^{1}H NMR spectrum of the commercial PEO and Figure 5-7(c) is the ^{1}H NMR spectrum of the extended PEO

polymer. From Figure 5-7(c), the molecular weight of the extended PEO is 17.4 kg/mol, which agrees well with our initial target molecular weight of 20 kg/mol.

5.3.4 Conclusion

Using azeotropic distillation to remove water and form potassium alkoxides directly from alcohols and KOH, we have demonstrated the synthesis of PEO from small molecular weight alcohols, the formation of PEO block copolymers, and the extension of PEO chains. Two methods, one under vacuum and the other at atmospheric pressure, were introduced. In addition, it avoids the often necessary removal of PEO homopolymers and compounds such as naphthalene from the final product. The presence of a co-solvent, DMSO, was also investigated, and it was found to be helpful only for the synthesis of PEO from macromers. This approach to the synthesis of PEO provides an attractive and useful alternative to the current practice of employing air sensitive and difficult to work with alkyl and aryl potassium reagents.

5.3.5 Supplemental Information

5.3.5.1 Images of anions

Figure 5-8. Image of anion from a small molecular weight alcohol initiator, 1-octanol, run with DMSO.

Figure 5-8 shows an image of the reaction mixture from the PEO growth from 1-octanol after distillation of the solvent THF on the vacuum line. The alkoxide was first created using method 2 or atmospheric pressure distillation. After the alkoxide is formed, the reaction mixture changes color, indicating an anion is present. The reaction was run with DMSO as the cosolvent.

Figure 5-9. Image of anion from a **s**mall molecular weight alcohol initiator, 1-octanol, run without DMSO.

The image of the anion from a reaction with 1-octanol, run without DMSO, is slightly different than the same reaction run with DMSO. Figure 5-9 shows that the reaction mixture did not change color when DMSO was not present as a cosolvent in the system. The reaction mixture remained clear.

Figure 5-10. Image of anion from a small molecular weight alcohol initiator, propargyl alcohol, run without DMSO.

The alkoxide was formed in the reaction using propargyl alcohol as a small molecular weight initiator using method 1 or vacuum distillation due to its thermal sensitivity. The image shown in Figure 5-10 is after heating the reaction mixture for 1 week. The reaction was run without DMSO as the cosolvent.

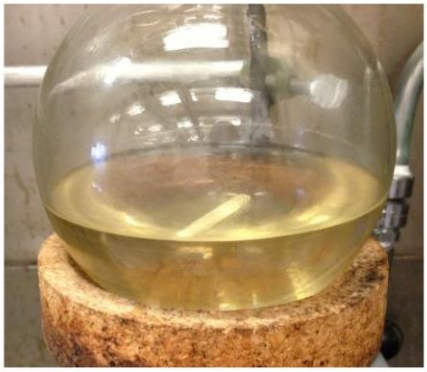

Figure 5-11. Image of anion from a PS-*b*-PEO synthesis with DMSO.

The reaction flask containing the anion from a diblock synthesis of PS and PEO is shown in Figure 5-11. The image was taken after heating the reaction mixture for 5 days. The solvent system was a THF/DMSO mixture.

Figure 5-12. Image of anion from a PS-*b*-PEO synthesis without DMSO.

Similarly to the PS-*b*-PEO reaction run with DMSO, the image of the anion of the reaction run without DMSO is shown in Figure 5-12. The image was taken after heating the reaction mixture for 5 days.

5.3.6 References

(1) Kataoka, K.; Harada, A.; Nagasaki, Y. *Adv. Drug Deliv. Rev.* **2001**, *47*, 113–131.

(2) Letchford, K.; Burt, H. *Eur. J. Pharm. Biopharm.* **2007**, *65*, 259–269.

(3) Wang, F.; Bronich, T. K.; Kabanov, A. V.; Rauh, R. D.; Roovers, J. *Bioconjug. Chem.* **2005**, *16*, 397–405.

(4) Kwon, G. S.; Forrest, M. L. *Drug Dev. Res.* **2006**, *67*, 15–22.

(5) Allen, C.; Maysinger, D.; Eisenberg, A. *Colloids Surfaces B Biointerfaces* **1999**, *16*, 3–27.

(6) Gaucher, G.; Dufresne, M.-H.; Sant, V. P.; Kang, N.; Maysinger, D.; Leroux, J.-C. *J. Control. Release* **2005**, *109*, 169–188.

(7) Lavasanifar, A.; Samuel, J.; Kwon, G. S. *Adv. Drug Deliv. Rev.* **2002**, *54*, 169–190.

(8) Adams, M. L.; Lavasanifar, A.; Kwon, G. S. *J. Pharm. Sci.* **2003**, *92*, 1343–1355.

(9) Liggins, R. T.; Burt, H. M. *Adv. Drug Deliv. Rev.* **2002**, *54*, 191–202.

(10) Alexandridis, P. *Curr. Opin. Colloid Interface Sci.* **1997**, *2*, 478–489.

(11) Ekizoglou, N.; Hadjichristidis, N. *J. Polym. Sci. Part A Polym. Chem.* **2001**, *39*, 1198–1202.

(12) Xie, H.-Q.; Xie, D. *Prog. Polym. Sci.* **1999**, *24*, 275–313.

(13) Raynaud, J.; Absalon, C.; Gnanou, Y.; Taton, D. *J. Am. Chem. Soc.* **2009**, *131*, 3201–3209.

(14) Arnal, M. L.; Balsamo, V.; Lopez-Carrasquero, F.; Contreras, J.; Carrillo, M.; Schmalz, H.; Abetz, V.; Laredo, E.; Muller, A. J. *Macromolecules* **2001**, *34*, 7973–7982.

(15) Alexandridis, P.; Hatton, T. A. *Colloids Surfaces A Physicochem. Eng. Asp.* **1995**, *96*, 1–46.

(16) Hillmyer, M. A.; Bates, F. S. *Macromolecules* **1996**, *29*, 6994–7002.

(17) Otsuka, H.; Nagasaki, Y.; Kataoka, K. *Adv. Drug Deliv. Rev.* **2012**, *64*, 246–255.

(18) Knop, K.; Hoogenboom, R.; Fischer, D.; Schubert, U. S. *Angew. Chem. Int. Ed. Engl.* **2010**, *49*, 6288–6308.

(19) Money, B. K.; Swenson, J. *Macromolecules* **2013**, *46*, 6949–6954.

(20) Ganta, S.; Devalapally, H.; Shahiwala, A.; Amiji, M. *J. Control. Release* **2008**, *126*, 187–204.

(21) Rösler, A.; Vandermeulen, G. W. M.; Klok, H.-A. *Adv. Drug Deliv. Rev.* **2012**, *64*, 270–279.

(22) Barthel, M. J.; Schacher, F. H.; Schubert, U. S. *Polym. Chem.* **2014**, *5*, 2647–2662.

(23) Kwon, G.; Naito, M.; Yokoyama, M.; Okano, T.; Sakurai, Y.; Kataoka, K. *Langmuir* **1993**, *9*, 945–949.

(24) Buskens, P.; Wouters, M.; Rentrop, C.; Vroon, Z. *J. Coatings Technol. Res.* **2013**, *10*, 29–36.

(25) Clinton, N.; Matlock, P. *Encyclopedia of Polymer Science and Technology*, 1st ed.

(26) Penczek, S.; Cypryk, M.; Duda, A.; Kubisa, P.; Slomkowski, S. *Prog. Polym. Sci.* **2007**, *32*, 247–282.

(27) Fallais, I.; Devaux, J.; Jerome, R. *J. Polym. Sci. Part A Polym. Chem.* **2000**, *38*, 1618–1629.

(28) Forster, S.; Kramer, E. *Macromolecules* **1999**, *32*, 2783–2785.

(29) Hadjichristidis, N.; Pispas, S.; Floudas, G. *Block Copolymers: Synthetic Strategies, Physical Properties, and Applications*; 2003.

(30) Allgaier, J.; Poppe, A.; Wilner, L.; Richter, D. *Macromolecules* **1997**, *30*, 1582–1586.

(31) Hruska, Z.; Hurtrez, G.; Walter, S.; Riess, G. *Polymer (Guildf).* **1992**, *33*, 2447–2449.

(32) Lanson, D.; Schappacher, M.; Borsali, R.; Deffieux, A. *Macromolecules* **2007**, *40*, 9503–9509.

(33) Castle, T. C.; Hutchings, L. R.; Khosravi, E. *Macromolecules* **2004**, *37*, 2035–2040.

(34) Knischka, R.; Lutz, P. J. *Macromolecules* **2000**, *33*, 315–320.

(35) Fragouli, P. G.; Iatrou, H.; Hadjichristidis, N. *Polymer (Guildf).* **2002**, *43*, 7141–7144.

(36) Ekizoglou, N.; Hadjichristidis, N. *J. Polym. Sci. Part A Polym. Chem.* **2002**, *40*, 2166–2170.

(37) Zhou, P.; Xie, H. *Polym. Commun.* **1985**, 124–130.

(38) Gitsov, I.; Simonyan, A.; Vladimirov, N. G. *J. Polym. Sci. Part A Polym. Chem.* **2007**, *45*, 5136–5148.

(39) Khan, T. N.; Mobbs, R. H.; Price, C.; Quintana, J. R.; Stubbersfield, R. B. *Eur. Polym. J.* **1987**, *23*, 191–194.

(40) Khan, A.; Siddiq, M. *J. Appl. Polym. Sci.* **2010**, *118*, 3324–3332.

(41) Jialanella, G. L.; Firer, E. M.; Piirma, I. *J. Polym. Sci. Part A Polym. Chem.* **1992**, *30*, 1925–1933.

(42) Esswein, B.; Moller, M. *Angew. Chem. Int. Ed. Engl.* **1996**, *35*, 623–625.

(43) Quirk, R. P.; Kim, J.; Kausch, C.; Chun, M. *Polym. Int.* **1996**, *39*, 3–10.

(44) Horsley, L. H. *Azeotropic Data - III (Advances in Chemistry Series 116)*; American Chemical Society, 1973.

Chapter 6:
Summary and Future Work

6.1 Summary

Graphene-stabilized water-in-oil emulsions, with graphene acting as a 2D surfactant, was shown to be a template for the synthesis of polymer/graphene nanocomposites. Bulk graphite exfoliates at a high-energy liquid/liquid interface and spreads at that interface to reduce the overall energy of the system. The self-assembled, overlapping graphene sheets are a percolated network that provides pathways for electrical and thermal conductivities in the resultant foams. These foams are unique due to the fact that they are made in a simplistic way and the method does not use high boiling solvents, surfactants, chemical treatments, or high temperatures. Bulk graphite, which is cheap and plentiful, is used and the process to exfoliate the graphite into graphene is thermodynamically driven. The process to produce these open-cell, lightweight, electrically conductive foams is scalable, tunable, and most importantly cost-effective.

In Chapter 1, the literature was surveyed regarding typical methods that are used to produce graphene. Most techniques available are expensive, require strict experimental conditions, and purification steps at the end. The final product, what researchers claim to be "graphene", is not entirely true. The material produced by the methods described in Chapter 1 without exception have residual functional groups and lattice defects that degrade the final properties. The technique developed in our lab, the interfacial trapping technique, is introduced and is the heart of the work to follow. In Chapter 2, an outline of the dissertation is presented in order to clearly follow the story of studying the polymer/graphene foams in optimizing their electrical and thermal properties, then further studying the same emulsions to understand the mechanism behind their size and stability and lastly developing a post-polymerization

modification technique for the porous materials to add hydrophilic characteristics through the synthesis of poly(ethylene oxide).

Chapter 3 provides a detailed study on the electrical and thermal properties of polymer/graphene nanocomposites as a function of graphene density. Within a single nanocomposite, different layers were analyzed to elucidate the effect of spheres packing prior to the structure being fixed by polymerization. In addition, graphite flake size was altered and the resultant change in properties was studied. Resistively heating the foams to ~100 °C was reproducible and did not degrade the material. In Chapter 4, the graphene-stabilized emulsions with different concentrations of graphite were studied further before polymerization using acoustic spectrometry. The average sphere size and distributions acquired through acoustic measurements were then compared to those obtained through SEM analysis, for the final composites post-polymerization. The ability to tune the cell size of the foams with the amount of graphite added to the system is important for filtration applications and was demonstrated through preliminary results in the adsorption of an organic dye and emulsified oil.

Lastly, in Chapter 5, a post-polymerization modification technique for hydrophobic, porous substrates was developed in order to add some hydrophilic components to the polymer/graphene foams. Poly (ethylene oxide) (PEO) was our polymer of choice however the formation of this polymer can be synthetically challenging. The new synthetic route that has been presented in this dissertation does not utilize moisture sensitive, pyrophoric organometallics, which are normally used. Instead, we used potassium hydroxide as the source for potassium cations. Azeotropic distillation, via two potential methods, was used to remove water from the equilibrium between an alcohol/KOH and alkoxide/water. We have shown the

mechanism can be used to grow PEO off small molecular weight alcohols, pre-formed PEO polymers, and hydroxyl terminated polymers to synthesize diblock copolymers.

To our knowledge, the study of polymer/graphene nanocomposites using pristine graphene has not been done before, but instead graphene oxide or reduced graphene oxide has been used but termed "graphene." The electrical and thermal properties of these foams were studied extensively in addition to the increase in the weight percent of initial graphite to see the change in the properties for resistive heating and adsorption applications. Furthermore, the synthetic route that is demonstrated in this dissertation is a new method for the formation of PEO and PEO block copolymers without the use of moisture sensitive, pyrophoric organometallics or the removal of unwanted compounds in the final polymer product.

6.2 Future Work

Current work being performed in the lab is continuing with the azeotropic distillation technique to grow PEO off of graphene oxide (GO). GO is hydrophilic and has oxygen functional groups on the sheets including hydroxyl groups, which can be used to form the potassium alkoxide required for the polymerization of ethylene oxide. Growing PEO with this method from other functional groups, such as amines and amides are of interest. Continuing with this same technique and modifying the porous polymer/graphene foams should be studied.

The polymer/graphene composites show great promise in adsorption and filtration applications, which should be further studied. Specifically, more work should be done with the butyl acrylate: *t*-butyl acrylate formulation made in metal pipes for a flow through setup with water. A 30:10 ratio was tried and subsequent hydrolysis, but other ratios should be used and polymerized in pipes.

Appendix A

A1.1 Reproducibility of thermal conductivity measurements

The thermal conductivity is measured using discs from top to bottom within a single composite. A PS/G composite with an initial loading of 1.3 wt% graphite is run in triplicate, with three different composite samples, to see the reproducibility of the technique with our foams. As shown in Figure A-1, the highest amount of error is with the slices at the bottom of the composite. This could be due to the density of the final composite decreasing as you move down the composite, regardless of the size of graphite used and initial graphite loading.

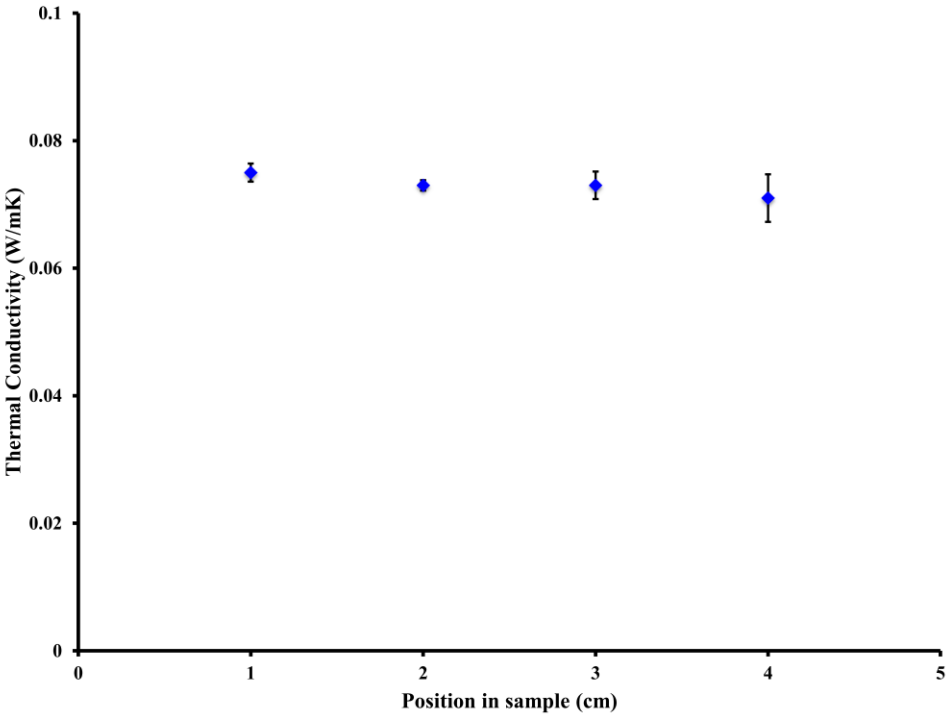

Figure A-1. Reproducibility of the thermal conductivity with respect to position in the sample of PS/G foams with 1.3 wt% graphite loading.

A1.2 Reproducibility of electrical conductivity

The reproducibility of the electrical measurements is studied using composites made with the same initial loading of graphite, 1.3 wt%, but with different graphite flake size. Figure A-2(A) illustrates the electrical conductivity of the PS/G foams made with the smaller graphite, which is 1 μm, with respect to position in the sample. Three slices of composite from three distinct samples were used in the measurements. The error is comparable irrespective of where you remove a slice from the composite. However, in Figure A-2(B), the error increases significantly from the top slice to the bottom slice of the composite made with the 10 μm graphite. This could be due to the density of the final composite decreasing more drastically in the material made with the larger flake graphite and the slices towards the bottom are therefore more fragile. This could create contact issues with the copper tape and lead to greater error towards the bottom of the sample.

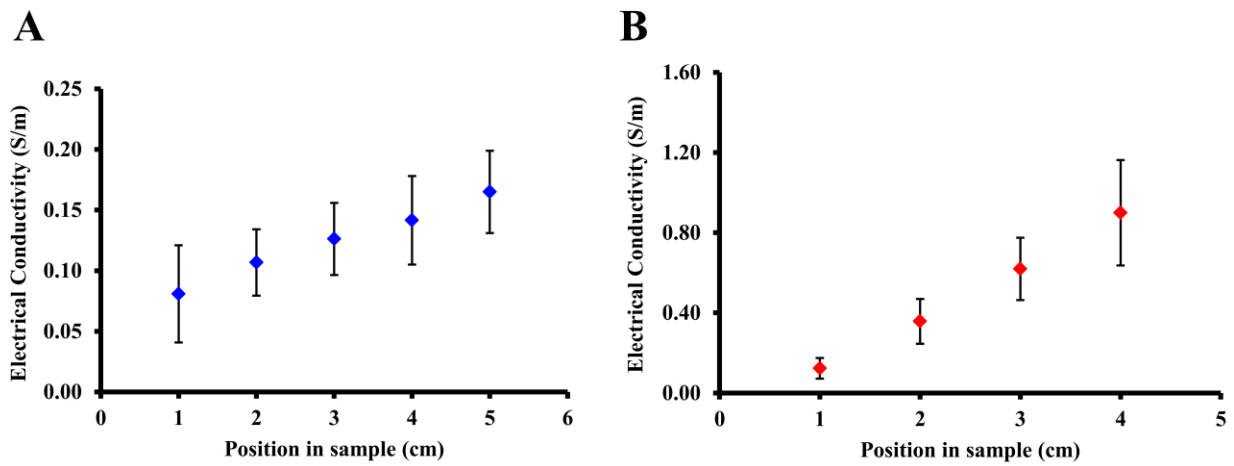

Figure A-2. Reproducibility of the electrical conductivity with respect to position in the sample of PS/G foams with 1.3 wt% graphite loading in a composite made with (A) 1 μm graphite (B) 10 μm graphite.

Figure A-3(A, B, and C) show the reproducibility of the electrical conductivity measurements for three different weight percentages of graphite in PS/G composites. All samples were run in triplicate, with three different composite samples, using the silver paste and copper tape method.

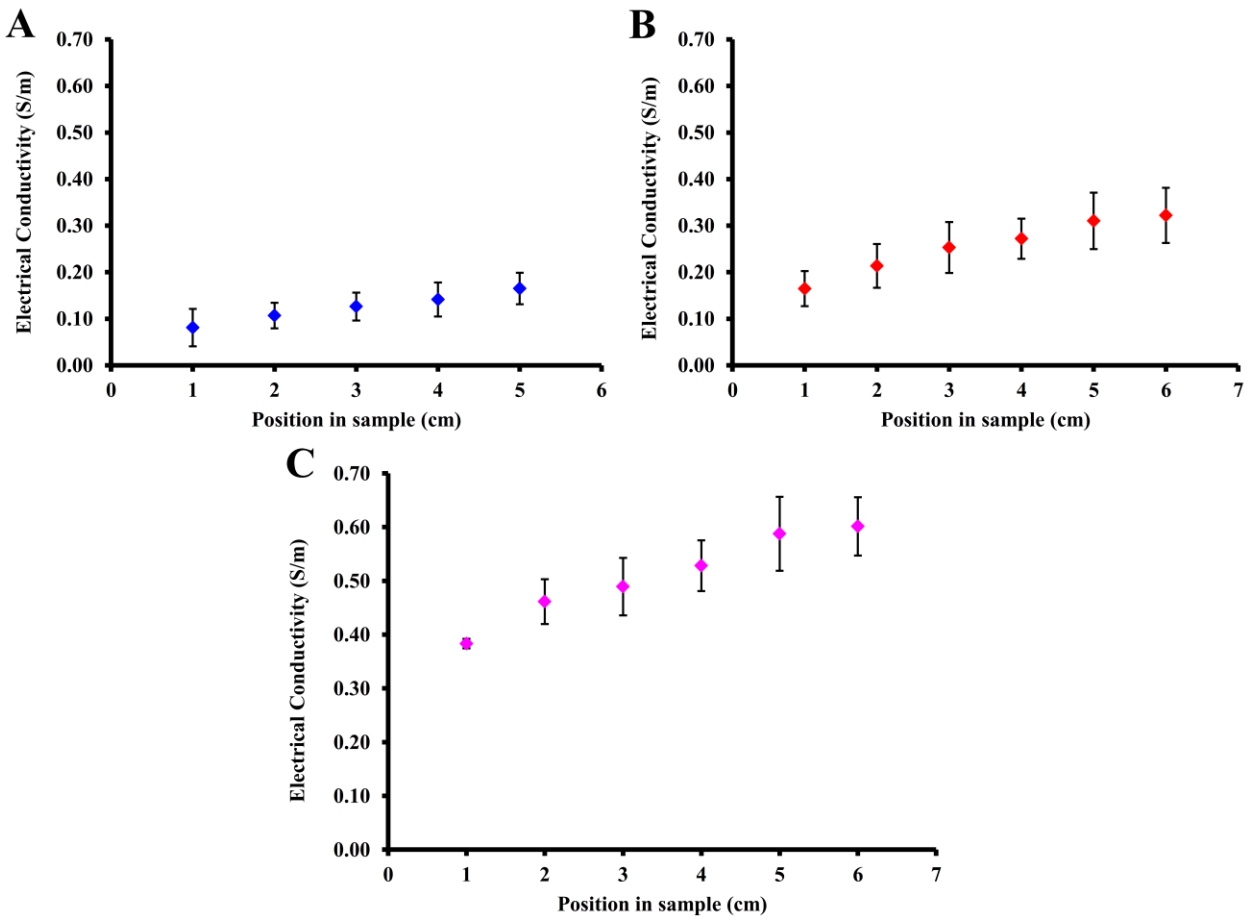

Figure A-3. Represents the reproducibility of the electrical conductivity measurements in (A) 1.3 wt% (B) 3.4 wt%, and (C) 6.9 wt% graphite.

A1.3 Thermal conductivity vs wt % of graphite

Figure A-4(A – D) further demonstrates that upon the addition of more graphite into the system, the thermal conductivity does not increase. The thermal conductivity actually decreases as the weight percent of graphite increases from 1.3 to 14. Only the graphite directly at the interface is completely exfoliated and aligned. As more and more graphite is added, the graphite becomes less aligned and less exfoliated therefore causing defects and edges within the system

where phonons can scatter in all directions. This bulk graphite further from the interface is not contributing to the properties of the material.

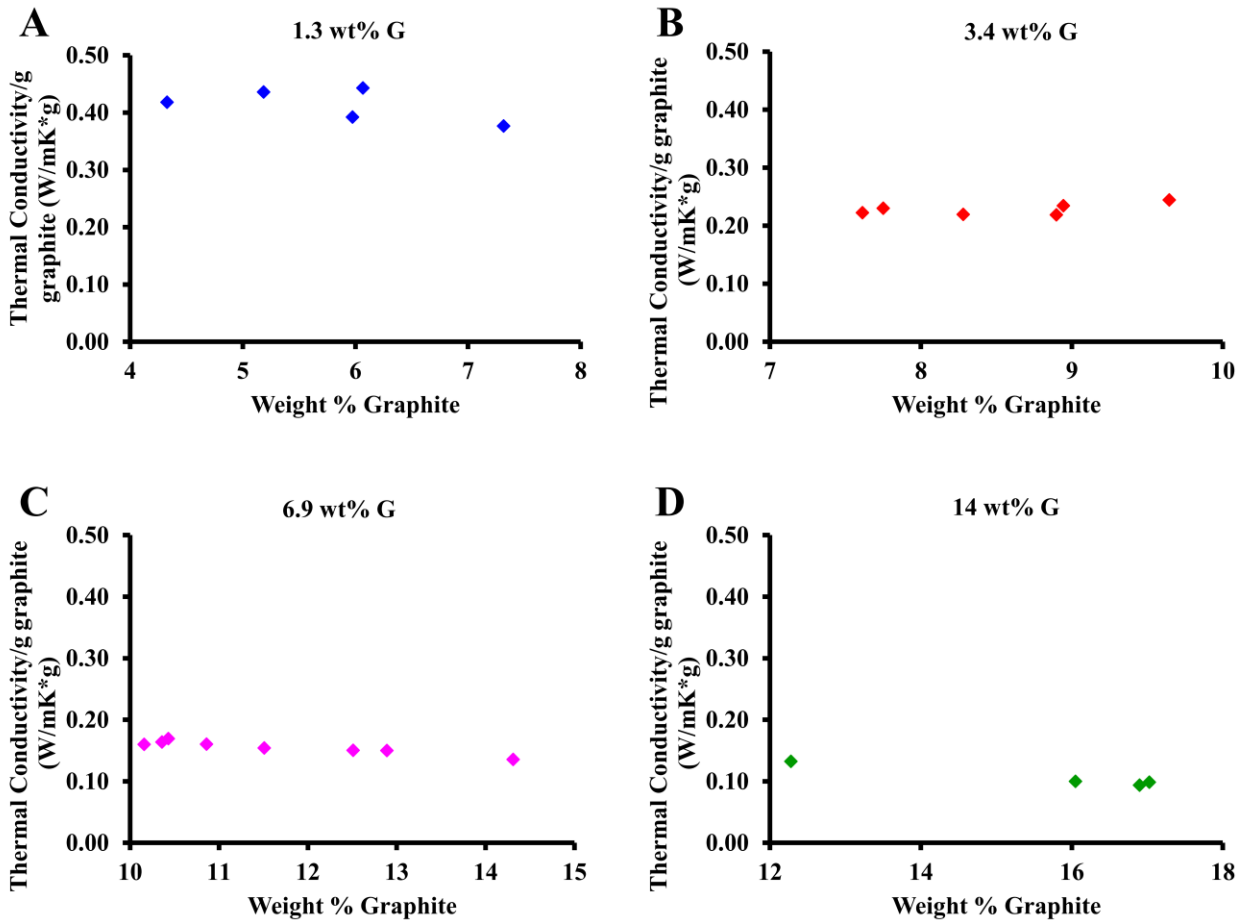

Figure A-4. Thermal conductivity normalized by grams of graphite collected by TGA versus the weight percent of graphite determined by TGA for four different initial loadings of graphite in PS/G foams: (A) 1.3 wt% (B) 3.4 wt% (C) 6.9 wt% (D)14 wt%.

A1.4 Electrical conductivity samples

Figure A-5 shows an image of two rectangles cut from a 6.9 wt% graphite polystyrene/graphene (PS/G) disc within a composite. The edges were painted with colloidal silver paste and then copper tape was adhered to the silver ends. The current was then measured using a Keithly Model 2420 sourcemeter. Based on the dimensions of the rectangular prisms and the average resistance, the conductivity was calculated. This method was performed for each disc within a composite, regardless of graphite loading or graphite sheet size.

Figure A-5. Two rectangular prisms of 6.9 wt% graphite initial loading in a PS/G composite with colloidal silver paste and copper tape on the edges for electrical conductivity measurements.

A1.5 SEM of 1.3 wt% PS/G using 10 μm graphite

SEM micrographs of a PS/G composite made with the 10 μm graphite flake size and a loading of 1.3 wt% graphite is shown in Figure A-6. A sphere-to-sphere contact point is shown in Figure A-6(A). If we further zoom into one of the sharp edges in between the two spheres, graphite can be seen, with visible layers, in Figure A-6(B).

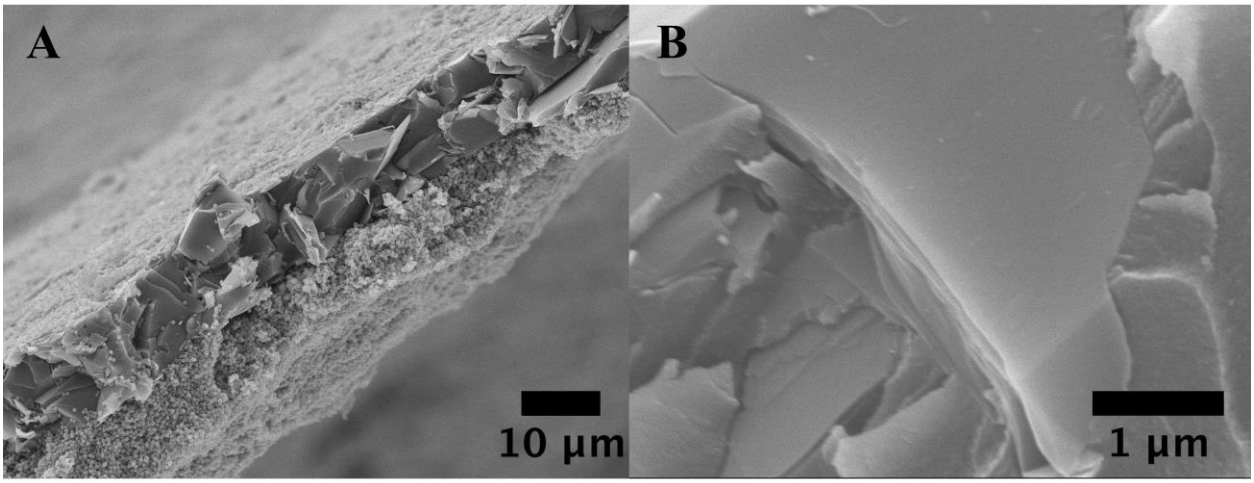

Figure A-6. (A) SEM image of sphere-to-sphere contact point with PS/G using 10 μm graphite flake size (B) Zoomed-in SEM image of graphite where the two spheres meet.

A1.6 Lower limit of graphite concentration

SEM micrographs of three different loadings of graphite in PS/G composites are shown in Figure A-7(A, B, and C). The three calculated loadings are 0.4, 0.8, and 1.3 wt%. A sample from the 2 – 3 cm position from each respective composite was taken and the morphology observed under SEM. As the loading of graphite is decreased, the average sphere size increases.

The 1.3 wt% graphite loading is our standard concentration of graphite and reducing that to 0.4 wt%, about 1/3 of the standard loading, leads to larger spheres and more holes in the spheres.

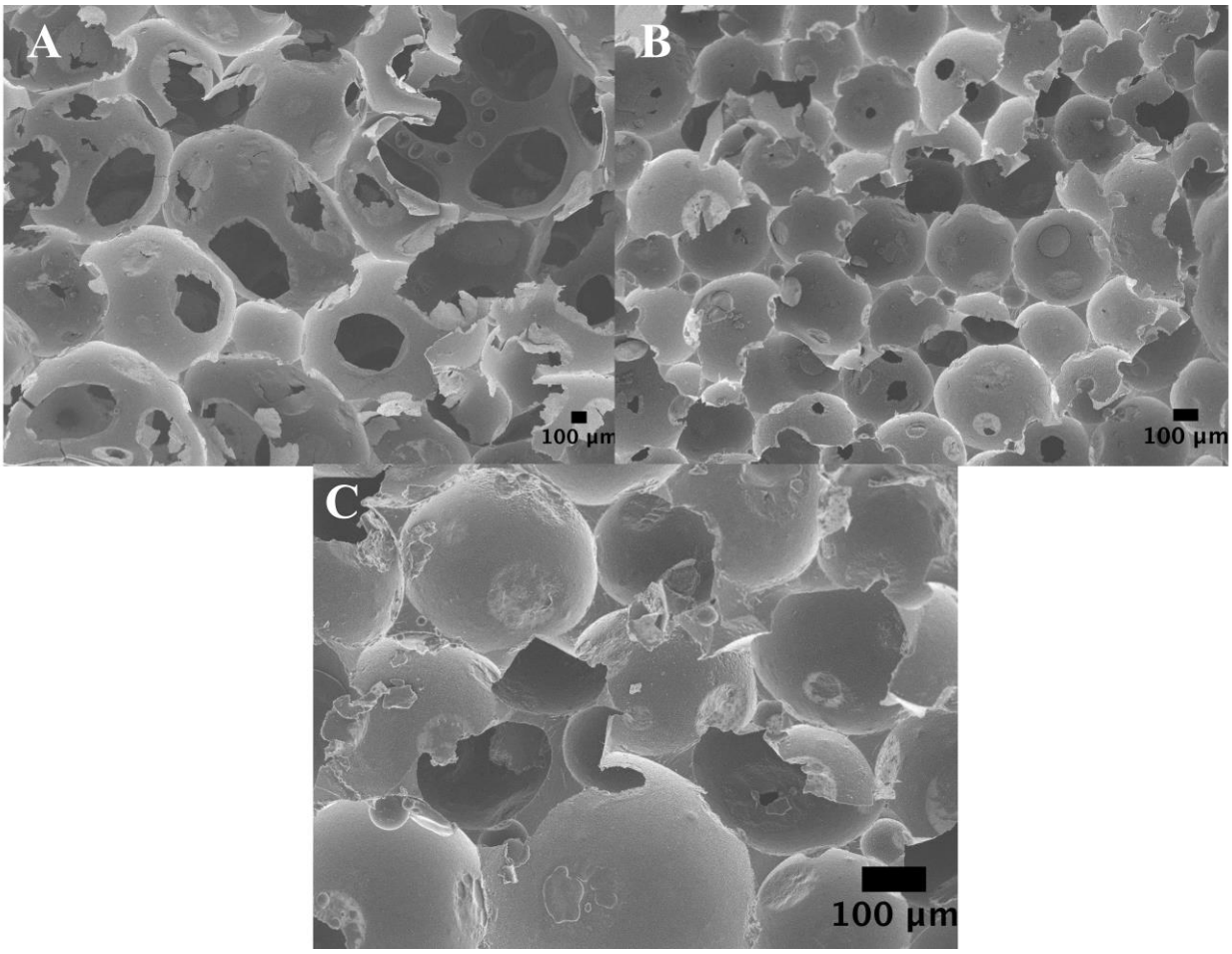

Figure A-7. (A) SEM micrograph of 0.4 wt% graphite PS/G composite (B) SEM micrograph of 0.8 wt% graphite PS/G (C) SEM micrograph of 1.3 wt% graphite PS/G.

The 0.4, 0.8, 1.3 wt% graphite PS/G composites were analyzed further by zooming into individual spheres to observe the graphene sheets via SEM. Figure A-8(A) shows the lowest graphite concentration, where many edges of graphene sheets are seen. Figure A-8(B) is an image of the interior of a single sphere in the 0.8 wt% graphite PS/G composite. Some smooth regions are visible, indicating PS regions as well as small PS spheres that result from a small

amount of the monomer solubilized in the water. Finally, in Figure A-8(C), the 1.3 wt% graphite PS/G interior lining of a sphere is shown. Many smooth PS areas are visible, with graphene sheets and PS spheres. These SEM micrographs are representative of the three different loadings of graphite.

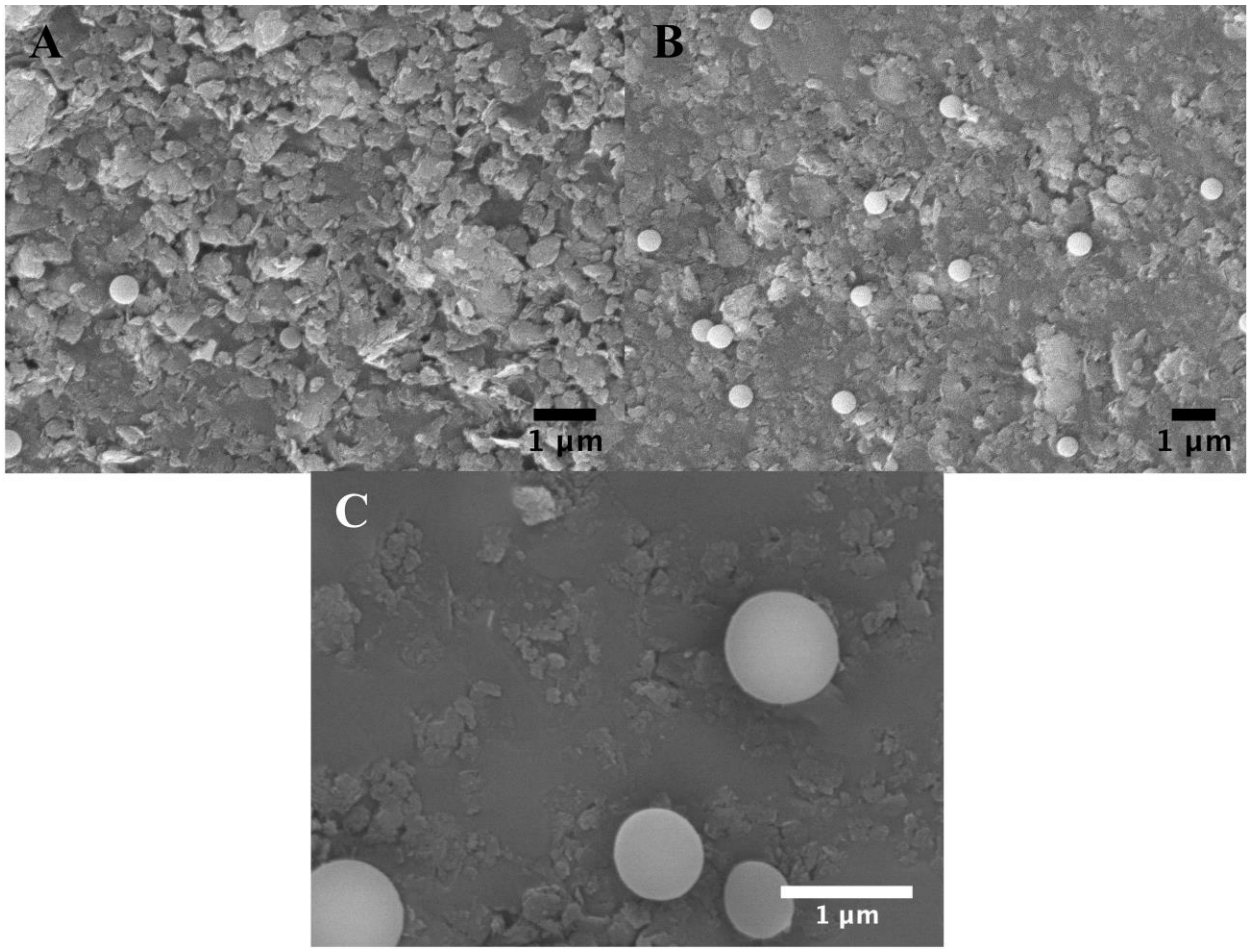

Figure A-8. SEM micrographs of (A) 0.4 wt% (B) 0.8 wt% (C) 1.3 wt% graphite in PS/G composites zoomed in to show graphene sheets lining the inner walls of the spheres.

A1.7 XRD of PS/G composite with controls

In Figure A-9, XRD spectra of a typical PS/G composite, of a 1.3 wt% graphite concentration, a PS control, and bulk graphite are overlaid. The composite was crushed with a mortar and pestle before XRD analysis. The PS control was synthesized the same way as the composite, just in the absence of graphite and a thin slice was used for analysis. The graphite control was a 1 micron synthetic derived graphite that was used as the 2D surfactant in making the PS/G composite. Both the PS/G composite and the PS control share broad peaks at 2θ values of ~9–10 and ~18–19[1], representing the polymer, in the blue and magenta curves in Figure 1-26, respectively. The graphite control, green trace in Figure A-9, has a sharp and narrow peak at a 2θ of ~26[1,2], which is also observed as a small, slightly broad bump in the PS/G composite XRD pattern.

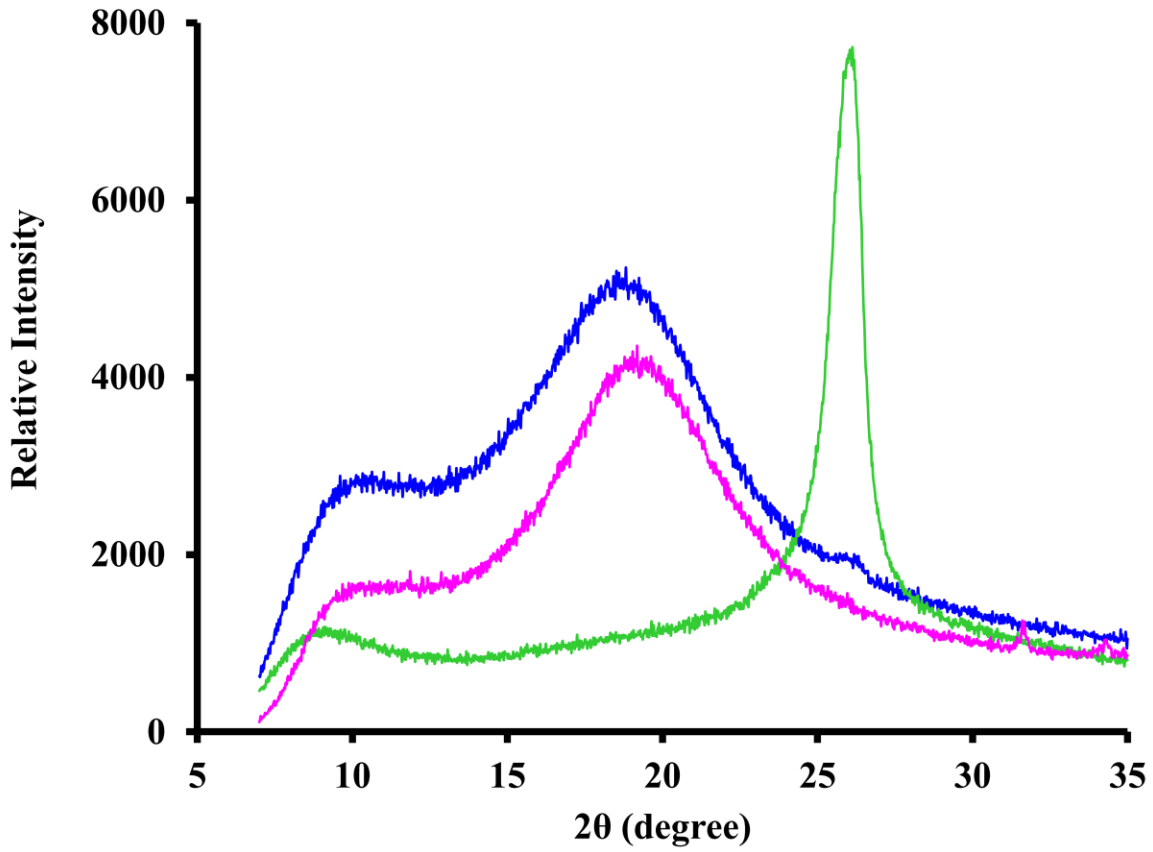

Figure A-9. XRD plot of 1.3 wt% graphite PS/G (blue), PS control (magenta), and Nano 24, 1 micron synthetic graphite (green).

The Graphite/Polystyrene (G/PS) net area is determined by XRD peak analysis using DIFFRAC.EVA software, Version 4.1.1 for five PS/G composite samples. The five samples have different loadings of graphite ranging from 0.4 to 14 wt%, which is the calculated weight percent. The actual weight percent of graphite is then determined by TGA. The G/PS net area is plotted versus the actual loading of graphite, as shown in Figure A-10. The more graphite that is put into the system, the greater the area under the graphite peak in XRD.

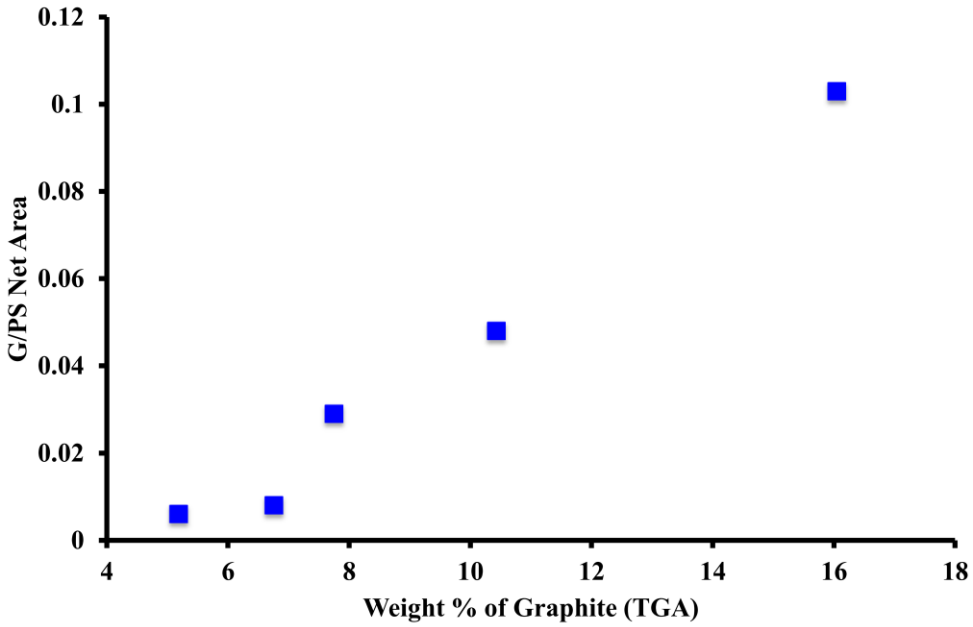

Figure A-10. Graphite/Polystyrene (G/PS) ratio of the net area from the XRD peak analysis vs weight percent of graphite determined by TGA of five different weight loadings of graphite.

Alternative method of measuring resistance of Polymer/Graphene composites

A1.8 Polymer/graphene composites with embedded wires

A different method, instead of the copper tape/silver paste method, was used to measure the current and obtain the average resistance of our composites to achieve better contact with copper wires embedded in the material. Embedded wires were placed in the emulsions before the continuous phase was polymerized. Different monomers such as styrene, butyl acrylate and methyl methacrylate were used. The distance between the wires was visualized using x-ray and

quantified, using a U.S. penny as a scale. The synthesis of the foams with embedded wires was as follows:

Polystyrene/Graphene (PS/G) foams with wires: The same method of preparing the emulsions was used as described previously. The following modifications have been made to the procedure. A ~100 mL scale of a 1.3 wt% graphite, 7/3 water/styrene emulsion was made and blended in a 125 mL jar. The copper wires, as shown in Figure A-11(A), were secured in place in a wide-mouth jar, which has a maximum capacity of ~ 470 mL, with duct tape before the emulsion was poured into the wide-mouth jar to cure. The wires were in an upside down "U" shape and the ends of the wires were splayed (~1/2 in). The top of the "U" was then cut in the middle after polymerization to have two ends to measure the average resistance of the composite. The jars were covered with aluminum foil to react in the oven. After the reaction was complete, the composites were removed from the jars and heated at ~70 °C for ~2 – 3 days to remove water. The amount of bulk layer was minimal and did not have to be removed. Figure A-11(B) shows the final PS/G composite with embedded wires.

Poly (butyl acrylate) (PBA/G) foams with wires: The same procedure that was used to synthesize the PS/G foams was used for the PBA/G foams, except for a different water/oil ratio. A 6/4 water/butyl acrylate ratio was used. Since the foams are flexible and not rigid, like the PS/G foams, the PBA/G composites with embedded wires can be slid right out of the jars without breaking them. The bulk layer of polymer on the PBA/G foams is very sticky and can be removed manually. An image of the PBA/G composite with embedded wires is shown in Figure A-11(C).

Poly (methyl methacrylate) (PMMA/G) foams with wires: The same formulation that was used to synthesize the PS/G foams was used for the PMMA/G foams. No visible bulk polymer layer is shown in the final PMMA/G composite with embedded wires in Figure A-11(D).

When making polymer/graphene composites with embedded wires, different types of wires were used. Wires with and without insulation were tried. Single wires were used. In addition, bundled thin and thick wires were also tried.

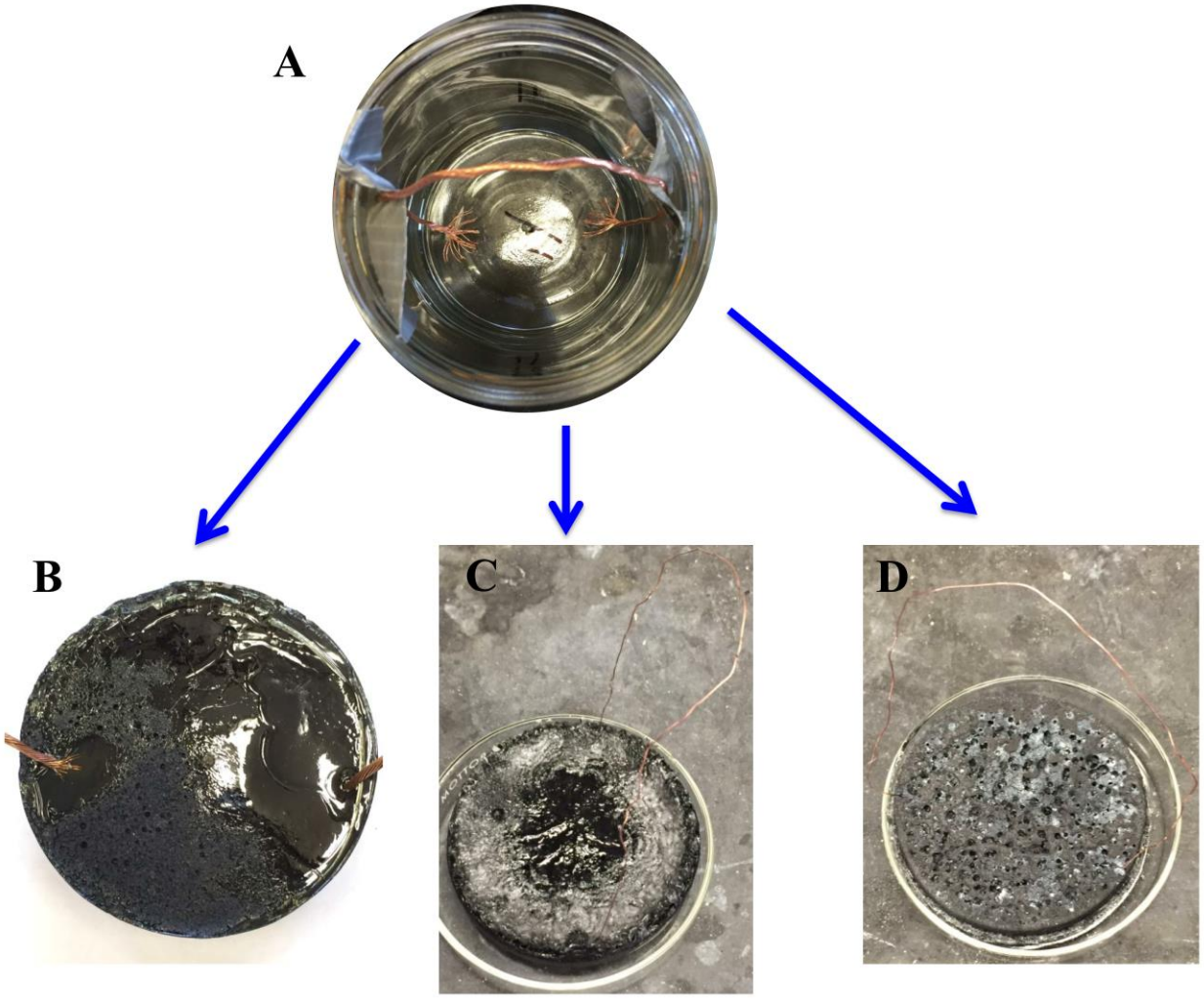

Figure A-11. (A) A wide-mouth glass jar with "U" shaped copper wires secured with duct tape before graphene-stabilized water-in-oil emulsion was poured into jar (B) PS/G composite with embedded wires after polymerization of the styrene continuous phase (C) PBA/G composite after polymerization of the butyl acrylate continuous phase (D) PMMA/G composite after polymerization of the methyl methacrylate continuous phase.

The same method of measuring the average resistance of the polymer/graphene composites with embedded wires was used as stated previously, using a Keithly Model 2420 sourcemeter. Instead of using copper tape and silver paste with the composites, the embedded wires were used to connect to the sourcemeter for better contact.

In order to visualize the placement and distance between the wires inside the polymer/graphene composites, the X-ray facility at the UConn infirmary was used. We thank the X-ray facility for allowing us to image our samples and the technicians for helping operate the equipment and software. An example of the X-ray images that were obtained are shown in Figure A-12. The example is of a PS/G composite with thin copper wires bundled with the X-ray images shown on the left and the actual composite used in the X-ray studies shown on the right.

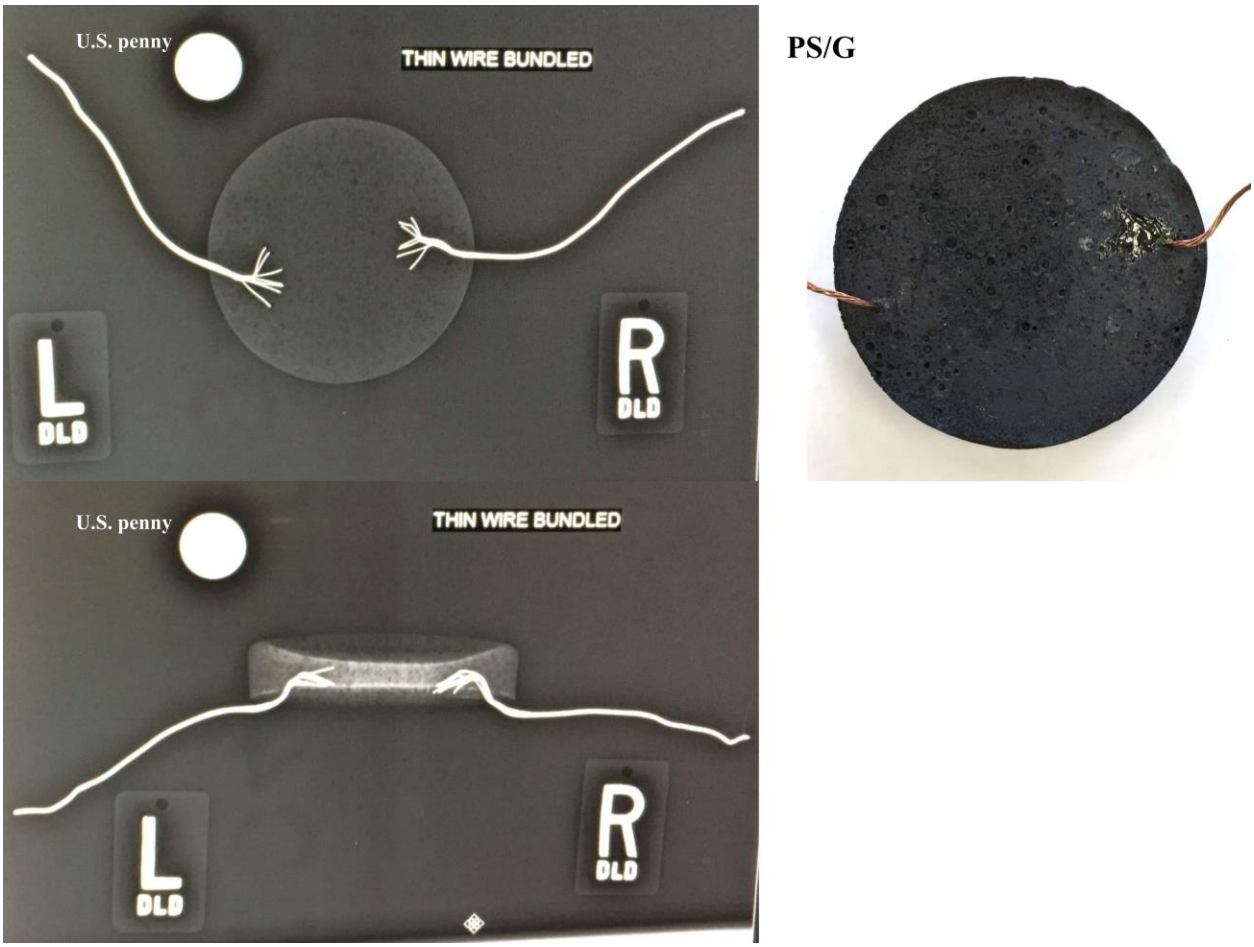

Figure A-12. X-ray image of a top view of PS/G composite with a U.S. penny for scale (top left) The actual PS/G composite used in X-ray studies in same position as viewed with X-ray (top right) X-ray image of a side view of PS/G composite with a U.S. penny for scale (bottom left).

The measured average resistance of the polymer/graphene composites made with thin bundled wire, without insulation was compared. All samples were run in triplicate. The average resistance of the PS/G composites with embedded wires was 1.51 kΩ. For the PMMA/G composites, the average resistance was 3.36 kΩ. Lastly, the average resistance of the PBA/G foams was the highest at 13.3 kΩ. The PS and PMMA graphene foams are similar in their structural integrity and are both rigid. They agree well in resistance measurements. However, the PBA/G composites are soft and flexible. The contact between the graphene-stabilized spheres,

where the inherent electrical conductivity comes from in the foams, might not be as strong, and therefore leads to a higher resistance value. The other possible reason is that there could be a thin layer of polymer coating the graphene sheets and thus increasing the resistance and lowering the conductivity. The procedure of embedding the wires before polymerization of the foams has been used for other projects within our lab such as creating electrodes for applications such as capacitive deionization.

A1.9 Thermal analysis of 1 vs 10 μm graphite

A typical TGA trace of a PS/G composite made with 1 μ m graphite flake size and 10 μ m graphite flake size is shown in Figure A-13. The same loading of graphite is used, 1.3 wt% graphite. The decomposition profile is the same regardless of the size of graphite used. The percent residue or experimental amount of graphite in the composites is taken at 795 °C.

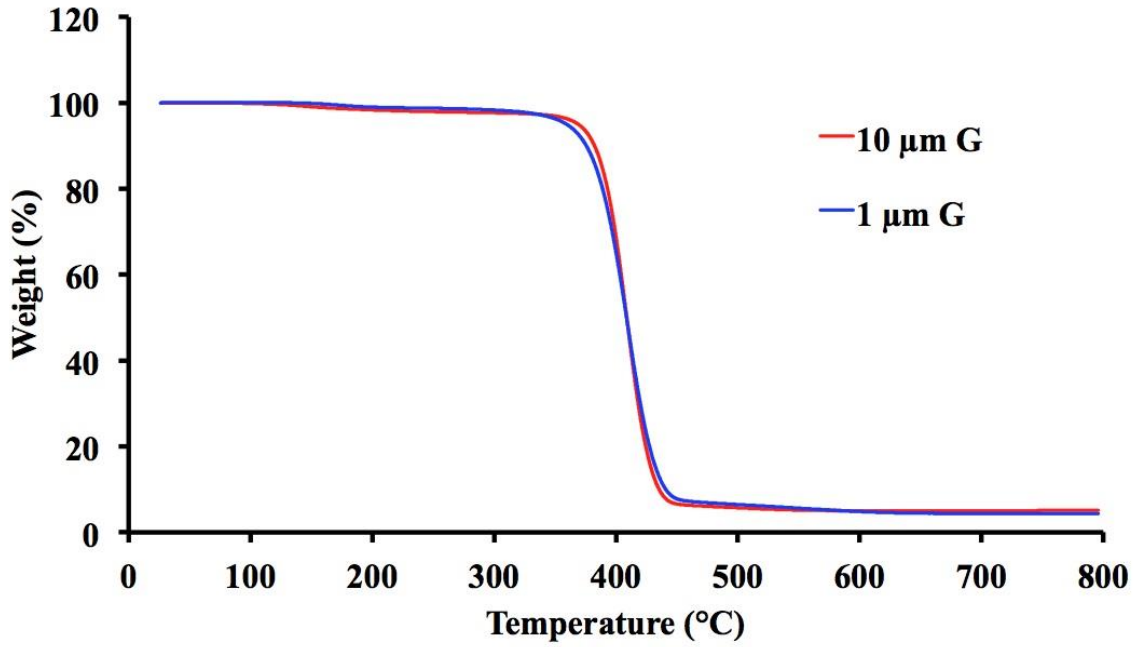

Figure. A-13. TGA trace of a PS/G composite made with 1 μm graphite (blue) and 10 μm graphite (red). The decomposition at 400 °C is due to the polymer in the composite, PS.

If samples are run from different positions within a composite made with the two different graphite flake sizes, the actual weight percent of graphite can be studied from the top of the composite, closest to the bulk layer of PS, to the bottom of the composite. As shown in Figure A-14, the amount of graphite increases moving towards the bottom of the composite, regardless of the flake size of graphite. Due to settling and packing of the spheres, interstitial polymer is squeezed out from in between the spheres. Due to the amount of polymer being less at the bottom, the relative density of graphite is greater. The same theoretical weight percent of graphite is used to synthesize the composites, which is a 1.3 wt% graphite. However, the PS/G composite with 10 μm graphite has more graphite in every position as compared to the 1 μm graphite flake size composite. Less emulsion is produced with the 10 μm graphite and therefore less composite. The material density is also less with the larger flake graphite. Both of these factors contribute to the greater amount of experimental weight percent graphite, as described previously in the results and discussion in Chapter 3.

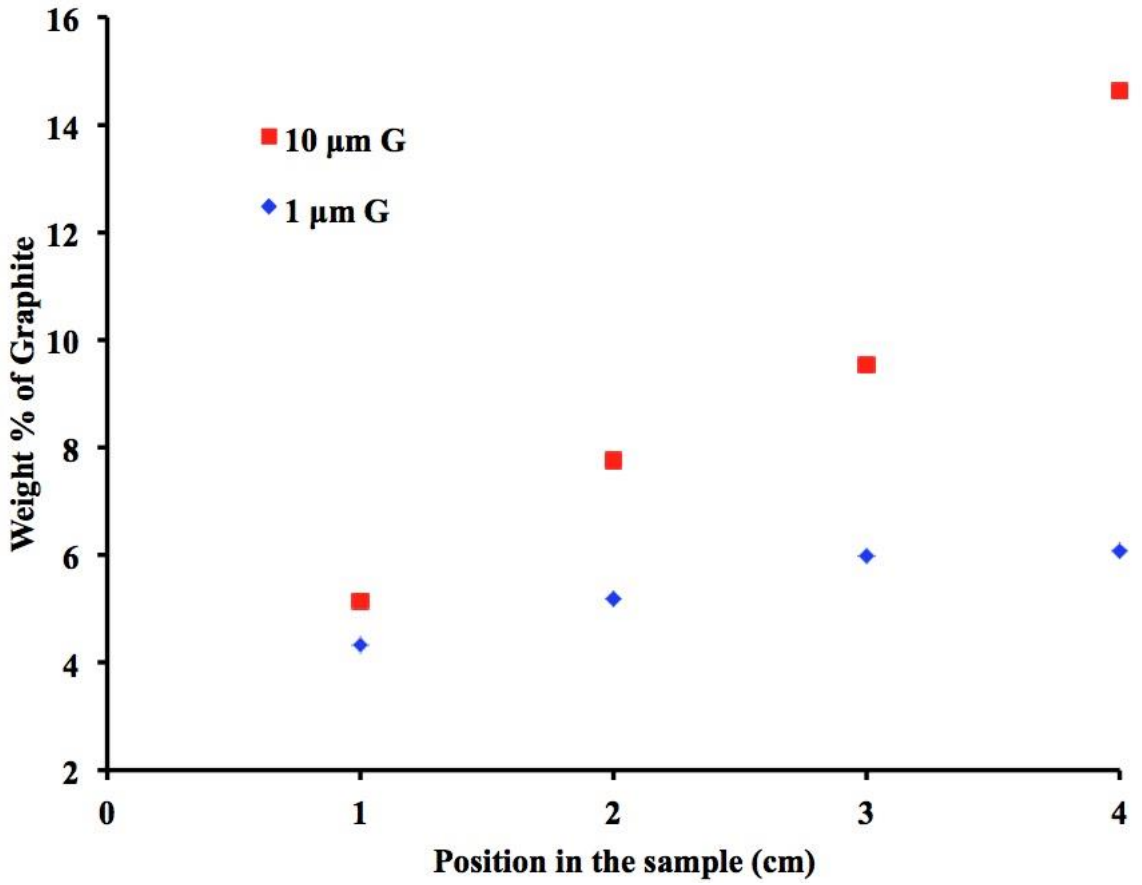

Figure A-14. Weight percent of graphite determined by TGA versus position in each sample with a PS/G composite made with 1 µm graphite (blue) and 10 µm graphite (red).

A1.10. Average resistance of PS/G foams

When studying the resistive heating properties of the PS/G foams, the current was measured using a Keithly Model 2420 sourcemeter and the average resistance was taken as the slope of the voltage vs current plot, as shown in Figure A-15. Before heating a theoretical 6.9 wt% graphite PS/G foam with a constant current of 0.09 A up to a stable temperature of ~100 °C, the average resistance was obtained. After 4 heating and cooling cycles with the same amperage, the current was measured using a voltage sweep of 0.001 to 0.1 V. The same average resistance was obtained pre and post-heating, at 158 Ω. This shows that there was no degradation of the material after 4 heating and cooling cycles.

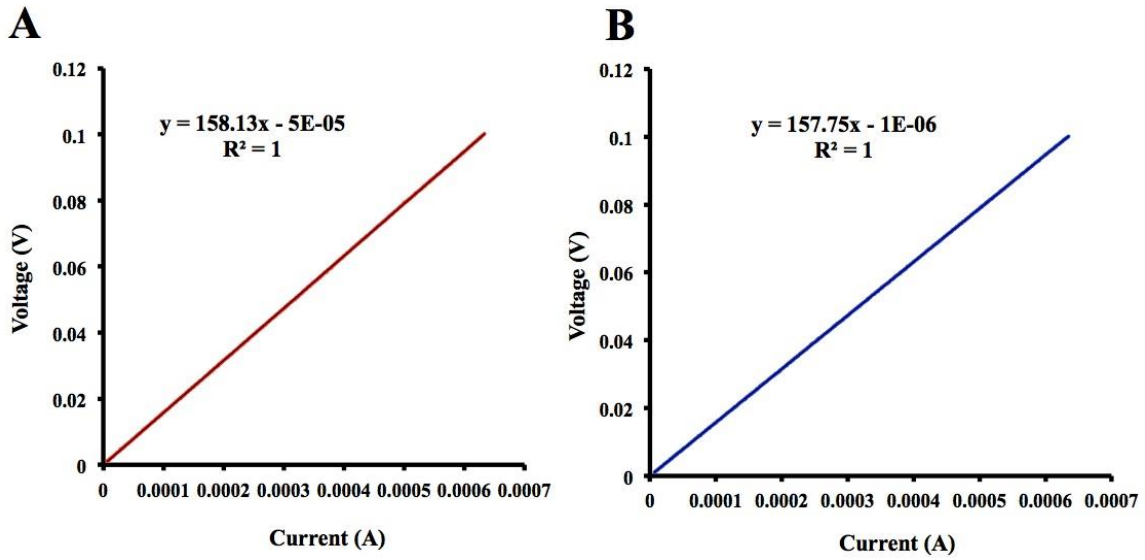

Figure.1-15. (A) Average resistance of PS/G composite pre-heating 4 cycles of constant current (0.09 A) through a PS/G composite (B) Average resistance of PS/G composite post-heating 4 cycles.

Appendix B

B1.1 Acoustic spectrometry: Sphere size distribution

Acoustic spectrometry is used to analyze the average sphere size and distribution in water-in-styrene emulsions containing three different loadings of graphite. Each sample was prepared immediately before loading the emulsion directly into the acoustic spectrometer chamber. At the beginning of each measurement, the curves in Figure B-1 show the droplet size distribution in the graphene-stabilized emulsions. The 1.3 wt% graphite (blue curve in Figure B-1), has the largest average sphere size of 43 μm. Increasing the weight percent to 3.4 wt% graphite, the sphere size decreases to 19 μm. Interestingly, the average sphere size of the 6.9 wt% graphite emulsions are somewhere in between the 1.3 and 3.4 wt% sphere sizes, even though we hypothesized they would be smaller, based on the SEM analysis of the final composites and acoustic spectrometry results of the emulsions later in the measurement. The average sphere size of the 6.9 wt% graphite emulsion is 27 μm.

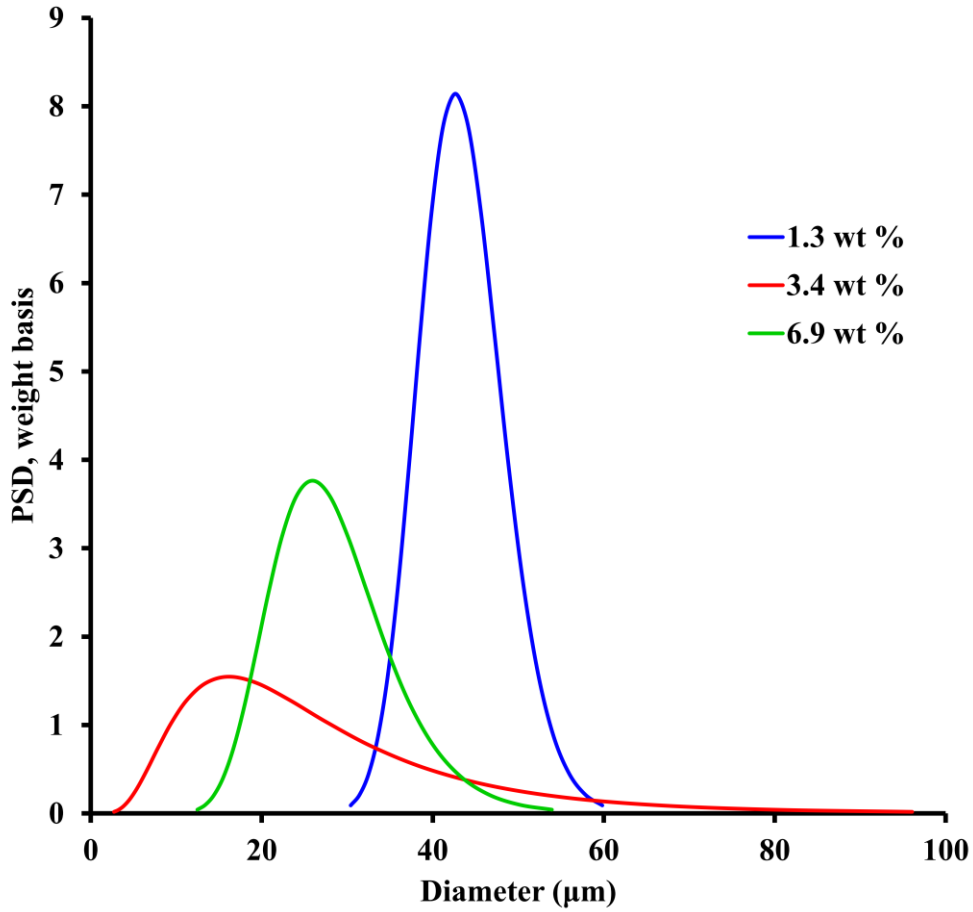

Figure B-1. Sphere size distribution determined by Acoustic Spectrometry of the three different concentrations of graphite: 1.3 wt% (blue), 3.4 wt% (red), 6.9 wt% (green) right after handshaking the emulsions.

B1.2 SEM analysis of higher wt% graphite

The PS/G composites with three different loadings of graphite were further analyzed with SEM. Zooming into an individual graphene-stabilized spheres, the amount of graphene sheets lining the spheres can be observed. Figure B-2(A) shows some sharp edges of graphene sheets but also many smooth regions of PS. The small spheres are PS spheres due to some of the styrene being soluble in the water phase. Continuing to increase the loading of graphite in Figure

B-2(B), to 3.4 wt%, there is a decrease in the amount of smooth regions of PS inside the spheres. Lastly, in Figure B-2(C), the amount of graphene has increased inside the spheres, as compared to Figure B-2(A and B). These images are representative of the PS/G composites with these loadings of graphite.

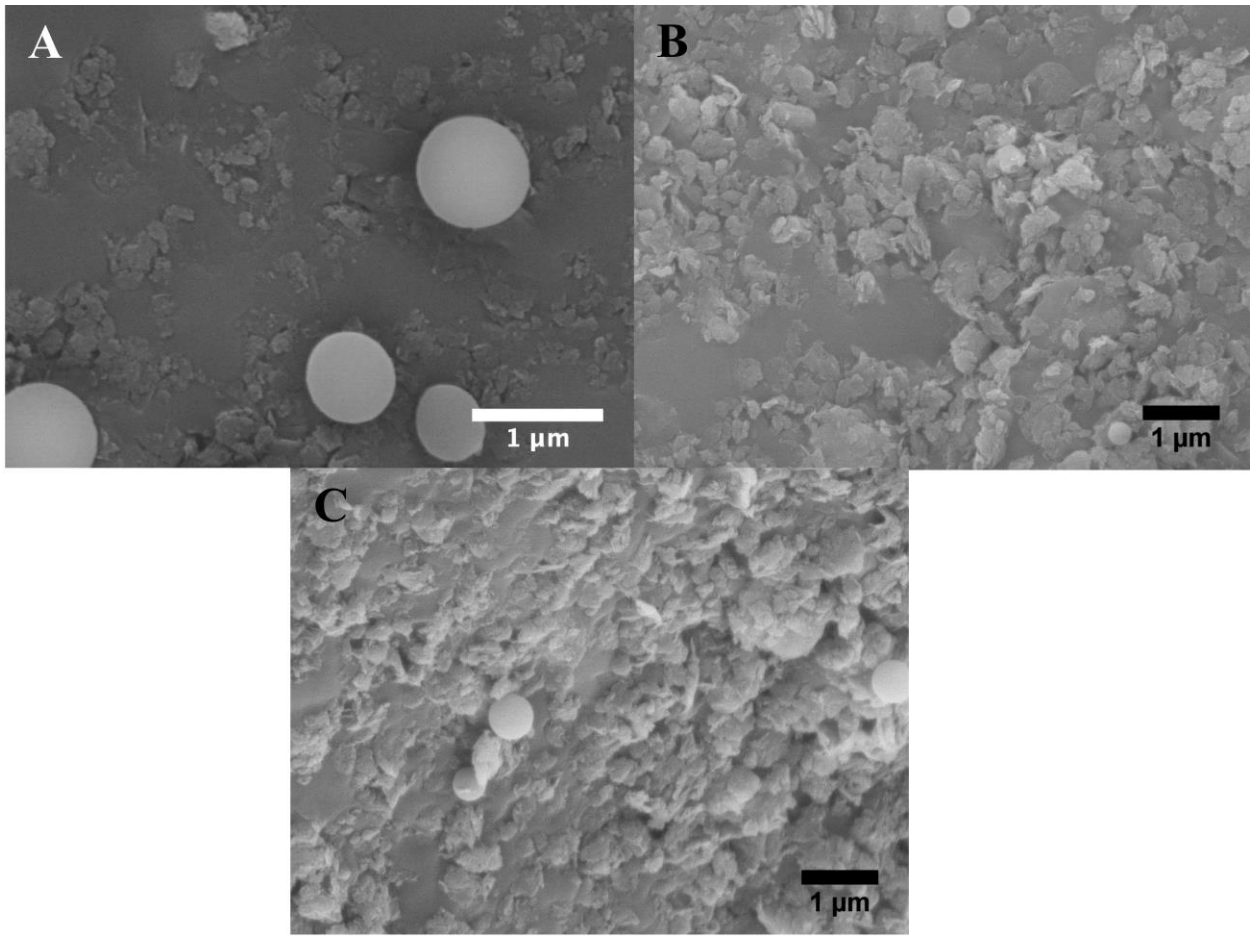

Figure B-2. SEM micrographs of (A) 1.3 wt% (B) 3.4 wt% (C) 6.9 wt% graphite in PS/G composites zoomed in to show graphene sheets lining the inner walls of the spheres.

B1.3 SEM of interstitial polymer in PS/G

Figure B-3 shows how the interstitial polymer between graphene-stabilized spheres changes dramatically as the weight percent of graphite is increased. In Figure B-3(A), the smooth region where three spheres meet is PS. The region where two spheres meet in Figure B-3(B)is very different in the amount of polystyrene and in the surface morphology. The region looks textured with a large amount of graphite/graphene present. The small beads within the larger cavities are due to some styrene dissolved in the water phase, as mentioned previously.

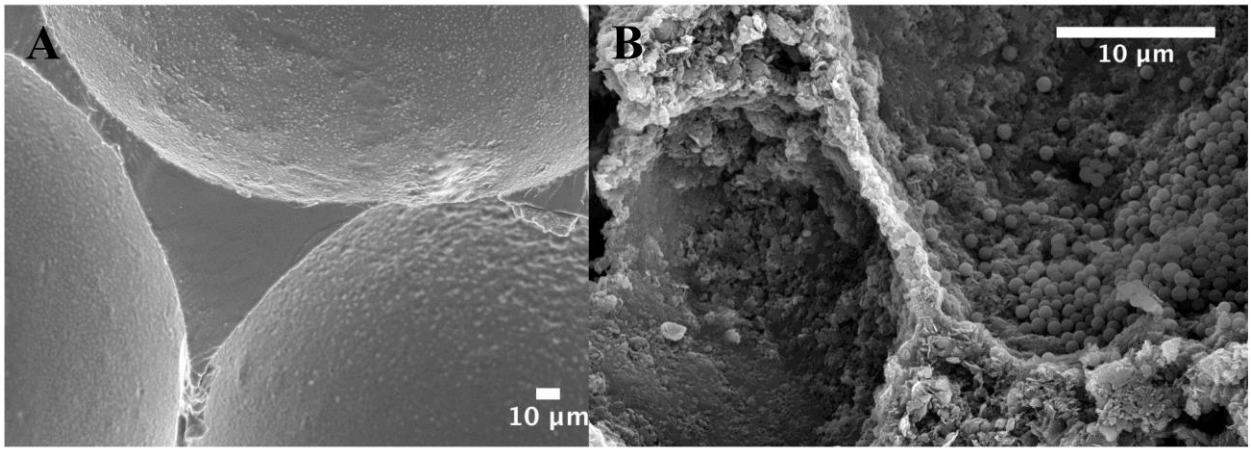

Figure B-3. (A) 1.3 wt% PS/G composite (B) 14 wt% PS/G composite.

B1.4 Raman spectroscopy of shaken vs blended PS/G

Two PS/G composites, both with a loading of 1.3 wt% graphite, were made exactly the same way except one was shaken for a minute and the other was emulsified using the Silverson laboratory mixer for one minute. Raman spectroscopy was used to analyze both samples to see if the way in which the emulsion was made had an effect on the number of graphene layers or extent of exfoliation in the final composite and if the properties of the two composites could be compared. As shown in Figure B-4, looking at the 2D peak at ~2700 cm^{-1}, there is no difference in the peak shape and shift.

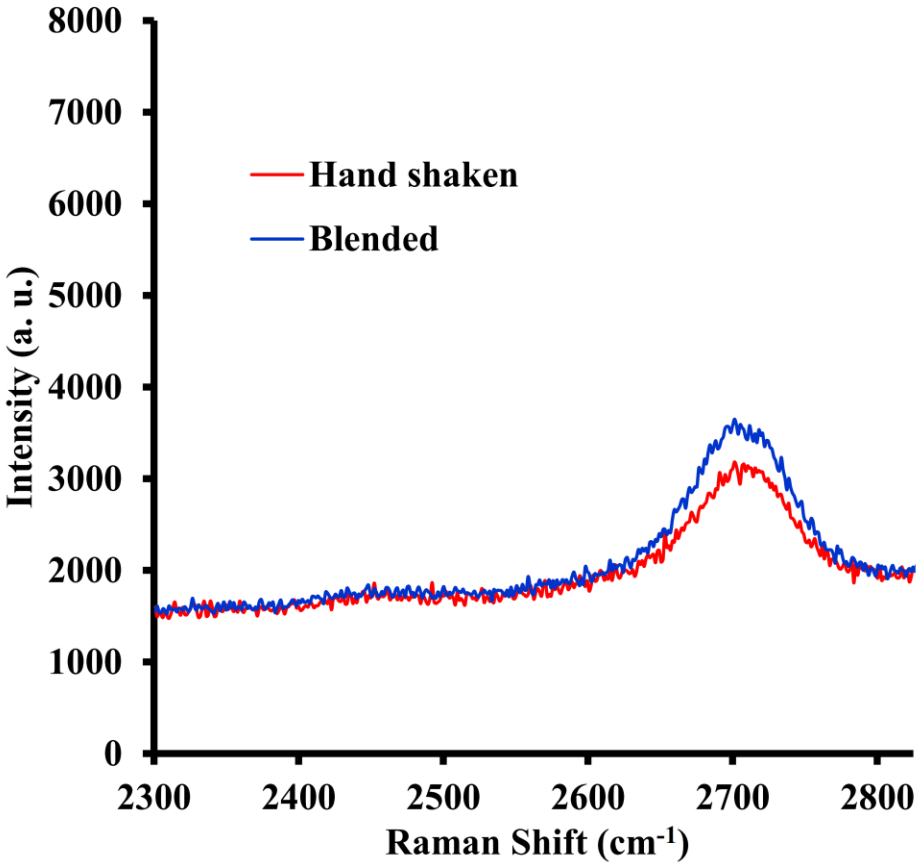

Figure B-4. Raman spectroscopy of the 2D peak of a shaken (red) and blended (blue) 1.3 wt% PS/G composite.

Comparing the 2D peak shape and shift from a PS/G composite, one made by blending the emulsion and one made by shaking, to the literature in Figure B-5, tells us that there appears to be two layers of graphene in our system. Therefore, there is the same number of graphene layers in the two systems, blending and shaking. When the viscosity increases in the higher graphite weight percent emulsions, shaking the sample can be compared to a sample that has been blended with the Silverson mixer, when looking at the electrical and thermal properties of the final composite.

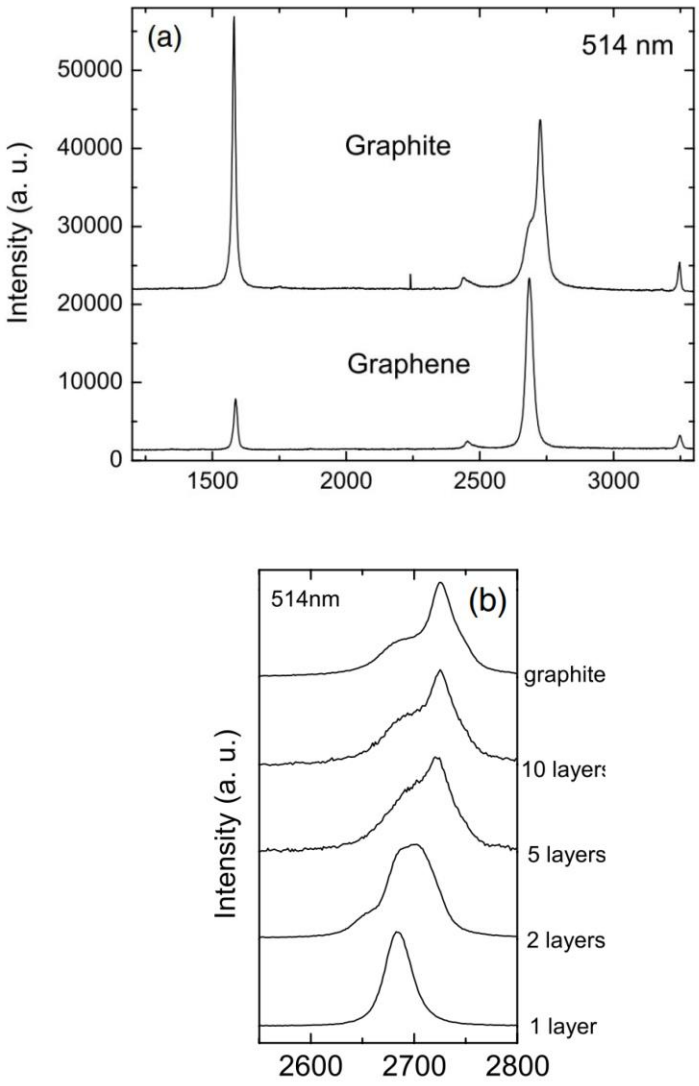

Figure B-5. (a) Raman spectra at 514 nm comparing bulk graphite and graphene (b) 2D peak shown at ~2700 cm^{-1} showing number of layers of graphene.[3]

B1.5 Poly(butyl acrylate)/poly (*tert*-Butyl acrylate) graphene (PBA/P*t*-BA/G) composites in pipes

In trying to find a different composite material that adheres well inside of a metal pipe, PBA/graphene foams have been tried in stainless steel pipes. A 6/4 water/oil ratio was used. However, the PBA foams are too soft and do not adhere well to the inner walls of the pipe. A different idea is combining PBA with P*t*-BA in order to further hydrolyze the P*t*-BA into poly (acrylic acid) (PAA) to create both a hydrophobic and hydrophilic material in one composite. We want the foam hydrophilic enough that when water flows through the pipe, the material swells and seals itself inside the pipe.

As before, a 6/4 water/oil ratio was used to form the emulsion in a 125 mL jar. A 1.3 wt% (0.44g) graphite concentration was used. In the 40 mL of oil, a 30:10 ratio was used of butyl acrylate (BA) to *tert*-butyl acrylate (*t*-BA). After the addition of oil phase, DI water (60 mL), DVB (0.5 mL), AIBN (0.12 g), and a stir bar, the mixture was allowed to stir on a stir plate for 1 minute. The stir bar was removed and the mixture was then shaken for 1 minute, emulsified with the Silverson laboratory mixer (Model L5M-A, Silverson Machines Inc.) for 1 minute, followed by shaking for 1 minute in order to get a stable emulsion. The emulsion was then allowed to sit for 30 minutes and some phase separation occurred (~25 mL), which was removed with a pipet. Similarly to the water/styrene emulsions, the emulsion was poured into the stainless steel pipes (4 in length, ½ in diameter). Teflon tape was used to wrap around the outer threads of the pipe to easily remove the bottom cap after polymerization. The bottom cap is sealed tightly so the emulsion does not leak and aluminum foil is placed on the top of the pipe, in order to

prevent pressure from building up inside the pipes. The pipe is placed into a convection oven (Blue M, Stabil-Therm) at ~70 °C for 24 h.

The cylindrical-shaped composites were removed from the pipe and dried at ~70 °C for 1 – 2 days. A typical procedure to hydrolyze the *t*-BA is as follows, based on work by Hautekeer *et al.*, where polystyrene-poly (*tert*-butyl acrylate) triblock copolymers were hydrolyzed using p-Toluenesulfonic acid (PTSA).[4] The mass of the dried cylindrical-shaped PBA/P*t*-BA composite was collected. The moles of *t*-BA were calculated and 5% of those moles was used to calculate the mass of the PTSA required for the hydrolysis. The PTSA was dissolved in hot toluene. Approximately 150 – 200 mL of toluene with the dissolved PTSA was placed in a 240 mL jar and the PBA/P*t*BA composite was placed into the jar. The composite swells immediately upon contact with the toluene/PTSA mixture. The jar was placed in an oil bath at 100 °C for 8 – 10 hours with continuous stirring in the jar and oil bath. While still in the jar, the composite shrinks once the hydrolysis is done. After air drying the hydrolyzed composite, it reduces back to its original size. The reaction of P*t*-BA to PAA using PTSA is shown in Figure B-6.

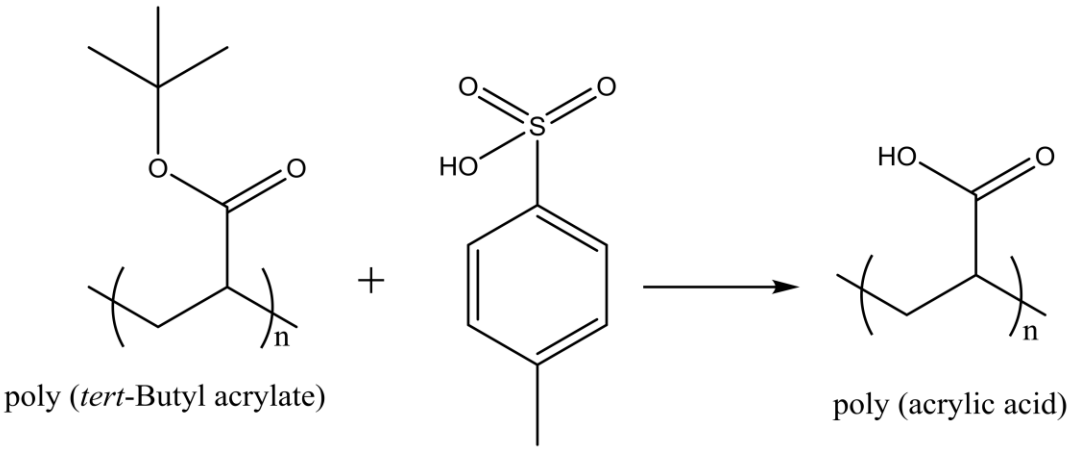

Figure B-6. Hydroylsis of poly (*tert*-butyl acrylate) (P*t*BA) to poly (acrylic acid) (PAA).

The 30:10 BA to *t*-BA seemed promising however the composite cracked after hydrolysis and therefore could not be re-inserted into a metal pipe and used in a flow through setup with water.

B1.6 Kinetic Study

The spreading of graphene sheets at a high energy liquid/liquid interface is driven by lowering the overall energy of the system. However, the kinetics of the emulsions is an important aspect and as the lateral sheet size of the graphite increases, the timescale of exfoliation should also increase. The kinetics of the exfoliation of three different graphite flake sizes, ~1, 10 and 50 μm, in a water/styrene system was monitored over a two-year period to see if the size of the graphite had an affect on the rate of exfoliation.

First, the morphology of the graphite we used in the study is observed with SEM. The average lateral sheet size of Asbury grade 2299 is on the order of a few microns, which was the smallest graphite used in the study. In Figure B-7(A, B, and C), the natural derived 2299 graphite can be seen, with a low amount of aggregation. 2299 is provided by Asbury Carbons.

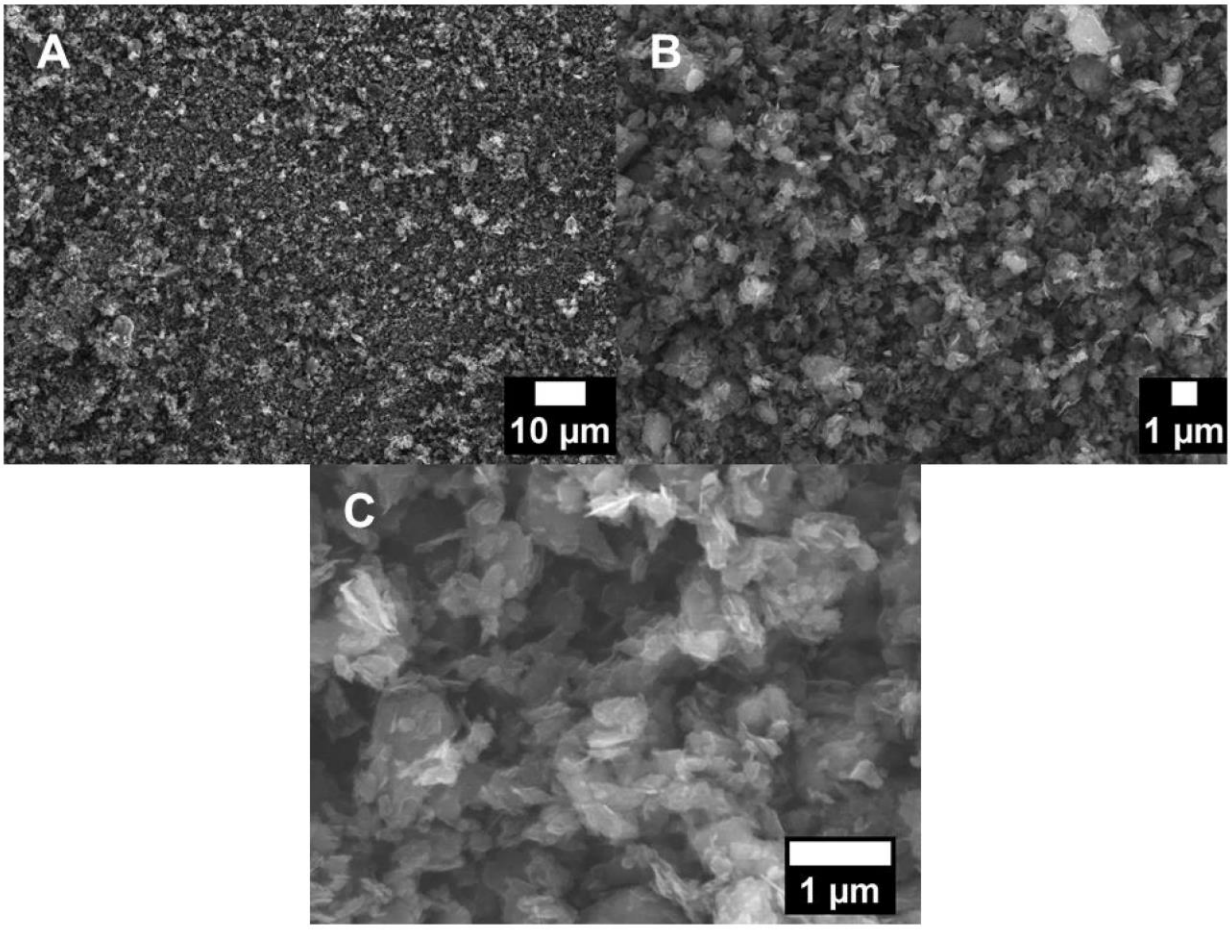

Figure B-7. Scanning electron microscopy images of Asbury Carbons graphite grade 2299.

For the middle-sized flake graphite, Asbury Micro 890 (~10 µm), which is a natural flake graphite, the SEM images were shown previously in Chapter 3. Asbury grade 3243 has the largest sheet size of the graphite that is used in the kinetic study of the emulsions, which is around 55 µm. The distribution of the lateral size of the graphite stacks is shown in Figure B-8(A). The composition of the larger aggregates, which are stacks of graphite, can be seen in Figure B-8(B). Lastly, zooming into one of the sample stacks, the thickness and layering can be visualized in Figure B-8(C).

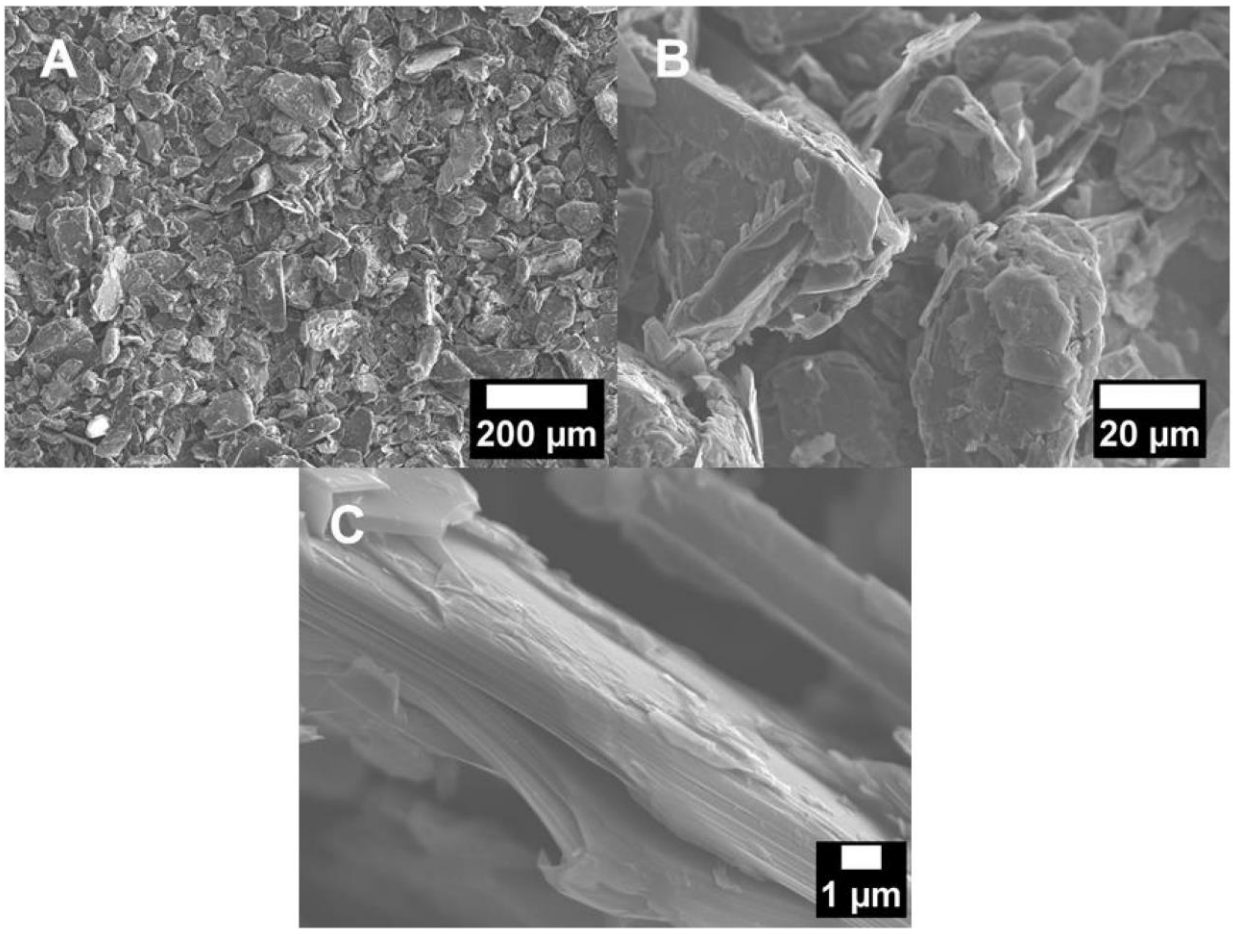

Figure B-8. Scanning electron microscopy images of Asbury Carbons graphite grade 3243.

The ratio of water to oil was held constant among the emulsions with different graphite flake size, with a 50:50 water:styrene ratio. Two different concentrations of graphite were studied: 4.4 mg/mL (880 mg in 200 mL emulsion or 1.3 wt% graphite) and 0.88 mg/mL (176 mg, 0.5 wt% graphite). Regardless of the sheet size and concentration of graphite, the same procedure was used as follows:

Graphite (880 mg or 176 mg), DI water (100 mL), styrene (100 mL), DVB (24 mL) and a magnetic stir bar were added to an Erlenmeyer flask. The contents were stirred on a stir plate for

30 s, bath sonicated (Branson 80W B2510DTH) for 30 s, and then emulsified using a POLYTRON® Mixer (Model PT 10/30, Kinematica GmbH) for 1 minute, placing the tip of the emulsifier at the oil – water interface. The emulsion was transferred to a 240 mL jar and capped. Pictures of the emulsions were taken with a ruler to document the size, shape, and quantity of emulsion produced. The samples were emulsified for 1 minute each at different time points throughout the year and pictures were taken before each blending cycle. At the ninth data point, a control sample was made for each graphite type and concentration. The control samples were blended for 9 consecutive minutes, which is equivalent to the actual sample blended 9 one-minute blending intervals over many months. The two samples in each graphite type and concentration were compared. Samples throughout the year, in the same graphite concentration and graphite flake size set were compared.

Many images were acquired during the kinetic study of three different sets of graphene-stabilized emulsions over a two-year time period. However, three different time points were selected here to represent and explain the events that occurred during the exfoliation of graphite into graphene over time. Figure B-9 shows six images that highlight those times points for two different concentrations of graphite in the water-in-styrene emulsions. The few micron natural graphite, grade 2299, was used. Figure B-9(A and D) were taken in 2014, Figure B-9(B and E) were captured in 2015, while Figure B-9(C and F) were taken in 2016. Comparing Figure B-9(A and D), the emulsion droplet size in the 0.88 mg/mL is larger than in the 4.4 mg/mL graphite concentration emulsion. As time progressed, more graphene climbing was observed on the inside walls of the jar. Although difficult to see inside the jars in Figure B-9(C and F), the styrene has auto-polymerized and a composite has formed. This observation was made in May of 2015 and the study began in July of 2014.

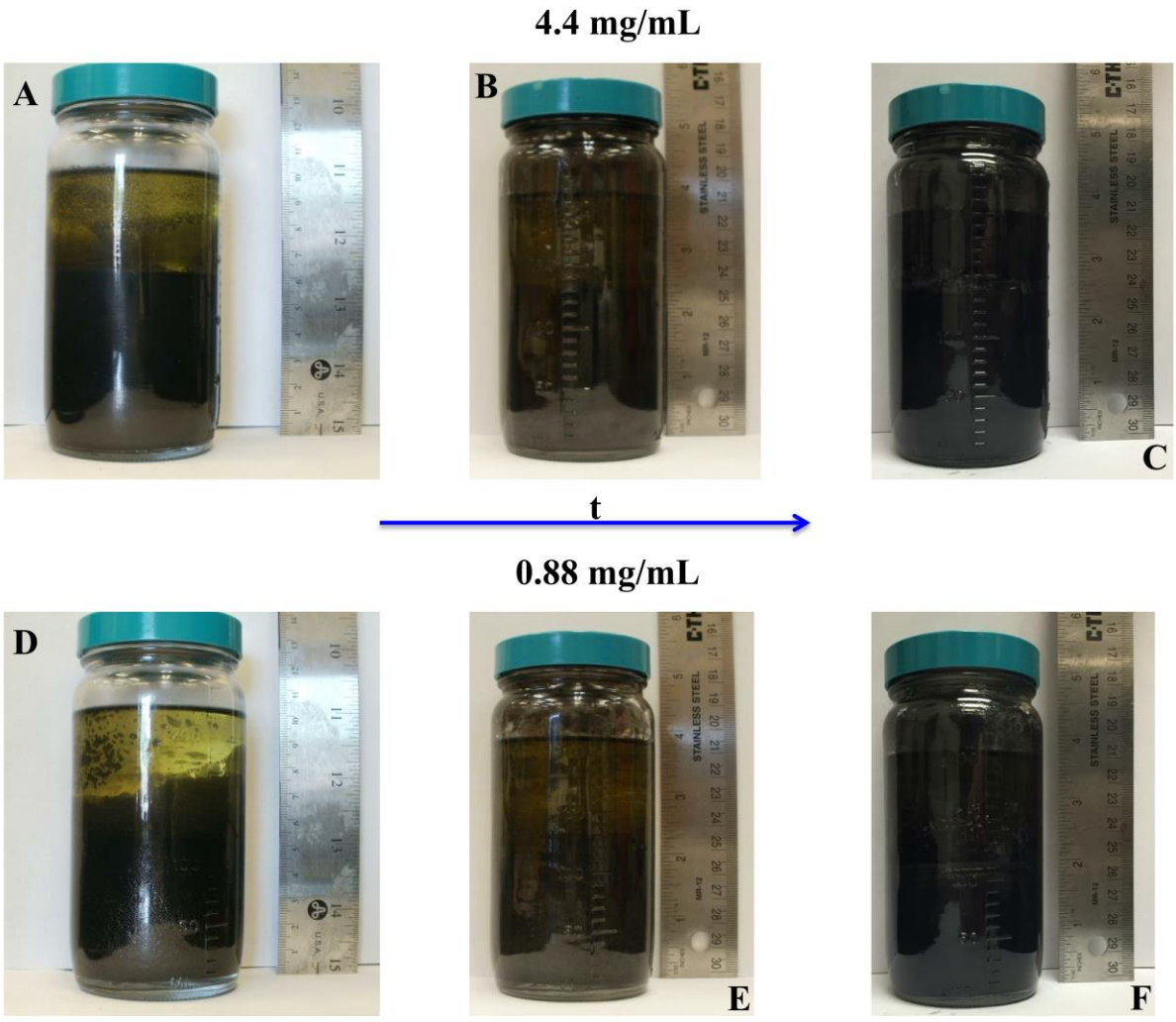

Figure B-9. Asbury Carbons graphite grade 2299 Kinetic Study: (A) – (C) 4.4 mg/mL graphite concentration, 2014, 2015, 2016 data points, respectively (D) – (F) 0.88 mg/mL graphite concentration, 2014, 2015, 2016 data points, respectively.

Figure B-10 demonstrates the same set of images at the same time points as in Figure B-9, but with the natural flake 10 μm graphite, Micro 890. The same observation was made with the emulsions that contained the Micro 890 as in the ones with the 2299, which was at a reduced concentration of graphite, the emulsion droplet size was larger, as shown in Figure B-10(A and D). For the 4.4 mg/mL concentration of graphite emulsions, more graphene climbing on the walls of the jar and a more grey emulsion was observed over time. Approximately 80 mL of

emulsion has polymerized and ~30 mL of emulsion has not in Figure B-10(C) as of August 2016. The 0.88 mg/mL emulsions with Micro 890 graphite has achieved a larger emulsion phase (by volume), a more stable emulsion, and smaller emulsion droplets over time, as visualized in Figures B-10(D – F). The graphene-stabilized emulsion with 0.88 mg/mL graphite concentration has not auto-polymerized.

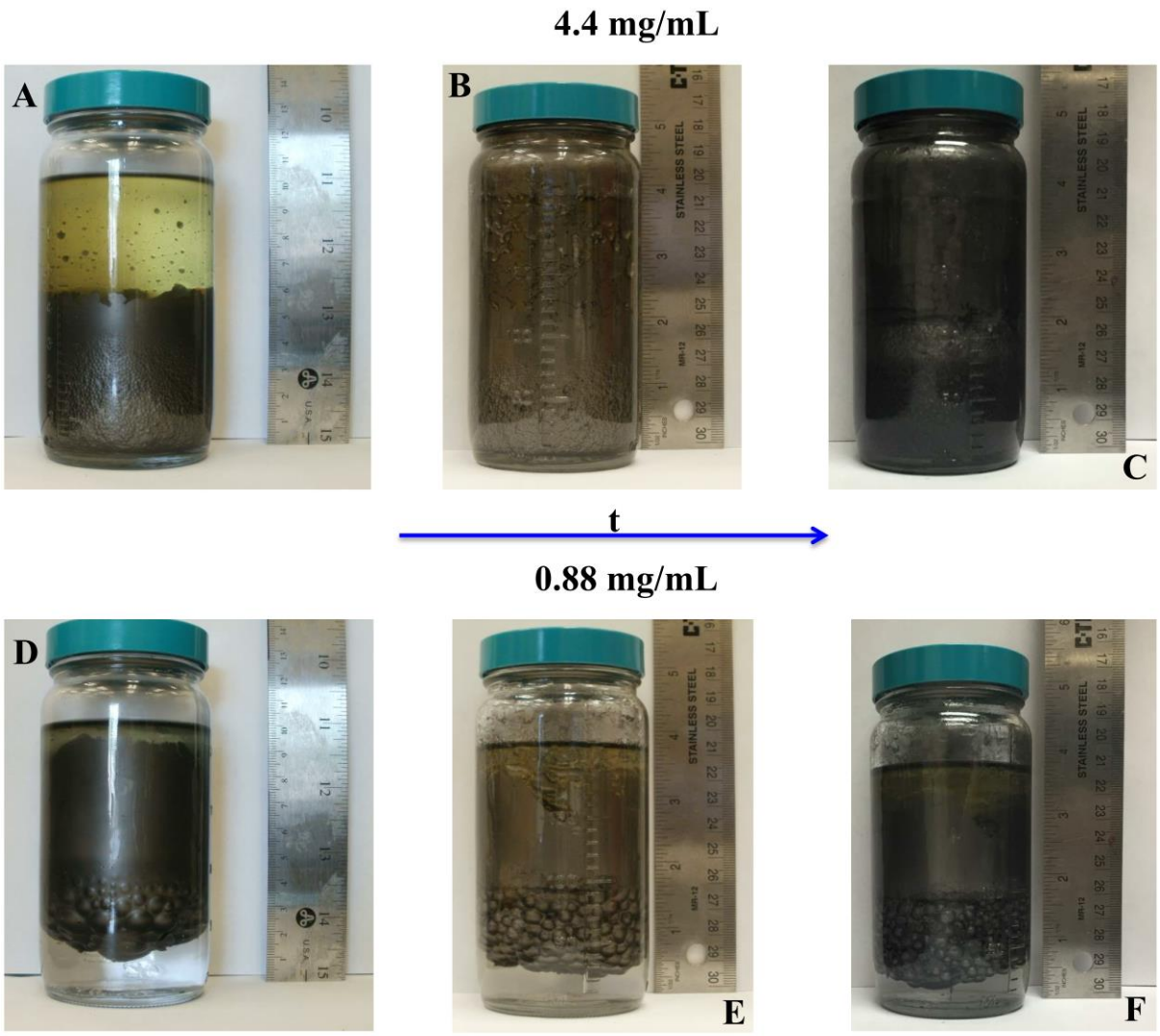

Figure B-10. Asbury Carbons graphite grade Micro 890 Kinetic Study: (A) – (C) 4.4 mg/mL graphite concentration, 2014, 2015, 2016 data points, respectively (D) – (F) 0.88 mg/mL graphite concentration, 2014, 2015, 2016 data points, respectively.

Lastly, the highlighted images at the same time points as the 1 and 10 μm graphite emulsions, for the largest flake size of graphite is shown in Figure B-11, which has a lateral sheet size of 50 μm and is grade 3243. The most dramatic change in the emulsion over time is seen with the 4.4 mg/mL graphite concentration with the 3243 graphite, as shown in Figure B-11(A – C). The emulsion has become more stable and the droplets have become smaller and more homogenous with time. The sample has not auto-polymerized. For the 0.88 mg/mL graphite concentration, an emulsion phase like the other samples regardless of graphite type or concentration, was never produced, however, in October of 2014 (test began in July of 2014), a glob of spheres was present at the interface between styrene and water, where most of the graphite/graphene is. This was the first time spheres were present. As shown in Figure B-11(E and F), that glob of spheres has fallen from the interface and sits on the bottom of the jar.

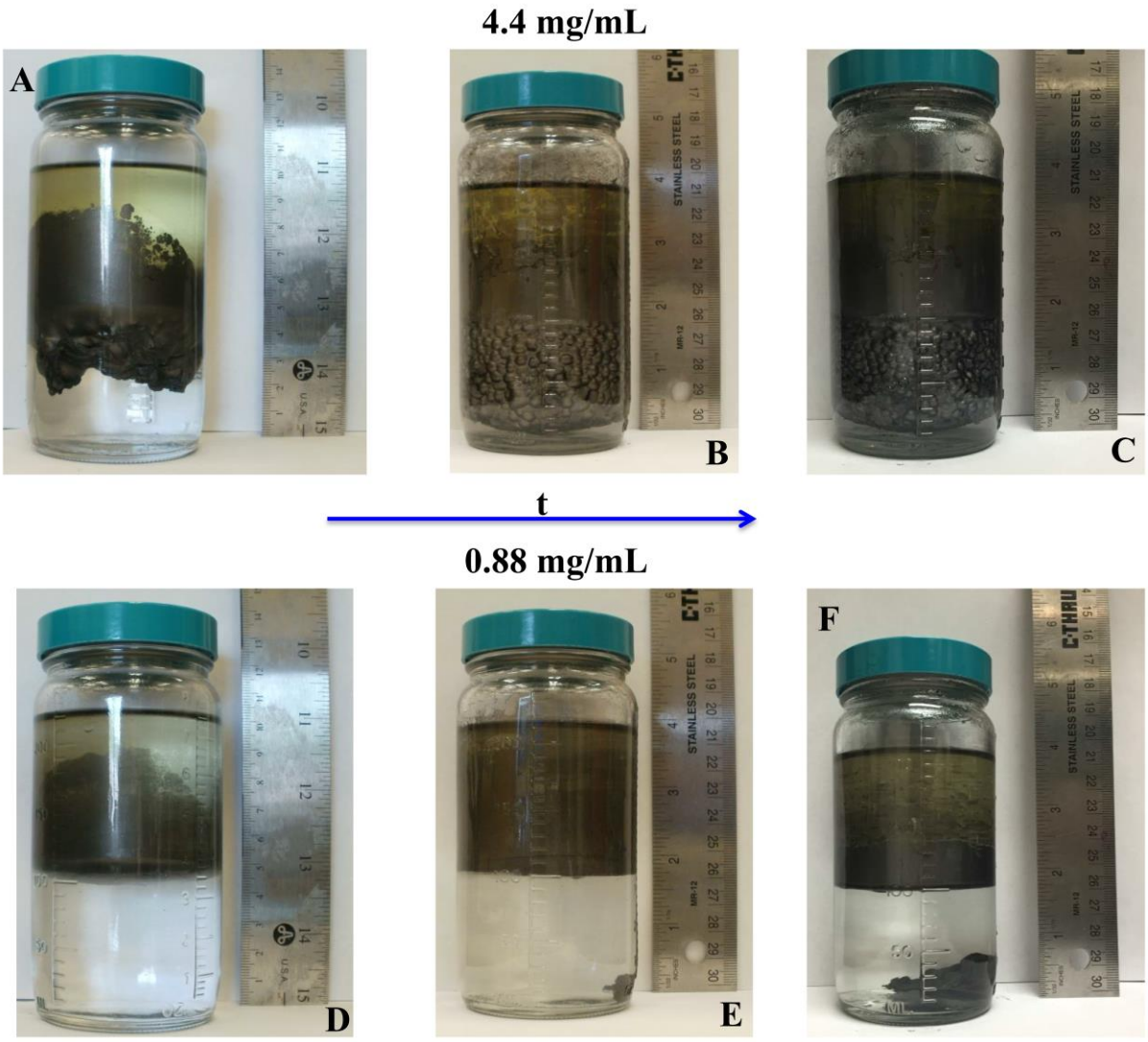

Figure B-11. Asbury Carbons graphite grade 3243 Kinetic Study: (A) – (C) 4.4 mg/mL graphite concentration, 2014, 2015, 2016 data points, respectively (D) – (F) 0.88 mg/mL graphite concentration, 2014, 2015, 2016 data points, respectively.

References

(1) Wu, N.; She, X.; Yang, D.; Wu, X.; Su, F.; Chen, Y. *J. Mater. Chem.* **2012**, *22*, 17254–17261.

(2) YAN, J.; CHEN, G.; CAO, J.; YANG, W.; XIE, B.; YANG, M. *New Carbon Mater.* **2012**, *27*, 370–376.

(3) Ferrari, A. C.; Meyer, J. C.; Scardaci, V.; Casiraghi, C.; Lazzeri, M.; Mauri, F.; Piscanec, S.; Jiang, D.; Novoselov, K. S.; Roth, S.; Geim, A. K. *Phys. Rev. Lett.* **2006**, *97*, 187401–1 – 187401–187404.

(4) Hautekeer, J.-P.; Varshney, S. K.; Fayt, R.; Jacobs, C.; Jerome, R.; Teyssie, P. *Macromolecules* **1990**, *23*, 3893–3898.